Title
Transcriptional and epigenetic control of Natural Killer cells during viral infection

Author
Riggan, Luke

Publication Date
2021

Peer reviewed|Thesis/dissertation

UNIVERSITY OF CALIFORNIA

Los Angeles

Transcriptional and epigenetic control of Natural Killer cells during viral infection

A dissertation submitted in partial satisfaction of the

requirements for the degree Doctor of Philosophy

in Molecular Biology

by

Luke Riggan

2021

ABSTRACT OF THE DISSERTATION

Transcriptional control of Natural Killer cells during viral infection

by

Luke Riggan

Doctor of Philosophy in Molecular Biology

University of California, Los Angeles, 2021

Professor Tim O'Sullivan, Chair

Natural killer (NK) cells are circulating group 1 innate lymphocytes (ILCs) that play a critical role during herpesvirus infection in mice and humans[1-3]. Although historically categorized as innate immune cells, circulating and tissue-resident group 1 ILCs can exhibit memory responses to mouse cytomegalovirus (MCMV)-associated glycoproteins through expression of germline encoded activating receptors[4-6]. NK cells possess traits of adaptive immunity, such as memory formation. However, the molecular mechanisms by which NK cells persist to form memory cells are not well understood. In chapter 2, we used single cell RNA sequencing to identify two distinct effector NK cell (NK_{eff}) populations following mouse cytomegalovirus (MCMV) infection. $Ly6C^-$ memory precursor NK cells displayed enhanced survival during the contraction phase in a Bcl2-dependent manner, and differentiated into $Ly6C^+$ memory NK cells. MP NK cells exhibited

distinct transcriptional and epigenetic signatures compared to Ly6C^{+} NK$_{eff}$ cells, with a core epigenetic signature shared with MP CD8^{+} T cells enriched in ETS1 and Fli1 DNA-binding motifs. Until recent years, studying gene function intrinsic to innate immune cell function was limited to Cre-inducible murine models. In order to increase the speed at which we can study gene function, we developed a novel method in Chapter 3 to study gene function in multiple innate immune cell linages during viral infection using a quick and robust protocol. Using this method, we were able to identify Fli1, a transcription factor, which controls memory precursor (MP) Natural Killer cell formation during viral infection. Fli1 was induced by STAT5 signaling *ex vivo,* and increased Bim levels in early effector NK cells following viral infection. Collectively, these results suggest that a NK cell-intrinsic checkpoint controlled by Fli1 limits MP NK formation by regulating early effector NK cell fitness during viral infection. In addition to transcriptional regulation, NK cells undergo dynamic chromatin remodeling during development and in response to viral infection[6,7]. However, the epigenetic regulators that are responsible for these genome-wide chromatin changes are unknown. In chapter 4, we identify ubiquitously transcribed tetratricopeptide repeat, X chromosome (UTX) as a critical regulator of the NK cell regulome. Deletion of UTX in NK cells results in global transcriptional changes and differences in chromatin accessibility at several gene loci involved in NK cell development, homeostasis, and effector function. Together, these results identify UTX as a critical epigenetic regulator of NK cells in mice. In summary, our work has developed a method for studying gene function in innate immune cells, identified novel transcriptional regulation of MP NK cells during memory NK cell formation and profiled epigenetic regulation of NK cell effector function during viral infection.

This dissertation of Luke Riggan is approved

Matteo Pellegrini

Yvonne Chen

Maureen Su

David Nathanson

Tim O'Sullivan, Committee Chair

University of California, Los Angeles

2021

This dissertation is dedicated to:

My parents and grandparents who have worked hard to allow me to live the life I have and to be presented with opportunities that allowed me to become who I am today.

And to all my mentors along the way, especially Mick Nyquist during my undergraduate studies and Tim O'Sullivan during my graduate studies at UCLA.

Table of Contents

List of Figures

Chapter 2

Chapter 3

Chapter 4

ACKNOWLEDGMENTS

I would like to first thank my mentor, Dr. Tim O'Sullivan. We have had an incredible journey over the last four years. Together with Andrew Hildreth we started the lab together. As the first graduate students of the lab, we have been through growing pains, lows, and highs. However, through all these challenging times, Tim has taught us to be rigorous in our work, do the best science possible and the rest will fall into place. Tim has shown us the value of maintaining multiple projects afloat at once and he provided incredible guidance on deciding when to start or stop a particular project. Tim was always available to talk about ideas or discuss project challenges. Tim has an incredible curiosity and imagination when it comes to science, we have come up with many fascinating ideas together, whether it be just talking in passing or putting ideas up on the whiteboard, we have generated many hypothesis driven ideas, and some of them worked out beautifully. Tim is also an incredible presenter and I have learned many attributes of data presentation and delivery from him, these skills have been invaluable as I prepare for the next stage of my career. Tim has excellent vision, he encouraged me to continue working on NK cells even though I joined his lab to work on a cancer project that initially failed. This turned out to pay off exceedingly, as the field of NK immunotherapy has exploded over the last few years and as a result, I have had an incredible number of quality job offers. Thanks Tim, thanks for encouraging me to stick with this project in times of doubt, thanks for helping me cut off projects that were not feasible and helping me drive a fascinating story about NK cell biology from a crazy idea to publication. Also thank you for your patience, guidance, and advice regarding life outside of the lab. I look forward to the opportunity to work together again one day

I cannot thank Andrew Hildreth enough, for the consistent support in and out the lab. Andrew has been a rock to me through my entire graduate school career. We joined Tim's lab together, I knew right away we would be good colleagues, but I had no idea I had also found a lifelong

friend. In the lab, Andrew always brings an extremely positive attitude and is willing to help in any way he can. We have troubleshooted numerous protocols together, discussed countless papers and crafted new hypotheses and ideas for future projects. Andrew is such an asset to have at work, I have no doubt he will go on to do incredible things. I hope we get the chance to work together in biotech down in San Diego one day.

I would also like to thank other members of the O'Sullivan lab, especially Joey Li. He joined as an MD-PhD student towards the end of my graduate career. Joey and I have worked together to accomplish an incredible amount of work in a short time period in order to finish the end of my thesis work. Joey is incredibly smart and a fast learner, I am looking forward to the results he generates over the next few years as he explores new questions which follow up some of my studies.

My committee members have all been incredibly helpful in different ways. Dr. Yvonne Chen, thank you for exposing me to the world of immunotherapy and for teaching me the importance of detail and showing me how to be a rigorous scientist during my rotation. Dr. Maureen Su, thank you so much for being a great co-mentor, I always appreciate our discussions in and outside of the lab. You have been incredibly supportive over the last four years. Dr. David Nathanson, thanks for always bringing positive energy to every conversation we have, I can't help but feel excited about science after any time we talk. Dr. Matteo Pellegrini, thank you for assistance with the bioinformatics and for being the head of my committee even though you didn't know me that well my first year at UCLA. And thank you all for the detailed criticism and advice regarding my projects over the last few years.

Feiyang Ma has been an incredible collaborator on two of my projects. I cannot thank him enough for his scientific contributions to the projects. He is an incredible bioinformatics expert

and has helped us make new discoveries in NK cell biology. Thanks so much Feiyang, hopefully we can celebrate one day when we are not separated by a pandemic and an entire ocean!

2021 was an incredible year for the O'Sullivan lab, we grew from just three members during the pandemic to about triple the size now. A huge thanks to Rana and Eddie, they are incredible to work with and have made sure everything in the lab stays in one piece. I'd also like to thank Vignesh Senthilkumar for helping out with daily experiments during the pandemic. I want to thank Siya Shah for writing a review article with me, completely virtually without ever meeting me in person prior to the opening of the lab post-pandemic. I want to thank former lab members Chris Huerta, Matt Mauldenhour and Ann Wong for helping out on numerous experiments including my initial project which ultimately failed but was an incredible learning experience

Elizabeth Fernandez was extremely helpful during our collaboration, from idea generating discussions to planning alternative protocols, thank you for your contributions.

Patrick Ho was a phenomenal mentor during my first rotation at UCLA. He taught me an incredible number of skills and how to think like a scientist in a matter of three months. It felt like a science bootcamp, but I cannot thank you enough.

Ryan Wong has been an incredible colleague and friend outside of the lab. I met Ryan during my second rotation during what some would call a chance encounter. I think it's so important to make the most of all these interactions because you never know what could come of it. Ryan is an incredible scientist, I always looked up to him and it has been a pleasure to watch him succeed. Ryan always provided great advice when it came to science and career advice. Thanks for everything Ryan and I look forward to the day we work together.

I would also like to thank Mick Nyquist, my undergraduate post-doc mentor, he provided an invaluable experience. He was willing to work with a kid who barely knew anything about science. By the end of our time at Fred Hutch, we were having detailed talks about science, and we successfully used CRISPR to investigate questions in prostate cancer at a time when CRISPR was revolutionary. Thank you for exposing me to so much cool science and getting me exciting about doing research.

Thank you to all my parents and step-parents, Mom, Dad, Mark and Carmen, you all have been incredibly supportive of my efforts to pursue education and research. Thank you to my Aunt Renee for your unconditional support and to my Uncle Cliff for providing me invaluable advice about research over the years and the biotech space as I enter the next stage of my career.

I also like to thank Jessica Scholes and Jeff Calimlim at the FACS core for their training and providing an essential resource. Without your help a majority of my experiments would not have been possible.

I'd also like to thank Deanna Linck for your incredible support outside of the lab. You were always willing to study with me through many late nights in the lab. You have been there for me in times of doubt and been incredibly supportive no matter what. We also joke and say you were my good luck charm, we made the discovery Fli1 right after I met you and proceeded to have the most productive and exciting 8 months of research. Thanks for being with me through such a crazy time.

Kaiser Atai, Ian Ford, Devin Gibbs, Nick Jackson, Michal Juda, Andrew Hildreth and Declan Evans. Thanks boys for being incredible friends and colleagues. UCLA would not have been the same without my fellow graduate student friends. Cheers to the times ahead!

VITA

EDUCATION

2013-2016 **University of Washington** Bachelor of Science, Biochemistry
2017- **University of California Los Angeles** (UCLA) MBIDP PhD program

WORK EXPERIENCE

2014-2016 Peter Nelson Lab – Fred Hutch Cancer Research Center – Undergraduate researcher

2015-2016 Elahe Mostaghel Lab – FHCRC – Undergraduate researcher

2016-2017 David Cobrinik Lab – Children's Hospital Los Angeles – Research Technician

2017 Lili Yang lab – UCLA - Graduate Student Researcher (Rotation)
Evaluated the development, activation and cytotoxicity of invariant Natural Killer T (iNKT) cells using humanized BLT (Fetal Bone Marrow, Liver, Thymus) mouse model

2017 Yvonne Chen lab – UCLA - Graduate Student Researcher (Rotation)
Designed smarter CAR T cells, successfully integrated 2100 bp bi-specific anti-CD20/CD19 CAR construct with high efficiency into TRAC locus of T cells to produce highly potent CAR T cells.

2018- Tim O'Sullivan Lab – UCLA – Graduate Student Researcher (current)

- Our work discovered new basic biology to further understand Group 1 Innate Lymphocyte responses during viral infection, tissue damage and anti-tumor responses.
- Developed CRISPR RNP infection model to study gene edited NK cells during murine cytomegalovirus infection (MCMV)
- Defined NK effector cell heterogeneity in response to MCMV using single cell sequencing, identified a memory precursor-like NK cell population and the novel transcriptional mechanism governed by Fli1 that controls the persistence of this population. We used our *in vivo* CRISPR model to explore the role of Fli1 which has never been profiled in NK cells.

PUBLICATIONS

Manuscripts in revision/preparation:

1. **Riggan L**, Ma F, Fernandez E, Nathanson D, Pellegrini M, O'Sullivan TE**.** Fli1 limits the formation of memory precursor NK cells during viral infection. *Nature Immunology.* Under Revision.

2. Cheng M., **Riggan, L,** Ma F., Chin S. Pellegrini M., O'Sullivan T.E., Su M. UTX controls NK cell development and effector function during viral infection. (In preparation).

Peer Reviewed Publications:

1. **Riggan L**, Shah S, O'Sullivan TE. Arrested development: suppression of NK cell function in the tumor microenvironment. *Clin Transl Immunology* 2021; **10**: e1238

2. **Riggan, L.,** Hildreth, A.D., Rolot, M., Wong, Y.Y., Satyadi, W., Sun R., Huerta C., O'Sullivan, T.E. CRISPR Cas9 Ribonucleoprotein-mediated Genomic Editing in Mature Primary Innate Immune Cells. *Cell Reports.* (2020)

3. Hildreth, A.D., **Riggan, L.** & O'Sullivan, T.E. CRISPR-Cas9 Ribonucleoprotein-Mediated Genomic Editing in Primary Innate Immune Cells. STAR Protocols (2020).

4. **Riggan, L.,** Freud, A.G., & O'Sullivan, T.E. True Detective: Unraveling Group 1 Innate Lymphocyte Heterogeneity. *Trends in Immunology* (2019)

5. Nabekura, T., **Riggan, L.,** Hildreth, A.D., O'Sullivan, T.E., Shibuya, A. Protective role of type 1 innate lymphoid cells in acute liver injury. *Immunity* (2019)

6. Weizman, O.E., Song, E., Adams, N.M., Hildreth, A.D., **Riggan, L.,** Krishna, C., Aguilar, O.A., Leslie, C.S., Carlyle, J.R., Sun, J.C., and O'Sullivan T.E. MCMV-experienced ILC1 acquire an m12-dependent memory response. *Nature Immunology*. (2019) PMID: 31263280

7. Tran HN, Singh HP, Guo W, Cambier, L., **Riggan, L.,** Shackleford, G. M., Thornton, M. E., Grubbs, B. H., Erdreich-Epstein, A., Qi, D. L., Cobrinik, D. Reciprocal Induction of MDM2 and MYCN in Neural and Neuroendocrine Cancers. *Front Oncol* 2020; **10**: 563156.

8. Michael D. Nyquist, Alexandra Corella, John Burns, Ilsa Coleman, Shuai Gao, Robin Tharakan, **Luke Riggan**, Changmeng Cai, Eva Corey, Peter S. Nelson and Elahe A. Mostaghel. *Molecular Cancer Research.* Exploiting AR Regulated Drug Transport to Induce Sensitivity to the Survivin Inhibitor YM155. Volume 15, Issue 5, pp. 521-531. May 2017.

PROFESSIONAL ACTIVITIES

2018-2021 UCLA MBIDP Orientation Student Ambassador
2019-2020 Biotech Connection Los Angeles – Outreach Lead
2019-2020 Co-Host of Finding Founders podcast
2019-2021 UCLA Annual MBI Retreat – Career Panel Advisor

HONORS AND SPECIAL AWARDS

2021 **UCLA MBIDP Dissertation Year Award**
2021 Warsaw Fellowship (1 year of funding)
2018 Cota Robles Fellowship recipient (2 years of funding)
2019 I3T UCLA Podium Presentation
2020 AAI Podium Presentation and Poster (Travel Award)
2020 UCLA MIMG travel award
2020 MBI Podium Presentation and Poster

Chapter 1: Introduction

Adaptive features of innate immunity, the transcriptional and epigenetic regulation of Natural Killer cells during pathogenesis and the importance of genetic editing as a tool to understand immune cell gene function

The innate immune system is a conserved host defense mechanism between plants, invertebrate and mammals[8]. Innate immune cells in mammals are found in nearly all organs, where specialized myeloid and lymphoid cells can become activated in response to physical breaks in barrier tissues, infiltration of infected cells or transformed malignant cells[9]. During pathogen encounter, germline encoded activating receptors such as pattern recognition receptors found on macrophages and dendritic cells, or natural cytotoxicity receptors found on Natural Killer (NK) cells can initiate an immune response in concert with the adaptive immune system to clear the pathogen or transformed cell and return the tissue to homeostasis[9]. NK cells were first defined, over 40 years ago, by their "Natural" ability to kill tumor cells *in vitro*[10]. NK cells are now also recognized to be important for protection against viral infection and for tissue homeostasis[11]. In mice, NK cells are defined based on the cell surface expression of NK1.1, with the absence of cell surface expression of other lineage (Lin) defining markers, including CD3, CD14, CD19, and T cell receptor (TCR) proteins[11]. Lin-NK1.1$^+$ cells were found to be heterogeneous for the expression of activating and inhibitory Ly49 receptors[11].

During Murine Cytomegalovirus (MCMV) infection, NK cells can exhibit features of adaptive memory demonstrated by a subset of epigenetically distinct Ly49H$^+$ NK cells which persist months post-infection and retain enhanced cytotoxicity against secondary MCMV infection in an antigen-dependent manner[12]. Prior to this finding, adaptive immunity has only been found in B and T cells, which require antigen receptor rearrangement to generate the diversity of receptors capable of recognizing the pathogen[12]. During infection, naive T cells undergo activation and proliferation, giving rise to progeny with effector and memory fates that can mediate short and long-term

protection[13]. Studies on CD8 T cell responses during lymphocytic choriomeningitis virus (LCMV) infection have revealed heterogeneity among effector T cells that determines, to some degree, the likely hood that a cell is programmed to survive and become a memory T cell or undergo apoptosis after executing effector functions[14-16]. CD8 T cells with high IL-7 receptor (IL-7R) expression and low KLRG1 expression (IL-7R^{high}KLRG1^{low}) have a much higher propensity to form memory T cells and are considered memory precursor (MP) cells, while nearly all IL-7R^{low}KLRG1^{high} CD8 T cells undergo apoptosis after pathogen clearance and can be considered terminally differentiated[14, 17, 18]. However, it should be appreciated that these markers are not completely exclusive and do not capture the full degree of heterogeneity that is present among effector CD8 T cells. For example, some KLRG1^{high} cells can be found after the resolution of an infection at a memory timepoint[19]. It remains incompletely understood if a collection of surface markers can entirely define memory precursor and terminal effector CD8 T cell populations during viral infection. However, in our studies in Chapter 2, we identify the first evidence of any surface marker which can define memory precursor NK cells during viral infection.

Previous studies over the last 10 years have demonstrated the adaptive features of NK cells during mouse and human cytomegalovirus infections[12]. In both mice and humans, stochastically expressed germline-encoded activating and inhibitory receptors as well as developmental subsets generate naive NK cell diversity and heterogeneity during homeostasis[4, 20, 21]. Furthermore, heterogeneity within the naive Ly49H^{+} NK cell pool can influence NK cell responses to MCMV. This involves preferential expansion of NK cells with a history of recombination-activating gene (RAG) expression, NK cells that lack expression of killer cell lectin-like receptor G1 (KLRG1) or the inhibitory receptor NKR-

P1B[22-24], and NK cells with a longer history of NKp46 expression[25]. Although subsets of naïve NK cells have been found to preferentially form Ly49H$^+$ effector NK (NK_{eff}) cells following MCMV infection, whether similar heterogeneity exists within expanded NK_{eff} cells remains unresolved. In Chapter 2, we found heterogeneity among the NK_{eff} pool using single cell sequencing. Furthermore, by examining differentially expressed surface markers in the NK_{eff} pool, we identified two subsets on Nk_{eff} cells defined by Ly6C. Ly6C$^-$ NK cells showed enhanced persistence in a BCL2-dependent manner. By examining differentially accessible regions of chromatin between the Ly6C NK cell subsets, using the assay for transposase-accessible chromatin using sequencing (ATAC-seq), we identified Friend of leukemia 1 (Fli1) as an important negative regulator during MP NK cell formation. Fli1 is considered a pro-oncogene and is embryonic lethal in mouse studies. The role of Fli1 is not well understood in NK cell biology. One study suggests heterozygous deletion of Fli1 in mice results in an increase of NK cell numbers during development[26]. A recent study in T cells revealed Fli1 restrained effector T cell formation and deletion of Fli1 enhanced effector T cell responses without compromising memory T cell formation. Therefore, we found the role of Fli1 of particular interest in NK cells, in Chapter 2, we profiled the effect of genetic deletion Fli1 in NK cells and the upstream signals which induce Fli1 during MCMV infection.

To understand these molecular mechanisms and others, we developed a novel protocol using CRISPR cas9 to interrogate gene function in primary murine NK cells, outlined in Chapter 3. Current strategies to specifically manipulate gene expression in the mouse innate immune system have been confounded by non-lineage specific Cre mouse transgenic lines. In the NK lineage, *Ncr1*^{Cre} mice induce gene deletion in NK cells, type 1

innate lymphoid cells (ILC1), and a subset of ILC3 [27]. Thus, the prevalent issue of non-specific gene targeting of innate immune cells significantly limits the precise mechanistic understanding of the innate immune system in models of host defense and disease *in vivo*. Recent advances in CRISPR-Cas9 genome editing provide and alternative gene manipulation tool that can be used on enriched primary immune cells [28]. Cas9 is a DNA endonuclease that can bind to a complementary region of the genome through its associated guide RNA (gRNA) to generate double strand breaks in the DNA that result in insertions and/or deletions (indels) in coding regions of proteins to permanently suppress their expression [29]. In Chapter 3, we describe an optimized strategy for non-viral CRISPR-Cas9 ribonucleoprotein (cRNP) genomic editing of primary mouse innate immune cells. Using these optimized conditions, we were able to achieve high knockout (KO) efficiency of cell surface proteins, intracellular signaling proteins, and transcription factors in innate immune cells using cRNP complexes. Furthermore, we describe two *in vivo* adoptive transfer models using cRNP-edited naive NK cells and dendritic cell precursors to reveal mechanistic details of antiviral gene function in these cell types during mouse cytomegalovirus (MCMV) infection. This general gene editing strategy may be further adapted to other primary immune cell types and *in vivo* transfer models to investigate protective or pathologic biological processes in the mammalian innate immune system.

In addition to transcriptional changes, NK cells undergo dynamic chromatin remodeling during development and in response to viral infection[6,7]. However, the epigenetic regulators that are responsible for these genome-wide chromatin changes are unknown. While previous work has identified distinct transcriptional and epigenetic states of mouse and human NK cells during development and viral infection[6,7, 30], the factors that control

the epigenetic landscape of NK cells during these processes remain unclear. In Chapter 4, our analysis of mice with NK cell-specific deletion of ubiquitously transcribed tetratricopeptide repeat, X chromosome (UTX) revealed increased peripheral immature NK numbers with a defect in effector responses to MCMV infection. UTX is a member of the Jumonji-C (JmjC) family of histone demethylases and is found on the X-chromosome. UTX functions by removing repressive methyl groups from histone H3K27 to promote gene transcription. However, the gene programs controlled by UTX are likely cell and context dependent. Therefore, we were interested in defining the role of UTX in NK cells during MCMV infection. In Chapter 4, we used ATAC-seq along with bulk RNA sequencing (RNA-seq) identified UTX-mediated changes in chromatin accessibility at several gene loci involved in NK cell development, homeostasis, and effector function. Together, these results identify UTX as a critical epigenetic regulator of NK cells in mice.

Chapter 2:

Fli1 restricts the formation of memory precursor NK cells during viral infection

Fli1 restricts the formation of memory precursor NK cells during viral infection

Luke Riggan[1,2], Feiyang Ma[3,4], Joey H. Li[1,2], Elizabeth Fernandez[5], David A. Nathanson[5], Matteo Pellegrini[3,4], and Timothy E. O'Sullivan[1,2,*,#]

[1]Department of Microbiology, Immunology, and Molecular Genetics, David Geffen School of Medicine at UCLA, Los Angeles, CA 90095
[2]Molecular Biology Institute, University of California, Los Angeles, Los Angeles, CA 90095, USA
[3]Department of Molecular, Cell, and Developmental Biology, University of California, Los Angeles, California, USA.
[4]Institute for Genomics and Proteomics, University of California, Los Angeles, California, USA.
[5]Department of Molecular and Medical Pharmacology, David Geffen UCLA School of Medicine, Los Angeles, California, USA.

[*]Corresponding Author
[#]Lead Contact

Correspondence:

Timothy E. O'Sullivan, PhD
David Geffen School of Medicine at UCLA
615 Charles E. Young Drive South, BSRB 245F
Los Angeles, CA 90095
Phone: 310-825-4454
Email: tosullivan@mednet.ucla.edu

Abstract

Natural killer (NK) cells are innate lymphocytes that possess traits of adaptive immunity, such as memory formation. However, the molecular mechanisms by which NK cells persist to form memory cells are not well understood. Using single cell RNA sequencing, we identified two distinct effector NK cell (NK_{eff}) populations following mouse cytomegalovirus (MCMV) infection. $Ly6C^-$ memory precursor (MP) NK cells displayed enhanced survival during the contraction phase in a Bcl2-dependent manner, and differentiated into $Ly6C^+$ memory NK cells. MP NK cells exhibited distinct transcriptional and epigenetic signatures compared to $Ly6C^+$ NK_{eff} cells, with a core epigenetic signature shared with MP $CD8^+$ T cells enriched in ETS1 and Fli1 DNA-binding motifs. Fli1 was induced by STAT5 signaling *ex vivo,* and increased Bim levels in early effector NK cells following viral infection. These results suggest that a NK cell-intrinsic checkpoint controlled by Fli1 limits MP NK formation by regulating early effector NK cell fitness during viral infection.

Introduction

The ability of the immune system to remember previous pathogen encounters by executing a specific and robust secondary response upon re-exposure to pathogen-associated antigens is termed immunological memory. During infection, this memory response is largely performed by the selective clonal proliferation and long-term persistence of adaptive lymphocytes that express somatically recombined antigen receptors (e.g. T and B cells). Adaptive lymphocytes form antigen-specific memory cells that are able to epigenetically maintain activation-induced transcriptional changes following clearance of pathogens[31, 32]. Coordination of stable epigenetic, transcriptional, and metabolic changes during T cell activation results in the cell-intrinsic capacity to form memory cells[31, 33, 34]. The kinetics of the adaptive immune response to infection consist of three distinct phases: clonal expansion, contraction and memory formation. During the contraction phase 90–95% of all expanded effector cells are eliminated through cell-intrinsic apoptosis, leaving memory T and B cells that persist long-term in the host[35]. Previous studies have demonstrated that expanded $CD8^+$ T cell populations consist of shorter-lived terminal effectors (TEs) that display decreased persistence during the contraction phase, and a smaller proportion of memory precursors (MPs) that contribute to the self-renewing memory $CD8^+$ T cell pool[14, 15, 35, 36]. However, whether MP-like cell states exist within the innate immune system is unknown.

Natural killer (NK) cells are circulating group 1 innate lymphocytes (ILCs) that play a critical role during herpesvirus infection in mice and humans[1-3]. Although historically categorized as innate immune cells, circulating and tissue-resident group 1 ILCs can exhibit memory responses to mouse cytomegalovirus (MCMV)-associated glycoproteins

through expression of germline encoded activating receptors[4-6]. Furthermore, NK cells exhibit clonal proliferation and persistence of a long-lived population of memory cells with enhanced protective capacity after secondary MCMV infection[12, 37]. In C57BL/6 mice, a subset of naïve Ly49H$^+$ NK cells initiate this adaptive response after recognition of the MCMV-encoded glycoprotein m157[6, 38, 39]. In both mice and humans, stochastically expressed germline-encoded activating and inhibitory receptors as well as developmental subsets generate naïve NK cell diversity and heterogeneity during homeostasis[4, 20, 21]. Furthermore, heterogeneity within the naïve Ly49H$^+$ NK cell pool can influence NK cell responses to MCMV. This involves preferential expansion of NK cells with a history of recombination-activating gene (RAG) expression, NK cells that lack expression of killer cell lectin-like receptor G1 (KLRG1) or the inhibitory receptor NKR-P1B[22-24], and NK cells with a longer history of NKp46 expression[25]. Although subsets of naïve NK cells have been found to preferentially form Ly49H$^+$ effector NK (NK_{eff}) cells following MCMV infection, whether similar heterogeneity exists within expanded NK_{eff} cells remains unresolved. Furthermore, whether a subset of NK_{eff} cells preferentially survives to form memory cells, and the molecular mechanisms that regulate memory cell fate in NK cells remain poorly understood.

Using single cell RNA sequencing (scRNAseq), we identified a MP-like transcriptional state of NK_{eff} cells following MCMV-driven expansion *in vivo*. We provide further evidence that Ly6C$^-$ NK_{eff} cells preferentially survive the contraction phase to generate memory NK cells in a Bcl2-dependent manner. MP NK cells displayed distinct transcriptional and epigenetic signatures compared to Ly6C$^+$ NK_{eff} cells, with an overlapping epigenetic signature shared with MP CD8$^+$ T cells enriched in ETS1 and Fli1

binding motifs. Fli1 regulated MP NK cell formation by promoting Bim levels in early effector NK cells to decrease the fitness of expanding NK cells during viral infection. These results suggest that memory NK cells, similar to memory T cells, are generated by a subset of epigenetically distinct MP cells that preferentially survive during the contraction phase of the response to viral infection and identify Fli as a critical regulator of MP NK cell formation.

Innate lymphoid cells (ILCs) are rapid producers of both proinflammatory and regulatory cytokines in response to local injury, inflammation, pathogen infection, or commensal microbiota perturbation[40-42]. The ability of ILCs to quickly respond to tissue stress and inflammation underpins their critical role in regulating tissue homeostasis and repair during infection or injury[3, 43]. Recent evidence suggests that ILCs contain developmentally imprinted open chromatin landscapes of stimulation-responsive elements (regulomes) that underpin their rapid responsiveness to environmental stimuli[7, 44-46]. However, the factors that maintain the “poised” epigenetic state of these elements during development and homeostasis are not well understood.

Natural Killer (NK) cells are cytotoxic group 1 innate lymphocytes that protect against viral infection and cancer formation through production of cytotoxic molecules (i.e. granzyme B) and cytokines such as interferon (IFN)-γ[4, 11]. While previous work has identified distinct transcriptional and epigenetic states of mouse and human NK cells during development and viral infection[6,7, 30], the factors that control the epigenetic landscape of NK cells during these processes remain unclear. Here, we identify

ubiquitously transcribed tetratricopeptide repeat, X chromosome (UTX; also known as *Kdm6a*) as a critical regulator of the NK cell regulome. Analysis of mice with NK cell-specific deletion of UTX revealed increased peripheral immature NK numbers with a defect in effector responses to mouse cytomegalovirus (MCMV) infection. Assay for transposase-accessible chromatin using sequencing (ATAC-seq) along with bulk RNA sequencing (RNA-seq) identified UTX-mediated changes in chromatin accessibility at several gene loci involved in NK cell development, homeostasis, and effector function. Together, these results identify UTX as a critical epigenetic regulator of NK cells in mice.

Results

Time-resolved scRNA-seq analysis reveals a MP-like NK cell state following MCMV infection

To determine whether transcriptional heterogeneity exists within NK_{eff} cells following viral infection, we adoptively transferred splenic $Ly49H^+$ NK cells into recipient $Ly49H^{-/-}$ mice and infected with MCMV. On day (D)7 post-infection (PI), NK_{eff} cells were sorted and then profiled using 10x Genomics Chromium droplet scRNA-seq (**Extended Data Fig. 1a**). The resulting NK_{eff} single cell dataset included 2,430 cells that were clustered based on differential expression of marker genes and visualized using a uniform manifold approximation and projection (UMAP) plot (**Fig. 1a, Supplementary Table 1**). Clustering analysis revealed 2 distinct clusters of NK_{eff} cells defined by differential expression of transcription factors (*Zeb2*, *Id2*, *Irf8*, *Runx3*), regulators of cell survival (*Gpx8*, *Shisa5*, *Bcl2*), and cell surface proteins (*Cx3cr1*, *Cd7*, *Ly6e*) (**Fig. 1c, Extended Data Fig. 1b**). While previous studies have identified two subsets of naïve mouse NK cells utilizing scRNA-seq[20], these subsets did not account for the distinct clusters of NK_{eff} cells identified within our dataset, because all $Ly49H^+$ NK cells analyzed displayed a mature phenotype ($CD27^-CD11b^+$) on D7 PI (**Extended Data Fig. 1c**). Gene ontology enrichment analysis indicated that specific pathways were differentially regulated between the two NK_{eff} cell clusters. Notably, significant terms related to regulation of apoptosis were enriched in cluster 1 in comparison to cluster 0, with cluster 1 expressing more transcripts of the pro-survival gene *Bcl2* than cluster 0 (**Fig. 1b,c**). These results suggested that transcriptional heterogeneity existed within NK_{eff} cells following viral infection, and that a specific effector cell state may preferentially persist during the contraction phase. Following MCMV-induced clonal proliferation, $Ly49H^+$ NK cells undergo a contraction phase from D7 to D28

PI during which most NK_{eff} undergo Bim-mediated apoptosis[47]. In order to address whether certain NK_{eff} cell states could persist during the contraction phase, adoptively transferred Ly49H$^+$ NK cells were sorted on D14 PI and profiled using scRNA-seq. Combining this dataset with Ly49H$^+$ NK cells analyzed from D7 PI resolved 4,399 cells that formed six distinct clusters which were visualized by UMAP dimensional reduction (**Fig. 1d, Supplementary Table 2).** While the majority of cells comprising clusters 1,2 (*Cx3cr1*, *Gpx8*, *Cma1*) and 4 (*Plac8, Gzmk, Thy1*) were derived from D7 PI NK_{eff} cells, Cluster 0 (*Cx3cr1*, *Sell*, *Cma1*) and 5 (*CD69*, *Ifng*, *Nfkbia*) predominantly contained cells from D14 PI NK cells and resembled terminally-differentiated and activated NK cells respectively **(Fig. 1d, Extended Data Fig. 1d).** Notably, cluster 3 (*Shisa5, Bcl2a1b, Il2rb*) contained a mix of cells from both D7 and D14 PI that were enriched in genes associated with response to stress and programmed cell death, suggesting that a distinct NK_{eff} cell state may persist during the contraction phase (**Fig. 1d, Extended Data Fig. 1d,e)**.

To test this hypothesis *in silico*, we utilized RNA velocity analysis[48] to determine the time-resolved transcriptional fates of D7 PI NK_{eff} cells (**Extended Fig. 2a**). Projection of the velocity field arrows onto the UMAP plot extrapolated future states of NK_{eff} cells showing 4 distinct manually averaged trajectories (**Extended Fig. 2b)**. Both clusters 2 and 4 transitioned through cluster 1 to cluster 3 (*trajectory 1*), while a subset of cluster 3 cells did not show directionality to any other cell state (*trajectory 2*) suggesting that cluster 3 represented a distinct cell state of NK_{eff} (**Extended Fig. 2a,b**). RNA velocity analysis also suggested that cluster 0 represented an end stage of NK_{eff} differentiation as both cluster 2 (*trajectory 3*) and a subset of cells from cluster 3 (*trajectory 4*) showed strong directionality toward this cell state (**Extended Fig. 2a,b**). Monocle pseudotime analysis

further corroborated *in silico* trajectories 1 and 4, showing that cluster 1 likely represented a transition state between cluster 4 and 3 on D7 PI, and that cluster 3 cells differentiated to cluster 0 on D14 PI (**Extended Fig. 2c)**. Trajectory 1 was defined by increased expression of *Bcl2* and *Il2rb*, while trajectory 4 was defined by increased expression of genes associated with NK cell terminal maturation such as *Zeb2* and *Irf8*[20, 49](**Extended Fig. 2d**). Because cluster 3 represented a distinct NK_{eff} cell state that persisted during the contraction phase and could putatively differentiate to the majority of NK cells present on D14 PI, we then tested whether cluster 3 represented a MP-like NK cell state using MP and TE $CD8^+$ T cell RNA-seq datasets described previously (GSE111902). Indeed, cluster 3 showed the highest enrichment for the MP $CD8^+$ T cell gene expression module score, while cluster 0 scored the highest for the TE $CD8^+$ T cell gene module score (**Fig. 1e).** Thus, these data suggest that D7 PI NK_{eff} cells contain a mixture of MP-like and other NK_{eff} cell states following viral infection.

Memory $Ly6C^+$ NK cells are derived from $Ly6C^-$ MP NK cells

To determine whether a distinct MP NK cell subset could be identified *in vivo*, we analyzed cell surface expression of several genes predicted by our scRNA-seq dataset to be differentially expressed at D7 PI. While several cell surface proteins identified (CD44, Sca1, NKG2D, CD16) did not display bimodal expression in effector NK cells, there were clear positive and negative populations of Ly6C and CX_3CR1 NK_{eff} cells on D7 PI (**Fig. 2a**). To test whether either of these markers could identify a subset of NK_{eff} cells with enhanced persistence during the contraction phase, we sorted congenically distinct $Ly6C^-$ and $Ly6C^+$ or CX_3CR1^- and CX_3CR1^+ $Ly49H^+$ NK_{eff} cells at D7 PI and adoptively

transferred equal mixtures of each into naïve Ly49H$^{-/-}$ mice (**Fig. 2b**). While we did not observe a change in the frequencies of CX_3CR1^- and CX_3CR1^+ NK_{eff} cells 12 days post-transfer (**Extended Data Fig. 3a**), there was a significant increase in the frequency of recovered Ly6C$^-$ compared to Ly6C$^+$ NK cells on D12 following transfer. (**Fig. 2c)**. These results were not due to differences in trafficking or proliferation of adoptively transferred Ly6C$^-$ NK_{eff} cells, as the percentage of adoptively transferred Ly6C$^-$ and Ly6C$^+$ Ly49H$^+$ NK cells remained similar in peripheral organs at various timepoints PI, and we did not observe differences in the frequencies of Ki-67$^+$ Ly6C$^-$ or Ly6C$^+$ Ly49H$^+$ NK cells on D7, D10, or D14 PI (**Extended Data Fig. 3b-d**). We also did not observe differences in single cell metabolic heterogeneity using SCENITH[50], or differential induction of mitophagy through analysis of TMRE and MitoGreen staining between Ly6C$^+$ and Ly6C$^-$ NK_{eff} at various timepoints during the contraction phase[51] (**Extended Data Fig. 4a,b**). Furthermore, D14 PI Ly6C$^+$ and Ly6C$^-$ NK_{eff} cells both displayed enhanced production of IFN-γ upon platebound antibody stimulation, and adoptively transferred D7 PI Ly6C$^+$ and Ly6C$^-$ NK_{eff} cells both rescued Ly49H$^{-/-}$ mice from lethal MCMV challenge (**Extended Data Fig. 4c,d)**. The observed enhanced survival phenotype was found to be intrinsic to Ly6C$^-$ NK_{eff} cells, as co-adoptive transfer of congenically distinct Ly6C$^-$ and Ly6C$^+$ NK_{eff} cells led to a higher ratio of Ly6C$^-$ to Ly6C$^+$ NK cells 12 days post transfer into distinct Ly49H$^{-/-}$ hosts that previously received adoptively transferred naïve NK cells and were infected with MCMV (**Fig. 2d,e**). These results suggest that Ly6C$^-$ NK_{eff} cells persist to a greater extent than Ly6C$^+$ NK_{eff} cells during the contraction phase to preferentially form memory NK cells.

Previous studies have suggested >95% of MCMV-induced memory NK cells are Ly6C$^+$ on D28 PI[52, 53]. However, our adoptive transfer data suggested that Ly6C$^-$ NK$_{eff}$ give rise to the majority of memory NK cells present 12 days following transfer, suggesting that Ly6C$^+$ NK$_{eff}$ likely do not represent MP NK cells (**Fig. 2c,e**). Notably, RNA velocity analysis indicated that a subset of MP-like NK cells transitioned to a terminal cell state that represented the majority of memory NK cells on D14 PI (**Extended Data Fig. 2a-d**). These results suggested that the Ly6C$^-$ NK$_{eff}$ population was likely enriched in the MP-like NK cell state identified by our scRNA-seq analysis. In support of this hypothesis, the percentage and numbers of adoptively transferred Ly6C$^-$ Ly49H$^+$ NK cells declined over time in the blood **(Fig. 3a-c)** and peripheral organs by D28 PI **(Extended Data Fig. 4e)**. Further examination of adoptively transferred Ly6C$^+$ and Ly6C$^-$ NK$_{eff}$ cells demonstrated that while a majority of the surviving Ly6C$^+$ memory NK cells were derived from D7 PI Ly6C$^-$ NK$_{eff}$ cells 12 days post transfer, ~80% of D7 Ly6C$^-$ NK$_{eff}$ cells upregulated Ly6C while Ly6C$^+$ NK$_{eff}$ did not lose expression of Ly6C **(Fig. 3d,e).** These results suggest that D7 PI Ly6C$^-$ NK$_{eff}$ cells (referred to as MP NK cells hereafter) preferentially persist and differentiate into Ly6C$^+$ memory NK cells during the contraction phase of the response to MCMV.

Bcl2 is required for the survival of NK$_{eff}$ cells during the contraction phase

To determine the mechanisms of MP NK cell persistence following MCMV infection, we adoptively transferred CD45.1$^+$Ly49H$^+$ NK cells into Ly49H$^{-/-}$ mice, infected with MCMV, sorted Ly6C$^+$ and Ly6C$^-$ Ly49H$^+$ NK cells from the spleens of the Ly49H$^{-/-}$ mice on D7 PI and performed RNA sequencing (RNA-seq). RNA-seq analysis identified 43 differentially expressed genes (DEGs) between Ly6C$^+$ NK$_{eff}$ and MP NK cells, with MP NK cells

displaying increased expression of *Bcl2* and the transcription factor *Zbtb33* (**Fig. 4a,b and Supplementary Table 3**). Conversely, Ly6C$^+$ NK$_{eff}$ cells displayed increased expression of the cell cycle inhibitor *Cdkn1b* (**Fig. 4b**). Analysis of common DEGs between MP vs TE CD8$^+$ T cells and MP NK cells vs Ly6C$^+$ NK$_{eff}$ cells revealed higher expression levels of *Bcl2* between MP CD8$^+$ T cells and MP NK cells **(Extended Fig. 5a**). However, MP CD8$^+$ T cells did not share an overlapping core transcriptional signature with MP NK cells. Instead, MP CD8$^+$ T cells expressed high levels of *Tcf7*, *Id3*, *P2rx7*, and *Espn*, which have been associated with early memory T cell progenitor stemness programs previously[54] (**Extended Fig. 5b**). In confirmation of our RNA-seq dataset, MP NK cells expressed higher levels of the pro-survival molecule Bcl2[55], whereas pro-apoptotic Bim levels were similar when compared to Ly6C$^+$ NK$_{eff}$ (**Fig. 4c**). Notably, bulk D7 PI NK$_{eff}$ cells displayed lower levels of Bcl2 compared to naïve NK cells (**Fig. 4d,e**), and were highly dependent on Bcl2 activity for survival as evidenced by increased release of intracellular cytochrome c following Bcl2 inhibition *ex vivo* (**Fig. 4f**).To determine whether Bcl2 was required for the persistence of Ly49H$^+$ NK cells during the contraction phase, we generated high efficiency CRISPR ribonucleoprotein (cRNP)-mediated deletion of *Bcl2* in primary mature NK cells[56] (**Fig. 4g)**. *Bcl2* cRNP-edited naïve (CD45.2) Ly49H$^+$ NK cells were co-adoptively transferred with control *Rosa26*-edited (CD45.1) Ly49H$^+$ NK cells into Ly49H$^{-/-}$ mice and subsequently infected with MCMV. We observed a significant survival defect in *Bcl2*-deficient NK cells during the contraction phase (D7-D28 PI) (**Fig. 4h**). Together, these data suggest that higher levels of Bcl2 in MP NK cells may contribute to their enhanced persistence during the contraction phase of the response to MCMV infection.

MP NK cells display a distinct epigenetic signature enriched in Fli1 binding motifs

To determine the mechanisms of MP NK cell formation following MCMV infection, we adoptively transferred CD45.1^{+}Ly49H^{+} NK cells into Ly49H$^{-/-}$ mice, infected with MCMV, sorted Ly6C^{+} and Ly6C^{-} Ly49H^{+} NK cells from the spleen of the Ly49H$^{-/-}$ mice on D7 PI and performed ATAC sequencing (ATAC-seq). ATAC-seq analysis identified 811 significantly differentially accessible (DA) peaks between Ly6C^{+} NK$_{eff}$ and MP NK cells (**Fig. 5a, Supplementary Table 4**). Using gene ontology analysis, we found that MP NK cells displayed an increase in accessible peaks associated with genes implicated in MAPK signaling while Ly6C^{+} NK$_{eff}$ cells showed increased accessibility in genes associated with the endosome and golgi (**Fig. 5b**). Next, we generated a core MP lymphocyte epigenetic signature consisting of 114 peaks that were significantly DA in MP CD8^{+} T and MP NK cells compared to TE CD8^{+} T cells and Ly6C^{+} NK$_{eff}$ (**Fig. 5c, Supplementary Table 5**). Peaks with greater accessibility in MP lymphocytes were associated with genes enriched in positive regulation of lymphocyte activation and differentiation such as the transcription factor *Lef1*, the chemokine receptor *Cxcr3*, and *Bcl2* (**Fig. 5d and Extended Data Fig. 6a-c**). Together, these results suggest that MP NK cells display a common epigenetic signature shared with MP CD8^{+} T cells that is enriched in genes associated with T cell memory formation and effector function. To determine core transcriptional regulators of MP lymphocyte formation, we performed HOMER motif analysis of DA peaks shared between MP CD8^{+} T cells and MP NK cells. We found that MP DA peaks were enriched in ETS1 and Fli1 binding motifs compared to Ly6C^{+} NK$_{eff}$ and CD8^{+} TE cell DA peaks that were enriched in Tbet, Runx1 and Runx2

binding motifs (**Fig. 5e**). These data indicated that MP NK cells display a distinct epigenetic signature compared to Ly6C^{+} NK$_{eff}$, and share a core epigenetic signature with MP CD8^{+} T cells.

Our ATAC-seq analysis suggested that Fli1 may be a critical transcriptional regulator of MP NK cells. Therefore, we examined whether mature NK cells express Fli1 during MCMV infection. RNA-seq analysis demonstrated that *Fli1* was repressed early during viral infection, but subsequently increased during the expansion phase of the response on D4 PI (**Fig. 6a**). A recent study found that IL-2 and IL-15 levels remain elevated in MCMV-infected tissues until D4 PI[44], suggesting that these cytokines may induce Fli1 expression. Using the RNA-seq datasets from this study, we determined that splenic NK cells stimulated with IL-2 and IL-15 *ex vivo* induced *Fli1* transcripts while IL-12 and IL-18 stimulated NK cells decreased *Fli1* expression **(Fig 6b).** To determine whether IL-2 or IL-15 induce Fli1 levels in mature NK cells, we examined Fli1 protein levels by western blot in purified splenic NK cells after 48 h culture with increasing doses of IL-2 or IL-15. While we observed that Fli1 was induced by both IL-2 and IL-15 in a dose-dependent manner in splenic NK cells, IL-15 induced higher Fli1 protein levels than IL-2 at each concentration **(Fig 6c).** Further analysis of previously published ATAC-seq and STAT5 ChIP-seq data sets[44] revealed that IL-2 and IL-15 stimulation of splenic NK cells increased accessibility of peaks within the *Fli1* locus that overlapped with enriched Stat5 ChIP-seq peaks, suggesting that Stat5 may directly induce Fli1 expression in NK cells in response to IL-2 or IL-15 stimulation *ex vivo* **(Fig 6d).** To test this possibility, we stimulated splenic NK cells with IL-15 in the presence of a Stat5 inhibitor or vehicle control. Indeed, Stat5 inhibition resulted in a ~50% reduction of Fli1 protein **(Fig 6e),**

suggesting that Fli1 protein levels are induced in mature NK cells by STAT5 signaling via IL-15 and/or IL-2 *ex vivo*.

Fli1 regulates BIM levels in early effector NK cells to limit MP NK cell formation

To determine the significance of Fli1 in regulating MP NK cells, we ablated Fli1 in mature NK cells using CRISPR cRNPs (**Fig. 7a**). We then adoptively transferred control or *Fli1*-edited Ly49H$^+$ NK cells mixed at a 1:1 ratio into Ly49H- mice and infected with MCMV 16 hours later. After D3 PI, Fli1-deficient NK cells represented a greater frequency of adoptively transferred Ly49H$^+$ NK cells at all time points analyzed and persisted in greater numbers in the blood and peripheral organs on D28 PI **(Fig. 7b-d).** While the frequency of Fli1-deficient NK_{eff} cells increased compared to control edited cells on D7 PI, there was a greater impact of Fli-deficiency on the frequency of MP NK cells compared to Ly6C$^+$ NK_{eff}. These results suggested that Fli1 restricts the formation of MP NK cells in addition to limiting NK_{eff} formation **(Fig. 7e).** We hypothesized that the effects of Fli1 loss could be attributed to either increased proliferation or prolonged survival of adoptively transferred Ly49H$^+$ cells. Analysis of adoptively transferred Fli1-deficient Ly49H$^+$ NK cells on D3 PI did not reveal differences in CTV dilution**,** proliferation kinetics**,** or Ki-67 staining **(Fig. 7f-h),** suggesting that Fli1 does not control proliferation of Ly49H$^+$ NK cells following viral infection. Instead, examination of Bim and Bcl2 protein by flow cytometry revealed that Fli1-deficient NK cells expressed significantly decreased levels of pro-apoptotic Bim versus control edited NK cells, while displaying similar levels of Bcl2 on D3 PI **(Fig. 7i)**. This increased Bim/Bcl2 ratio in Fli1-deficient NK cells coupled with their increased

persistence *in vivo* suggested that Fli1 restricts the fitness of early effector NK cells through regulation of Bim levels during viral infection **(Extended Data Fig. 7a,b)**.

Discussion

We utilized single cell sequencing to identify a MP-like NK cell state following mouse cytomegalovirus (MCMV) infection. Ly6C$^-$ NK$_{eff}$ cells displayed enhanced survival during the contraction phase and were determined to be the main precursors of Ly6C$^+$ memory NK cells. MP NK cells displayed distinct transcriptional and epigenetic signatures compared to Ly6C$^+$ NK$_{eff}$ cells, with increased protein expression of Bcl2. While Bcl2 was required for the survival of Ly49H$^+$ NK cells during the contraction phase, Stat5 signaling likely induced Fli1 in early effector NK cells to increase Bim levels and restrict the formation of MP NK cells.

Time-resolved trajectory analysis of our scRNA-seq data suggested that a subset of D7 PI NK$_{eff}$ cells transition to a cell state enriched in the MP CD8$^+$ T cell transcriptional signature. Although bulk RNA-seq analysis demonstrated that MP CD8$^+$ T cells and MP NK cells did not display overlapping gene signatures, they both display higher expression of Bcl2 transcript and protein, which is required for effector T cells to preferentially survive during the contraction phase of the anti-viral response[57, 58]. These data suggest that *Mcl1* expression, which is required for NK cell survival during homeostasis[55, 59], is not sufficient to inhibit apoptosis in NK$_{eff}$ cells due to the decreased levels of Bcl2 observed on D7 PI. The discrepancy between our bulk RNA-seq and scRNA-seq data may be explained by the possibility that D7 PI Ly6C$^-$ NK$_{eff}$ cells contain a mixture of transitional NK$_{eff}$ and MP

NK cells rather than a homogenous MP cell state identified by scRNA-seq. Furthermore, because a small frequency of adoptively transferred Ly6C$^+$ NK$_{eff}$ persist during the contraction phase, it is possible that D7 PI Ly6C$^+$ NK$_{eff}$ contain a small fraction of transitional NK$_{eff}$ that survive to generate memory NK cells on D14 PI. Irrespective of these points, our adoptive transfer data suggest that the majority of memory NK cells present on D19 PI are derived from D7 PI Ly6C$^-$ NK$_{eff}$ cells, making this a functional MP population.

RNA velocity analysis suggested that MP-like NK cells undergo continuous differentiation to a terminally differentiated state on D14 PI, which could explain the constant decay of memory NK cell numbers observed in all studies to date following the expansion phase in response to MCMV infection[60]. Indeed, monocle trajectory analysis identified *Zeb2* expression increasing towards the terminally differentiated memory NK cell state on D14 PI, and Zeb2 has been implicated in the terminal maturation of naïve NK cells during homeostasis as well as the terminal differentiation of effector CD8$^+$ T cells following viral infection[49, 61, 62]. However, our results indicate that Zeb2 is required for the expansion of NK$_{eff}$ cells, but not the terminal differentiation of MP-like NK cells (data not shown). Similarly, Id2 has been shown to maintain the terminal differentiation of effector CD8$^+$ T cells through sustained repression of central memory-associated transcriptional programs in addition to regulating NK cell development and epigenetic regulation of effector functionality[63-66]. While we observed higher expression of Id2 in the D7 PI MP-like NK cell cluster from our scRNA-seq analysis, we did not observe an increase in MP NK cells following inducible deletion of Id2 during the contraction phase following MCMV infection (data not shown). Together, these findings suggest that there may be important

epigenetic differences between effector NK and $CD8^+$ T cells that dictate lineage specific terminal differentiation programs, although future studies will be necessary to support this hypothesis.

Our ATAC-seq dataset revealed that $Ly6C^+$ NK_{eff} and TE $CD8^+$ T cells share common enrichment in Runx1, Tbet, and Runx2 binding motifs, with $Ly6C^-$ NK_{eff} and MP $CD8^+$ T cells show enrichment for Fli1 and ETS1 binding motifs. While Tbet and Runx1 are important for NK cell survival during homeostasis and MCMV infection[67, 68], the precise roles of these transcription factors during NK_{eff} terminal differentiation will need to be studied in further detail. In mouse and human NK cells, ETS-1 has been shown the be required for mature NK cell development and regulation of gene involved in apoptosis, and can be induced by IL-2/IL-15 signaling in human NK cells[69-71]. Similarly, we found that Stat5 signaling induced expression of Fli1 in mature mouse NK cells in response to IL-2 and IL-15 *ex vivo*. Interestingly, CRISPR-mediated deletion of *Fli1* in mature naïve NK cells leads to decreased Bim levels and a greater persistence of early effector NK cells following MCMV infection, with a larger proportion of MP NK cells persisting through the contraction phase as a result. This finding suggests that Fli1 acts as a repressor of MP NK cell formation, likely to limit bystander immunopathology of expanded $Ly49H^+$ NK cells following clonal proliferation. Similarly, Fli1-deficient $CD8^+$ T cells accumulate more effector cells following LCMV infection[72], implicating Fli1 as a critical intrinsic checkpoint regulator of effector lymphocyte formation. While future studies will be needed to determine the epigenetic and/or transcriptional mechanisms by which Fli1 represses early effector lymphocyte fitness, these results identify an important regulator of effector lymphocyte formation. Thus, understanding the transcriptional and epigenetic pathways

that induce MP states in NK cells could inform strategies aimed at enhancing adaptive NK cell adoptive immunotherapies.

Acknowledgements

We thank members of the O'Sullivan and Sun labs for helpful discussion. T.E.O. was supported by the NIH (AI145997) and UC CRCC (CRN-20-637105).

The authors declare no financial conflicts of interest.

Author Contributions

L.R., and T.E.O. designed the study; L.R. J.H.L., and E.F. performed the experiments; F.M. and M.P. performed bioinformatics analysis; D.N. provided reagents; T.E.O., and L.R. wrote the manuscript.

Competing Interests Statement

The authors declare no competing interests.

Figure 1. Single cell RNA sequencing reveals two clusters of NK_{eff} cells following MCMV infection.

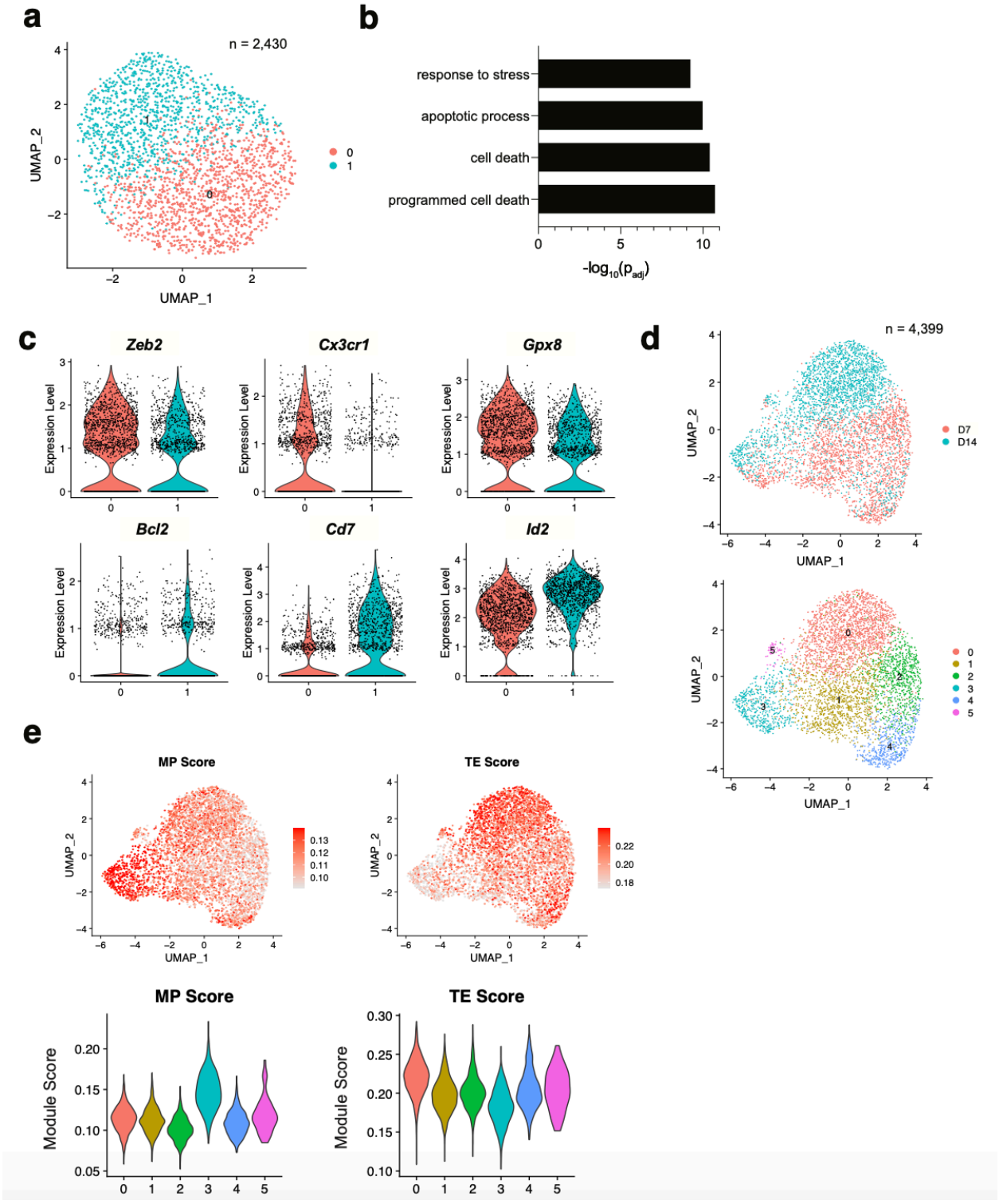

Ly49H^{+} NK cells were transferred into naïve Ly49H$^{-/-}$ mice and infected with MCMV i.p. 16 hours later. TCRβ^{-}CD3^{-}NK1.1^{+}Ly49H^{+}KLRG1^{+} NK cells were sorted on D7 and D14 PI. Cells were immediately processed using 10x Genomics Chromium droplet single cell RNA sequencing. **(a)** UMAP plot of 2,430 D7 PI NK_{eff} cells colored by cluster identities. Each dot represents an individual cell. **(b)** Gene Ontology (GO) enrichment analysis of upregulated genes in cluster 0 compared to cluster 1 from D7 PI NK_{eff} cells. Terms were considered statistically significantly enriched if $-\log_{10}(p_{adj})<0.05$. **(c)** Violin plots showing the relative expression of six differentially expressed genes in the two clusters of D7 PI NK_{eff} cells. Each dot represents a cell. **(d)** UMAP plot of 4,399 cells combined from D7 and D14 PI NK_{eff} cells, colored by timepoint analyzed (top) and cluster identity based on differential gene expression (bottom). Each dot represents an individual cell. **(e)** UMAP plot showing memory precursor (MP) and terminal effector (TE) CD8^{+} T cell gene module scores (top) and violin plots showing the distribution of MP and TE gene module scores for each cluster (bottom).

Figure 2. Ly6C$^-$ NK$_{eff}$ cells preferentially persist following MCMV infection.

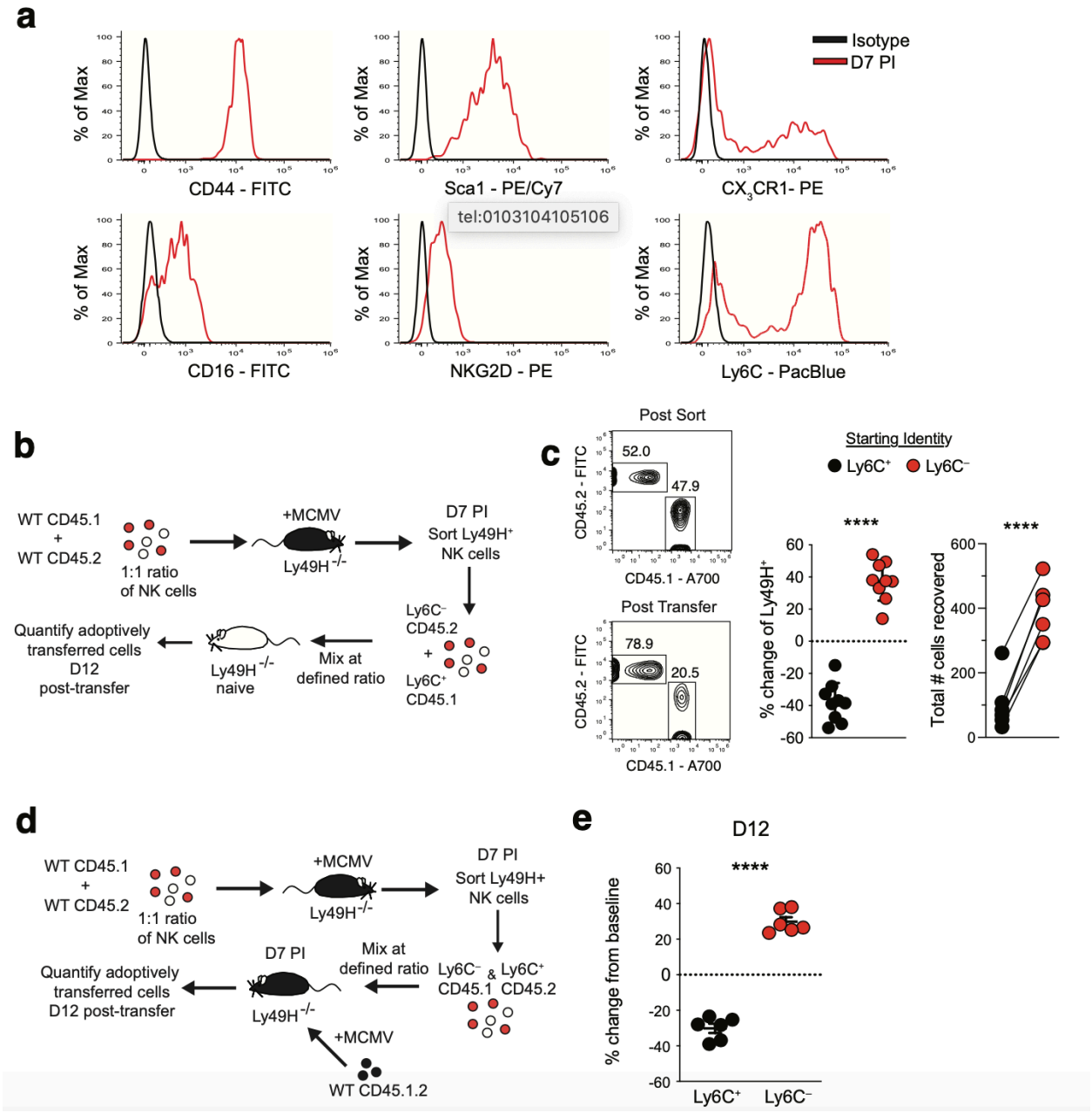

Splenic Ly49H$^+$ NK cells were transferred into Ly49H$^{-/-}$ mice i.v. and infected i.p with MCMV 16 hours after adoptive transfer. **(a)** Histograms of indicated cell surface marker expression from D7 PI Ly49H$^+$ NK$_{eff}$ cells (red) compared to isotype controls (black). **(b)** Experimental schematic. A mixture of purified WT splenic CD45.1 and CD45.2 Ly49H$^+$ NK cells were transferred into Ly49H$^{-/-}$ mice and infected i.p with MCMV 16 hours after

adoptive transfer. On D7 PI, TCRβ^{-}CD3^{-}NK1.1^{+}Ly49H^{+}KLRG1^{+}CD45.1^{+}Ly6C^{+} and TCRβ^{-}CD3^{-}NK1.1^{+}Ly49H^{+}KLRG1^{+}CD45.2^{+}Ly6C^{-} NK_{eff} were sorted and then transferred into naïve Ly49H$^{-/-}$ hosts at a 1:1 ratio. Recipient spleens were harvested 12 days post transfer and analyzed by flow cytometry. **(c)** Representative flow cytometry plots and statistical analysis of co-adoptively transferred Ly6C^{+} (CD45.1) and Ly6C^{-} (CD45.2) Ly49H^{+} NK cell subsets before transfer (post sort) and harvested from recipient Ly49H$^{-/-}$ mice on D12 (post transfer). Change from post sort frequency (middle) and numbers (right) of recovered cells 12 days post transfer. **(d)** Experimental schematic. Indicated CD45.1 and CD45.2 NK_{eff} cell subsets were transferred into Ly49H$^{-/-}$ hosts that were previously adoptively transferred with CD45.1 x CD45.2 naïve NK cells and infected with MCMV 7 days prior. **(e)** Quantification of the change in frequency of co-adoptively transferred Ly6C^{+} (CD45.1) and Ly6C^{-} (CD45.2) Ly49H^{+} NK cells subsets harvested from recipient mice on D12 (post transfer). Data are representative of 2-3 independent experiments with n = 3 mice per group. Samples were compared using two-tailed Student's t test with Welch's correction, assuming unequal SD, and data points are presented as individual mice with the mean ± SEM (***$p < 0.001$, ****$p < 0.0001$).

Figure 3. Ly6C$^-$ NK$_{eff}$ cells differentiate into Ly6C$^+$ memory NK cells.

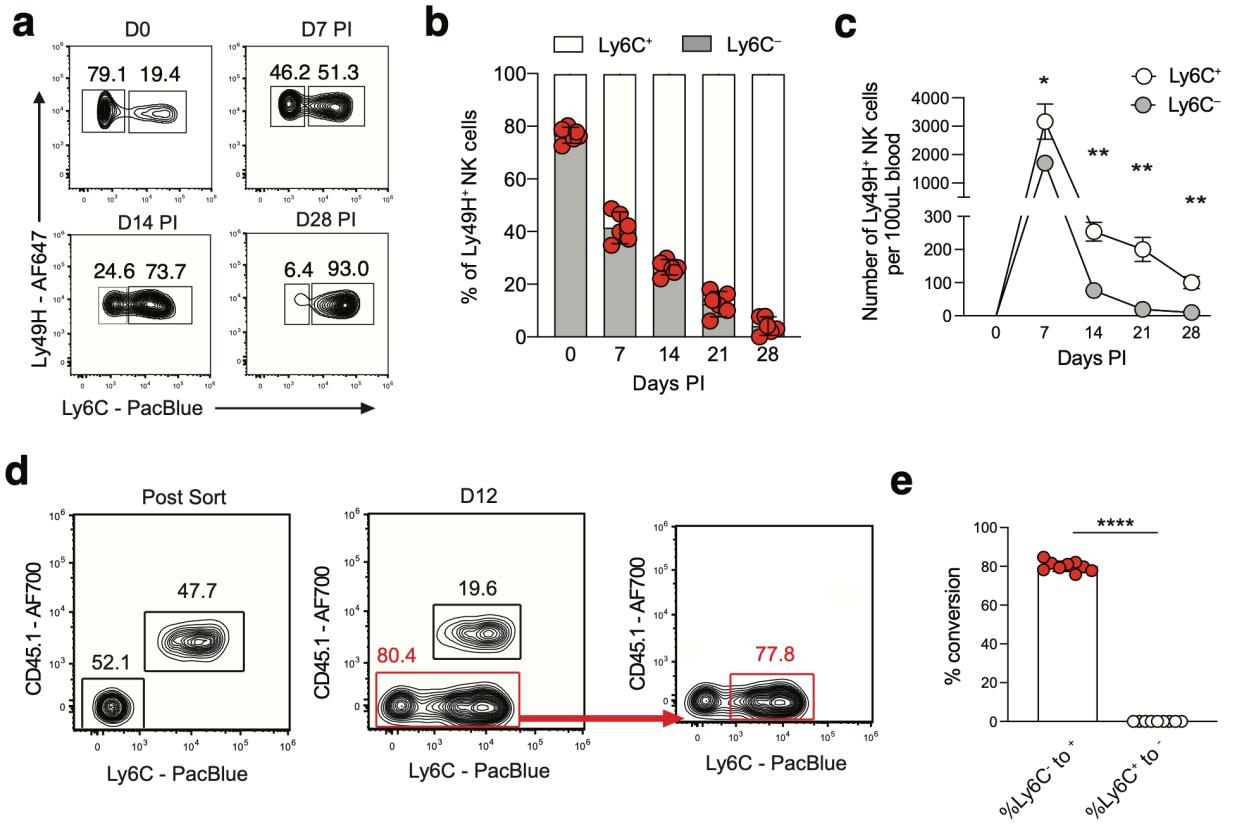

(a-c) Ly49H$^+$ NK cells were adoptively transferred into Ly49H$^{-/-}$ mice and infected with MCMV i.p. 16 hours later. **(a)** Representative flow plots and **(b)** frequency of adoptively transferred Ly49H$^+$ Ly6C$^-$ NK cells at indicated timepoints following MCMV infection. **(c)** Absolute numbers of Ly6C$^+$ and Ly6C$^-$ Ly49H$^+$ NK cells in the blood at indicated timepoints post MCMV infection. **(d)** Representative flow plots showing Ly6C expression in indicated adoptively transferred NK$_{eff}$ cell subsets from Fig. 2C on D12 post transfer. **(e)** Frequency of Ly6C$^-$ to Ly6C$^+$ conversion or vice versa at D12 post transfer. Data are representative of 2-3 independent experiments with **a-c,e**: n = 3 mice per group. Samples were compared using two-tailed Student's t test with Welch's correction, assuming unequal SD, and data points are presented as individual mice with the mean ± SEM (*p < 0.05, **p < 0.01, ****p < 0.0001).

Figure 4. MP NK cells are transcriptionally distinct and require Bcl2 for optimal survival during the contraction phase of the response to MCMV.

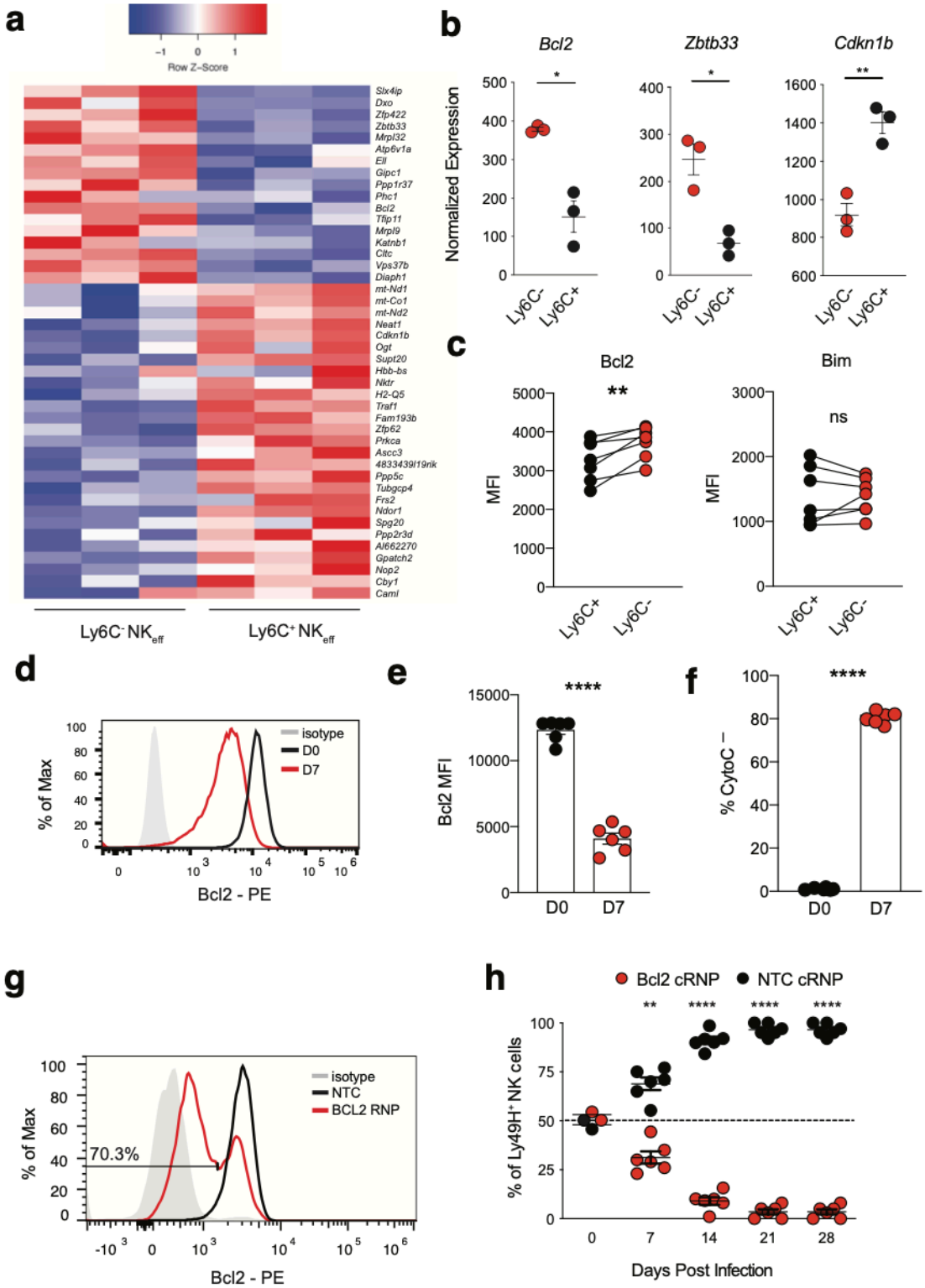

(a-b) Splenic Ly49H$^+$ NK cells were transferred into Ly49H$^{-/-}$ mice i.v. and infected i.p with MCMV 16 hours after adoptive transfer. Splenic TCRβ$^-$CD3$^-$NK1.1$^+$KLRG1$^+$Ly49H$^+$Ly6C$^+$ and TCRβ$^-$CD3$^-$NK1.1$^+$KLRG1$^+$Ly49H$^+$Ly6C$^-$ NK$_{eff}$ were sorted from recipient mice on D7 PI. Sorted NK cells were immediately processed for mRNA extraction, library preparation and sequencing. **(a)** Heatmap showing differentially expressed genes between Ly6C$^+$ and Ly6C$^-$ D7 PI NK$_{eff}$ cells ($p_{adj} < 0.05$). **(b)** Normalized read counts of selected genes shown in **(a)**. **(c)** MFI of Bcl2 and Bim in D7 PI Ly6C$^+$ and Ly6C$^-$ NK$_{eff}$ cells. **(d)** Representative histogram and **(e)** MFI of intracellular Bcl2 expression in naïve (D0) and D7 PI Ly49H$^+$ NK$_{eff}$ cells. **(f)** Quantification of the frequency of intracellular cytochrome c negative cells following Bcl2 inhibition with ABT-199 in naïve and D7 PI Ly49H$^+$ NK$_{eff}$ cells *ex vivo*. **(g,h)** IL-15 pre-activated congenically distinct NK cells were electroporated in the presence of either *Rosa26* NTC cRNP (CD45.1) or *Bcl2* cRNP (CD45.2) before being transferred i.v. into Ly49H-deficient recipients at a 1:1 ratio. **(g)** BCL2 protein expression shown by histogram of *Bcl2* cRNP or *Rosa26* NTC RNP CRISPR edited NK cells 3 days post gene edit *ex vivo*. **(h)** Recipient mice were infected i.p with MCMV 16 hours after adoptive transfer. Quantification of adoptively transferred Ly49H$^+$ NTC cRNP or *Bcl2* cRNP-edited NK cells in the blood of recipient mice at various timepoints PI. Data are representative of 2-3 independent experiments with n = 3-4 mice mice per group. Samples were compared using two-tailed Student's t test with Welch's correction, assuming unequal SD, and data points are presented as individual mice with the mean ± SEM (*$p < 0.05$, **$p < 0.01$, ****$p < 0.0001$).

Figure 5. MP NK cells share a core epigenetic signature with MP CD8⁺ T cells.

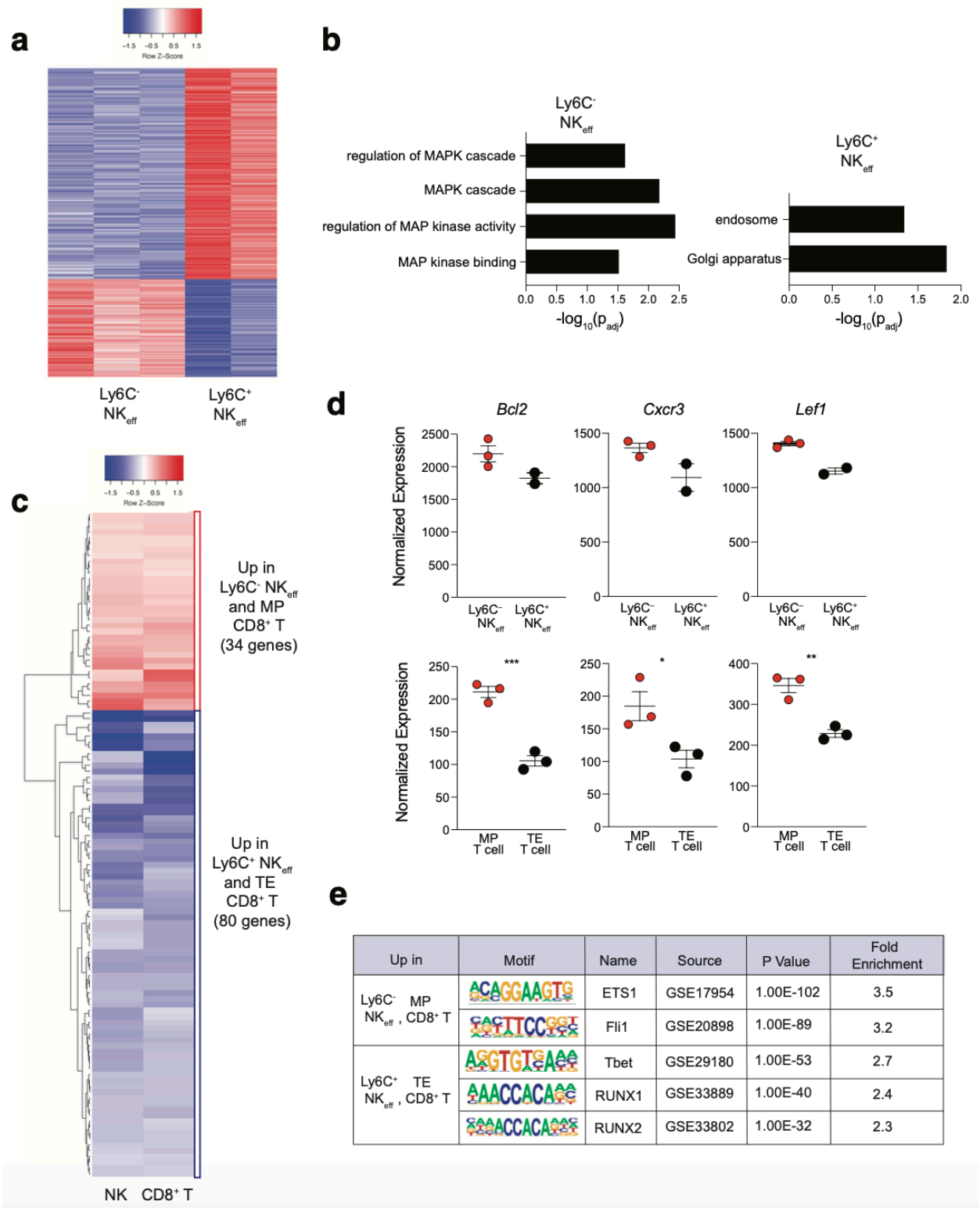

e

Up in	Motif	Name	Source	P Value	Fold Enrichment
Ly6C⁻ NKeff, MP CD8⁺ T		ETS1	GSE17954	1.00E-102	3.5
		Fli1	GSE20898	1.00E-89	3.2
Ly6C⁺ NKeff, TE CD8⁺ T		Tbet	GSE29180	1.00E-53	2.7
		RUNX1	GSE33889	1.00E-40	2.4
		RUNX2	GSE33802	1.00E-32	2.3

Splenic Ly49H$^+$ NK cells were adoptively transferred into Ly49H$^{-/-}$ mice i.v. and infected i.p with MCMV 16 hours after adoptive transfer. Splenic TCRβ$^-$CD3$^-$ NK1.1$^+$KLRG1$^+$Ly49H$^+$Ly6C$^+$ and TCRβ$^-$CD3$^-$NK1.1$^+$KLRG1$^+$Ly49H$^+$Ly6C$^-$ NK$_{eff}$ were sorted from recipient mice on D7 PI. Sorted NK cells were immediately processed for ATAC library preparation and sequencing. **(a)** Heatmap showing differentially accessible peaks between Ly6C$^+$ and Ly6C$^-$ NK$_{eff}$ cells. Peaks with $p_{adj} < 0.15$ were plotted. **(b)** GO enrichment analysis on genes related to differentially accessible peaks in Ly6C$^+$ and Ly6C$^-$ NK$_{eff}$ cells. Terms were considered statistically significantly enriched if $-\log_{10}(p_{adj})<0.05$. **(c)** Heatmap showing common differentially accessible peaks in the comparisons of Ly6C$^-$ to Ly6C$^+$ NK$_{eff}$ cells and MP to TE CD8$^+$ T cells ($p_{adj} <0.05$). **(d)** Normalized read counts of peaks related to selected genes which have differential accessibility between indicated NK$_{eff}$ cells (top) and T cells (bottom). **(e)** HOMER motif analysis displaying common transcription factor binding site motifs in differentially accessible peaks between D7 PI Ly6C$^-$ NK$_{eff}$ and MP CD8$^+$ T cells and D7 PI Ly6C$^+$ NK$_{eff}$ and TE CD8$^+$ T cells. Samples were compared using two-tailed Student's t test with Welch's correction, assuming unequal SD, and data points are presented as individual mice with the mean ± SEM (*p < 0.05, **p < 0.01, ***p <0.001).

Figure 6. Fli1 is induced by IL-15-mediated STAT5 signaling in mature NK cells.

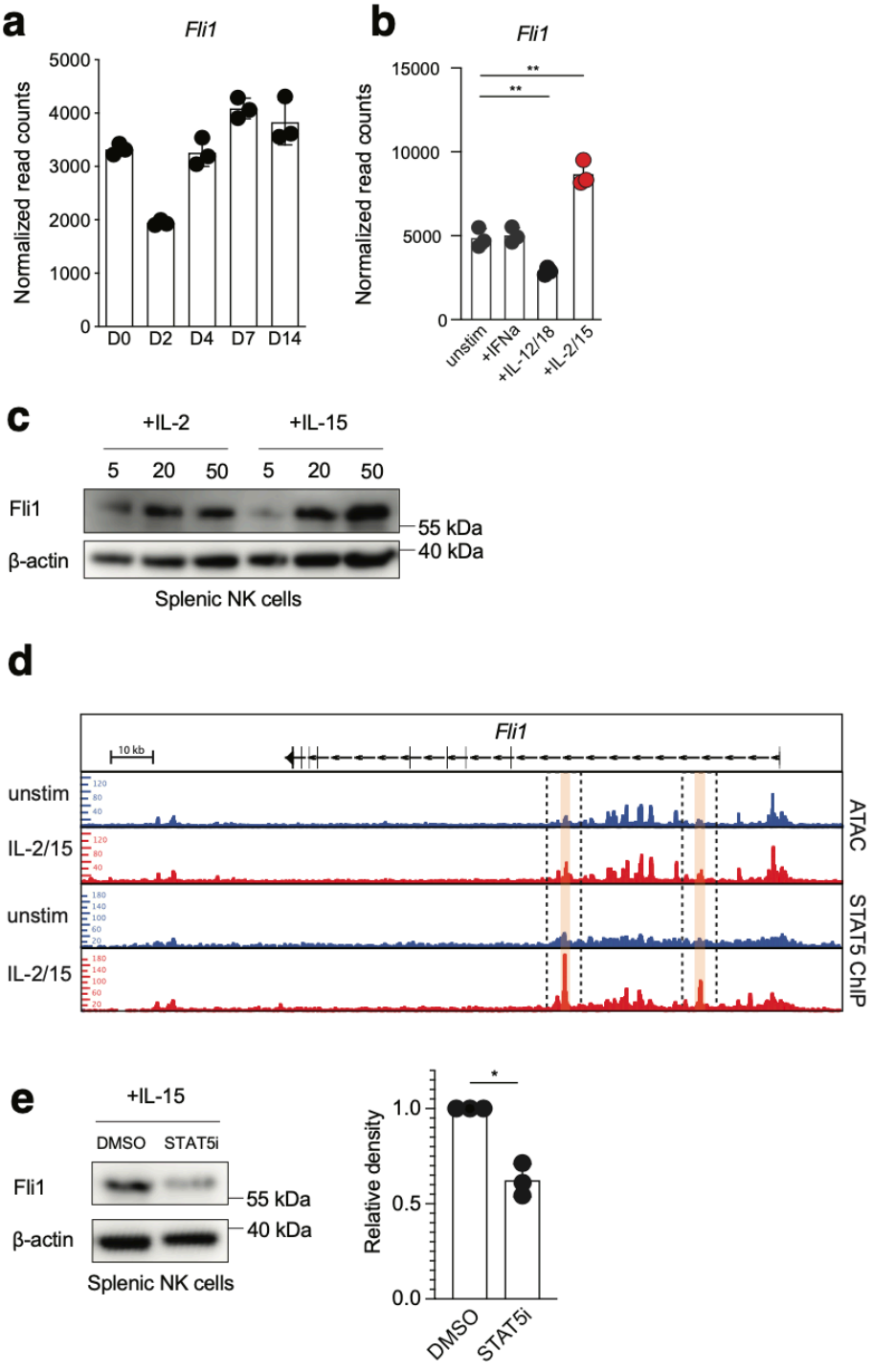

(a) Normalized read counts from bulk RNA-seq analysis of Ly49H^{+} NK cells at indicated time points PI. **(b)** Normalized read counts of *Fli1* in splenic NK cells 3 hours after

indicated cytokine stimulation *ex vivo*. **(c)** Western blot showing Fli1 and β-actin loading control protein levels in unstimulated, IL-2-stimulated, or IL-15-stimulated splenic NK cells. **(d)** Upper two rows, ATAC-seq peaks in the *Fli1* locus; Lower two rows, STAT5 ChIP-seq peaks in the *Fli1* locus in unstimulated or IL-2/IL-15-stimulated splenic NK cells. **(e)** Western blot showing Fli1 and β-actin loading control protein levels in IL-15-stimulated + DMSO, or IL-15 stimulated + STAT5 inhibitor (CAS 285986-31-4) treated splenic NK cells. Samples were compared using two-tailed Student's t test with Welch's correction, assuming unequal SD. **(a,b)** data points are presented as individual mice with the mean ± SEM (*$p < 0.05$, **$p < 0.01$). **(c,e)** Data represent 2-3 independent experiments with: n = 3 mice pooled per data point with the mean ± SEM (*$p < 0.05$, **$p < 0.01$).

Figure 7. Fli1 restricts the formation of MP NK cells during viral infection.

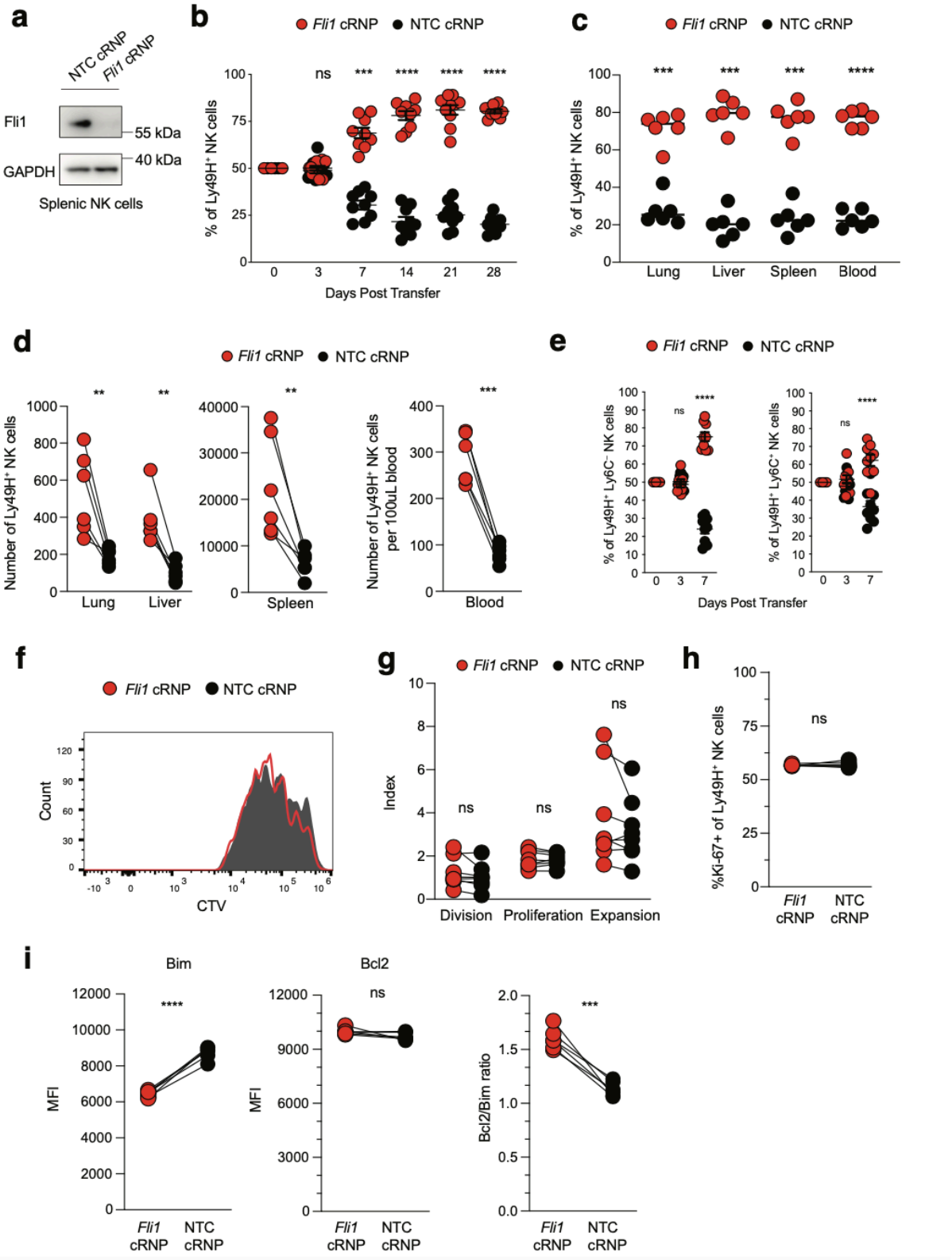

(a) Protein levels of Fli1 shown by western blot of *Fli1* cRNP or *Rosa26* NTC cRNP CRISPR edited NK cells 3 days after editing *ex vivo*. **(b-i)** IL-15 pre-activated congenically distinct NK cells were electroporated in the presence of either *Rosa26* NTC cRNP (CD45.1) or *Fli1* cRNP (CD45.2) before being transferred i.v. into Ly49H-deficient recipients at a 1:1 ratio. Recipient mice were infected i.p with MCMV 16 hours after adoptive transfer. **(b)** Quantification of adoptively transferred Ly49H$^+$ NTC cRNP or *Fli1* cRNP-edited NK cells in the blood of recipient mice at various timepoints PI. (**c)** The percentage and **(d)** number of Ly49H$^+$ NTC cRNP or *Fli1* cRNP-edited NK cells are quantified in the spleen, lung, liver, and blood of D28 recipient mice. **(e)** The percentage of Ly6C$^-$ or Ly6C$^+$ NK cells is shown in Ly49H$^+$ NTC cRNP or *Fli1* cRNP-edited NK cells at various timepoints PI. **(f,g)** *Fli1* cRNP or *Rosa26* NTC cRNP CRISPR edited NK cells were labeled with CTV dye before being transferred i.v. into Ly49H-deficient recipients and splenic NK cells were isolated on D3 PI. **(f)** Representative histograms displaying CTV dilution of *Fli1* cRNP and NTC cRNP Ly49H$^+$ NK cells. **(g)** Quantification of division, proliferation and expansion index calculated using FlowJo V10 software. **(h,i)** Splenic NK cells were isolated Day 3 PI. Dot plots displaying quantification of **(h)** %Ki-67$^+$ and **(i)** MFI of Bim, Bcl2 and Bcl2/Bim ratio in *Fli1* cRNP and NTC cRNP Ly49H$^+$ NK cells. **(a)** Data represent 2 independent experiments with: n = 3 mice per group. **(b-i)** Data represent 2-3 independent experiments with: n = 3-4 mice per group. Samples were compared using two-tailed Student's t test with Welch's correction, assuming unequal SD, and data are presented as individual mice with the mean ± SEM (*$p < 0.05$, **$p < 0.01$, ***$p < 0.001$, ****$p < 0.0001$)

Extended Data Figure 1. Phenotypic and single cell sequencing analysis of naïve, D7 PI and D14 PI Ly49H^{+} NK cells.

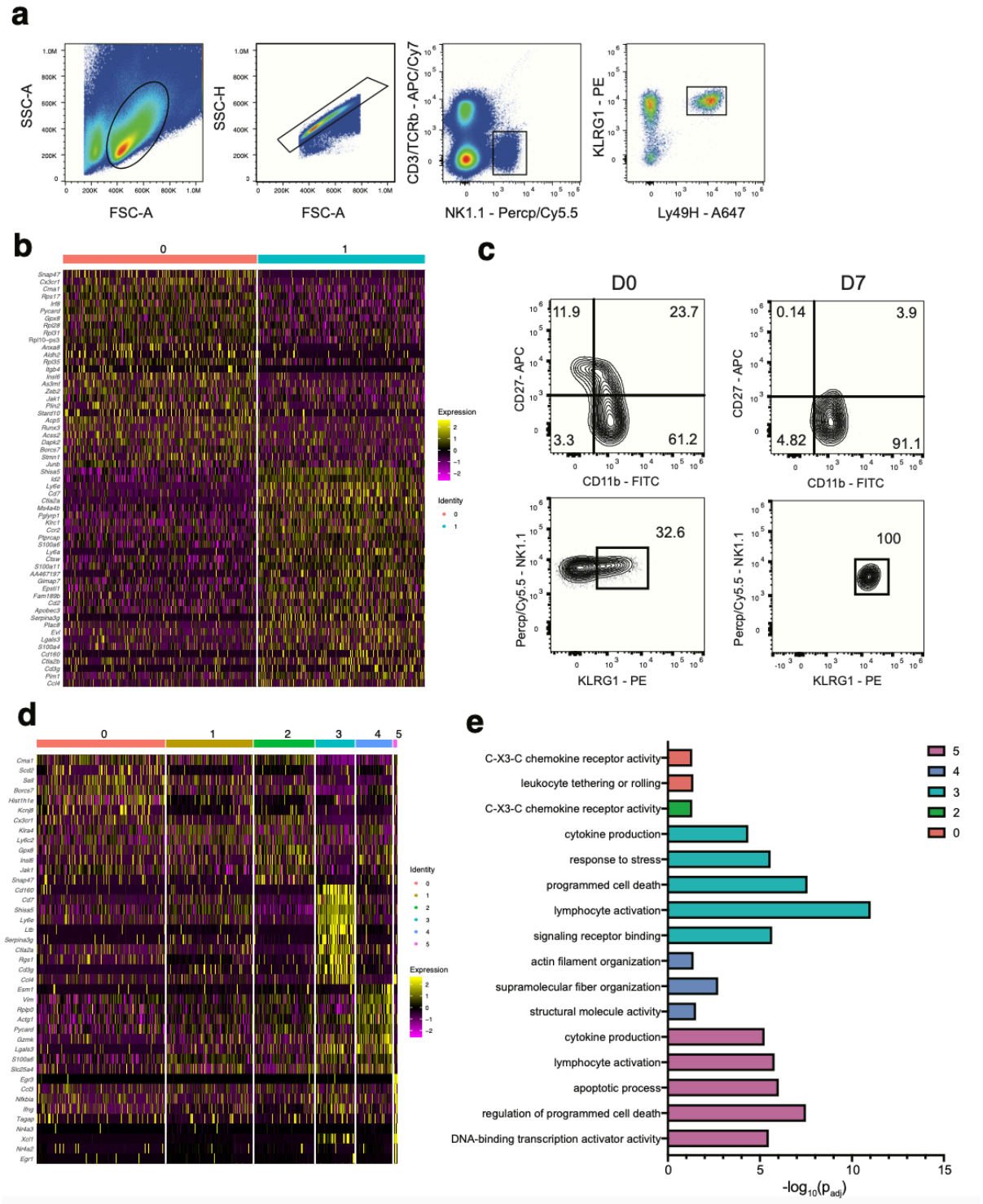

(**a**) Gating strategy to sort adoptively transferred TCRβ^{-}CD3^{-}NK1.1^{+}KLRG1^{+}Ly49H^{+} NK cells from the spleen of recipient Ly49H$^{-/-}$ mice on D7 and D14 following MCMV infection. (**b**) Representative flow plots of cell surface expression of CD27, CD11b, NK1.1 and KLRG1 on naïve (left) and D7 PI (right) TCRβ^{-}CD3^{-}NK1.1^{+}Ly49H^{+} NK$_{eff}$ cells. **(c-e)** Ly49H^{+} NK cells were adoptively transferred into Ly49H$^{-/-}$ mice and infected with MCMV i.p. 16 hours later. TCRβ^{-}CD3^{-}NK1.1^{+}Ly49H^{+}KLRG1^{+} NK cells were sorted on D7 and D14 PI. Cells were immediately processed for single cell sequencing using 10x Genomics Chromium droplet single cell RNA sequencing. (**c**) Heatmap showing the top differentially expressed genes between the two clusters of D7 PI NK cells ($p_{adj} < 0.05$). (**d**) Heatmap showing the top differentially expressed genes between the six clusters from NK cells at D7 and D14 PI ($p_{adj} < 0.05$). (**e**) GO enrichment analysis of marker genes for each cluster from (d). Terms were considered statistically significantly enriched if $-\log_{10}(p_{adj})<0.05$.

Extended Data Figure 2. Time-resolved putative differentiation pathways of NK_{eff} and MP NK cells during MCMV infection.

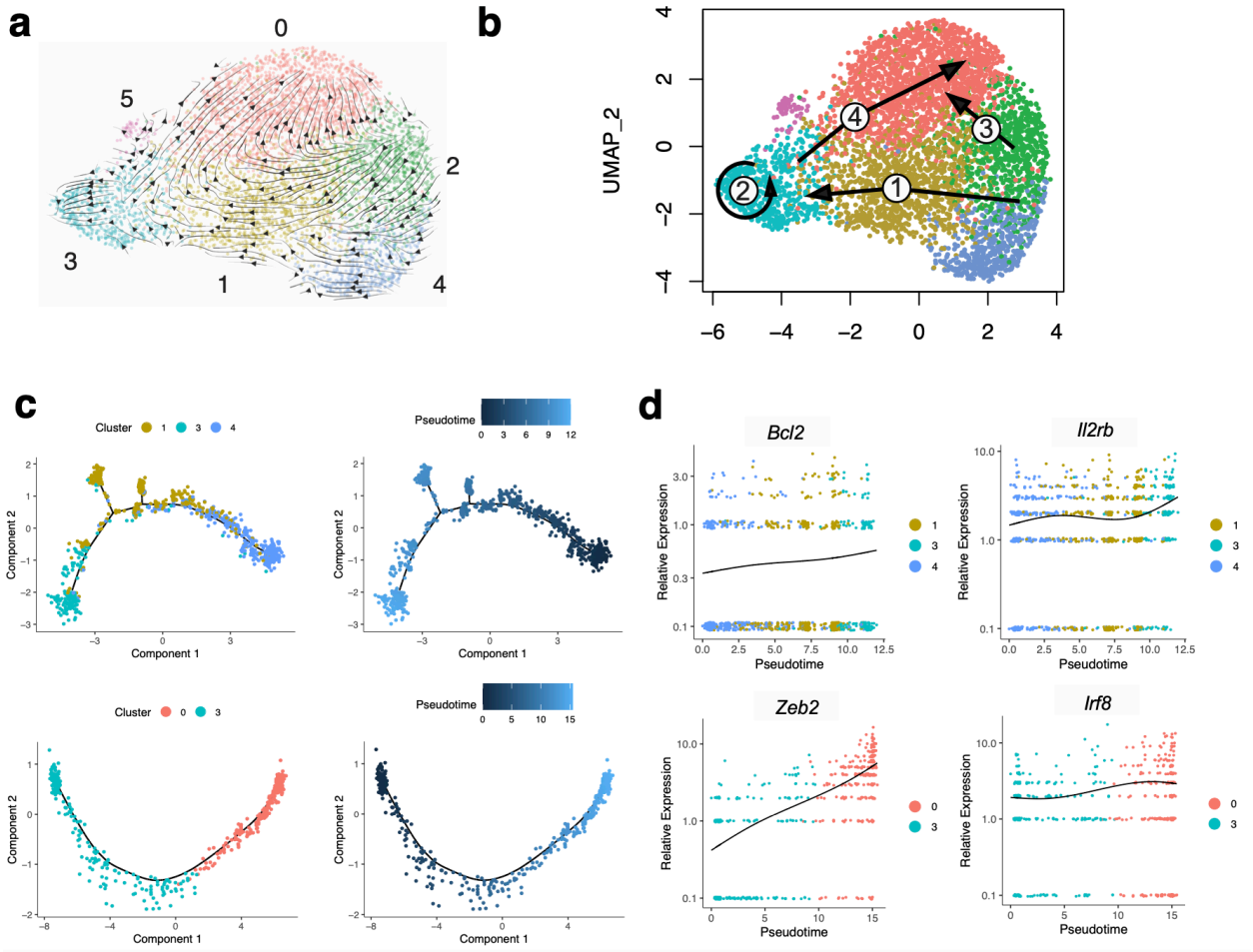

(a-d) Ly49H^{+} NK cells were adoptively transferred into Ly49H$^{-/-}$ mice and infected with MCMV i.p. 16 hours later. TCRβ^{-}CD3^{-}NK1.1^{+}Ly49H^{+}KLRG1^{+} NK cells were sorted on D7 and D14 PI. Cells were immediately processed for single cell sequencing using 10x Genomics Chromium droplet single cell RNA sequencing. (**a**) RNA-velocity analysis of D7 and D14 NK_{eff} cell clusters with velocity field arrows projected onto the UMAP plot. (**b**) Arrows show the local average velocity evaluated on a regular grid and indicate the extrapolated future states of cells. (**c**) Monocle pseudotime analysis of NK cell clusters,

indicating cluster identities (left) and pseudotime (right). **(d)** Scatter plot displaying relative expression (y-axis) of selected genes along pseudotime (x-axis).

Extended Data Figure 3. NK_{eff} subsets do not demonstrate differential trafficking or proliferation following MCMV infection.

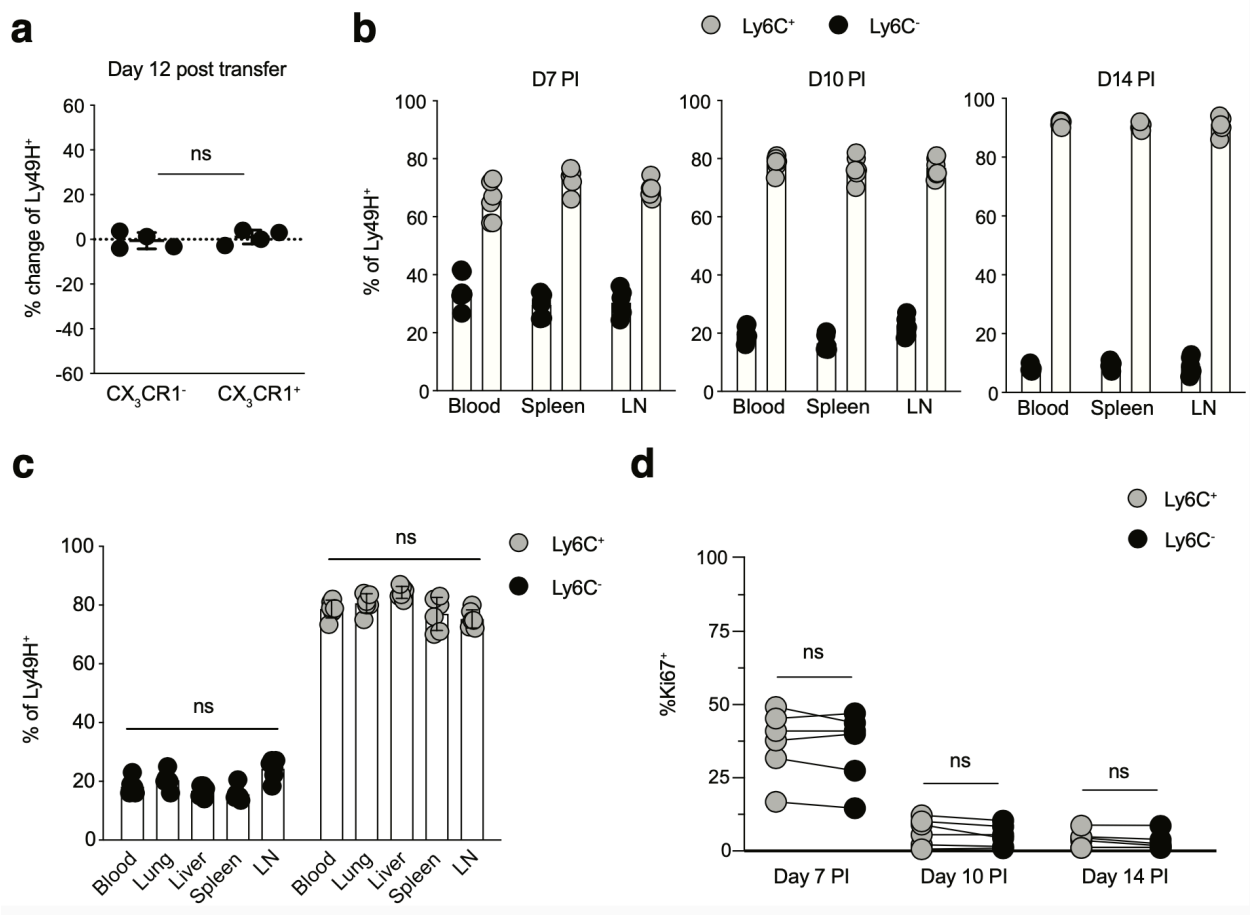

WT splenic CD45.1 and CD45.2 Ly49H$^+$ NK cells were transferred into Ly49H$^{-/-}$ mice, and infected with MCMV i.p. 16 hours later. 7 days after MCMV infection, TCRβ$^-$CD3$^-$ NK1.1$^+$Ly49H$^+$KLRG1$^+$CD45.1$^+$CX$_3$CR1$^+$ and TCRβ$^-$CD3$^-$ NK1.1$^+$Ly49H$^+$KLRG1$^+$CD45.2$^+$CX$_3$CR1$^-$ NK_{eff} were sorted and then transferred into naïve Ly49H$^{-/-}$ hosts at a 1:1 ratio. Recipient spleens were harvested 12 days post transfer and analyzed by flow cytometry. **(a)** Quantification of the change in frequency of CX$_3$CR1$^+$ (CD45.1) and CX$_3$CR1$^-$ (CD45.2) Ly49H$^+$ NK cells subsets from recipient mice on D12 (post transfer). (**b-d**) Splenic WT Ly49H$^+$ NK cells were transferred into Ly49H$^{-/-}$ mice and infected with MCMV i.p. 16 hours later. (**b**) Quantification of Ly6C$^+$ and Ly6C$^-$ Ly49H$^+$

NK cells from the indicated peripheral organs at various timepoints PI and (**c**) D10 PI. (**d**) Quantification of Ki-67$^+$ Ly49H$^+$ splenic NK cells at D10 PI. (**a**) Data represent 2 independent experiments with n = 4 mice per group. (**b-d**) Data represent 2 independent experiments with n = 6 mice per group. Samples were compared using two-tailed Student's t test with Welch's correction, assuming unequal SD, and data points are presented as individual mice with the mean ± SEM (ns = not significant).

Extended Data Figure 4. Ly6C^{+} and Ly6C^{-} NK$_{eff}$ cells do not display differences in mitophagy, cell-intrinsic metabolism and memory functionality.

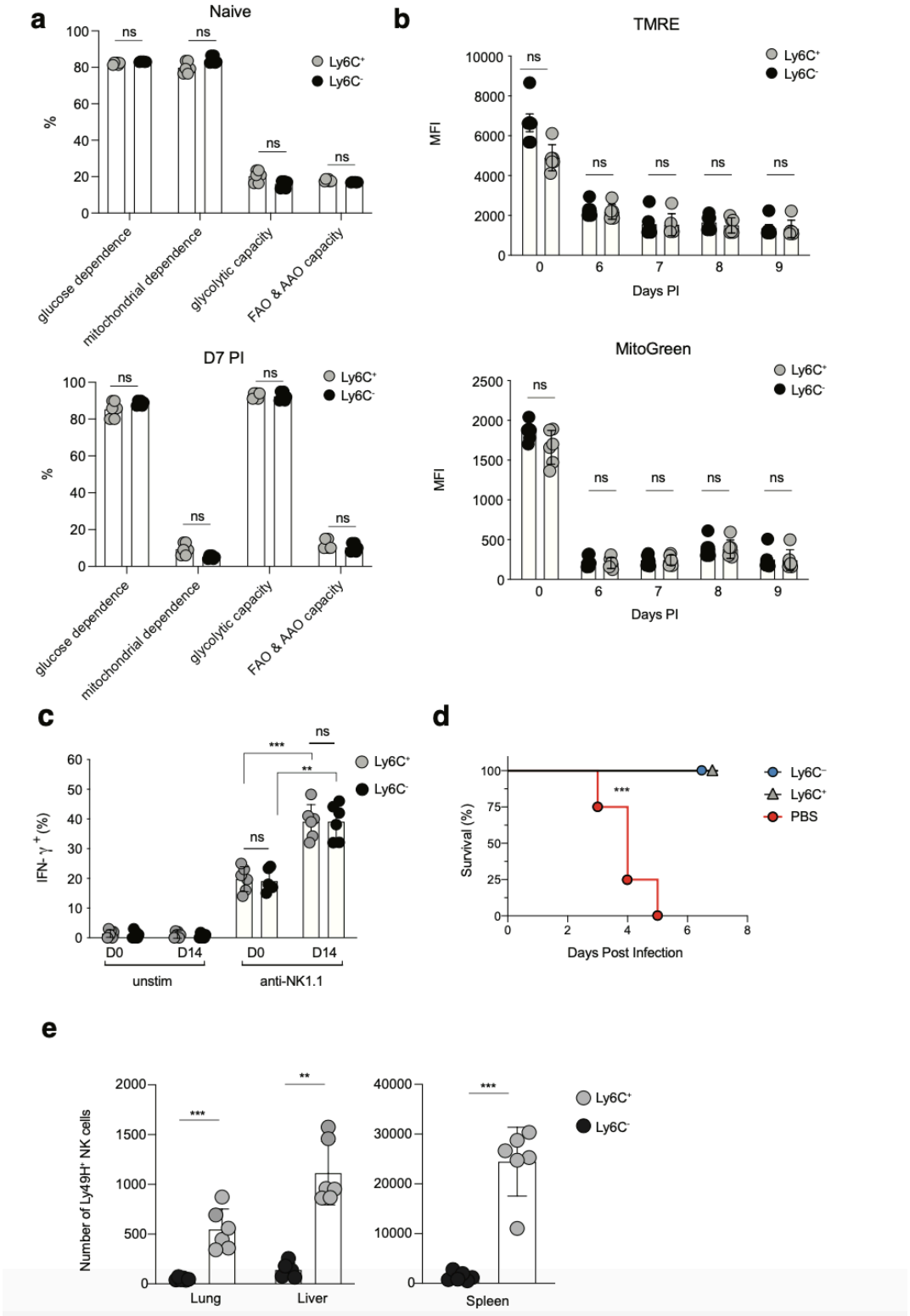

(**a-e**) Splenic Ly49H^{+} NK cells were transferred into Ly49H$^{-/-}$ mice i.v. and infected i.p with MCMV 16 hours after adoptive transfer. (**a**) Single cell metabolic analysis of naïve (top) or D7 PI (bottom) NK_{eff} using SCENITH. (**b**) MFI for tetramethylrhodamine ethyl ester (TMRE) staining (top) or MitoTracker Green staining (bottom) in adoptively transferred Ly49H^{+} NK cells from recipient spleens at the indicated time points PI. (**c**) Percentage of IFN-γ^{+} naïve or adoptively transferred D14 PI Ly6C^{+} or Ly6C$^{–}$ Ly49H^{+} NK cells following no stimulation or 4hr stimulation *ex vivo* with anti-NK1.1 monoclonal platebound antibody. (**d**) 2.5 x 10^3 D7 PI sorted TCRβ^{-}CD3$^{–}$NK1.1^{+}KLRG1^{+}CD45.1^{+}Ly49H^{+}Ly6C^{+} or TCRβ^{-}CD3$^{–}$NK1.1^{+}KLRG1^{+}CD45.1^{+}Ly49H^{+}Ly6C^{-} NK cells were adoptively transferred i.v. into naïve Ly49H$^{-/-}$ mice and infected with MCMV 7 days later. (**d**) Kaplan-Meier survival curves of Ly49H$^{-/-}$ mice that received PBS or indicated sorted NK cell populations i.v. (**e**) The number of Ly6C^{+} and Ly6C$^{–}$ Ly49H^{+} NK cells was quantified in various organs at D28 PI. (**a-c,e**) Data represent 2-3 independent experiments with n = 3 mice per group. Samples were compared using two-tailed Student's t test with Welch's correction, assuming unequal SD, and data are presented as individual points with the mean ± SEM. (**d**) Data are pooled from 2 independent experiments with n = 4–5 mice per group per experiment. Data points are presented as individual mice. Conditions were compared using the Log-rank (Mantel-Cox) test with correction for testing multiple hypotheses. (**p < 0.01, ***p < 0.001).

Extended Data Figure 5. MP NK cells are transcriptionally distinct from MP CD8 T cells.

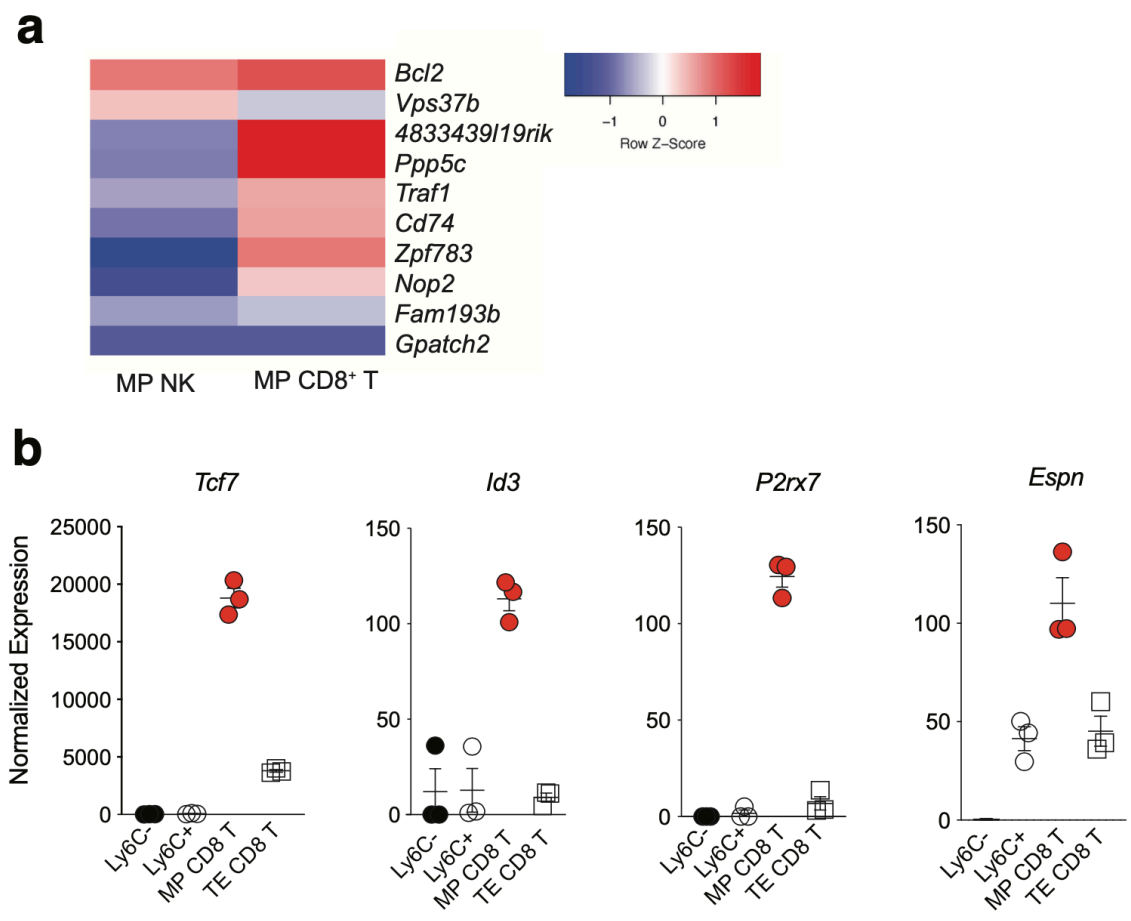

Splenic Ly49H$^+$ NK cells were transferred into Ly49H$^{-/-}$ mice i.v. and infected i.p with MCMV 16 hours after adoptive transfer. Splenic TCRβ$^-$CD3$^-$NK1.1$^+$KLRG1$^+$Ly49H$^+$Ly6C$^+$ and TCRβ$^-$CD3$^-$NK1.1$^+$KLRG1$^+$Ly49H$^+$Ly6C$^-$ NK$_{eff}$ were sorted from recipient mice on D7 PI. Sorted NK cells were immediately processed for mRNA extraction, library preparation and sequencing. (**a**) Differentially expressed genes common between MP Ly6C$^-$ NK and Ly6C$^+$ NK$_{eff}$ cells compared to MP and TE CD8$^+$ T cells ($p_{adj} < 0.05$). (**b**) Normalized read counts of selected genes in indicated cell types.

Extended Data Figure 6. MP NK cells and MP CD8$^+$ T cells display similar chromatin accessibility at specific gene loci.

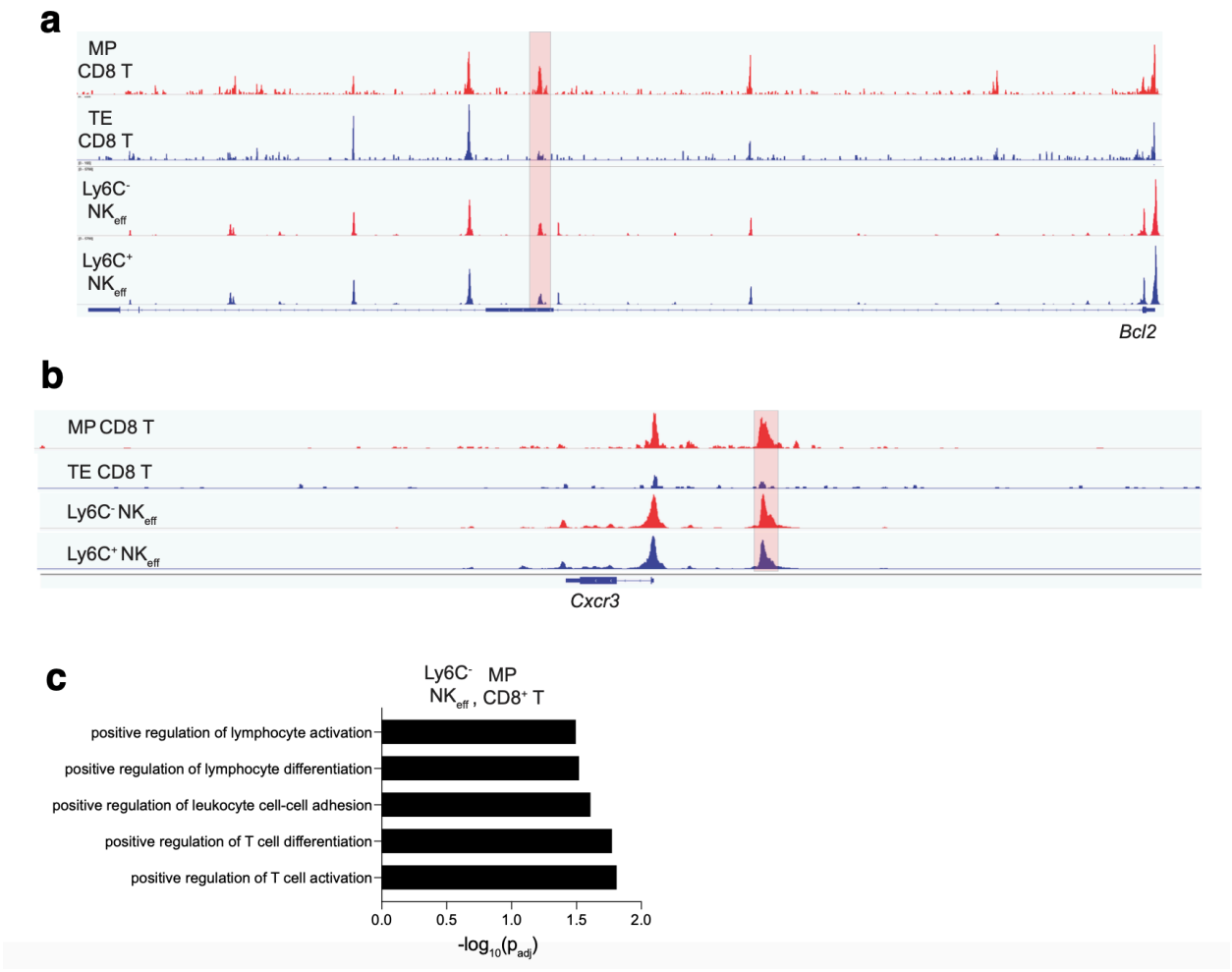

ATAC sequencing reads from Fig. 5 in the indicated cell subsets mapping to the **(a)** *Bcl2* locus and **(b)** *Cxcr3* locus. Highlighted peaks represent differentially accessible peaks (p_{adj} <0.15). **(c)** GO term analysis from differentially accessible peaks shared between MP NK cells and MP CD8$^+$ T cells. Terms were considered statistically significantly enriched if -log$_{10}$(p_{adj})<0.05. Data are representative of three independent replicates for MP and TE CD8$^+$ T cells, D7 PI Ly6C$^-$ NK$_{eff}$ and two independent replicates for D7 PI Ly6C$^+$ NK$_{eff}$.

Extended Data Figure 7. Proposed model of MP NK cell formation and mechanism of Fli1 induction.

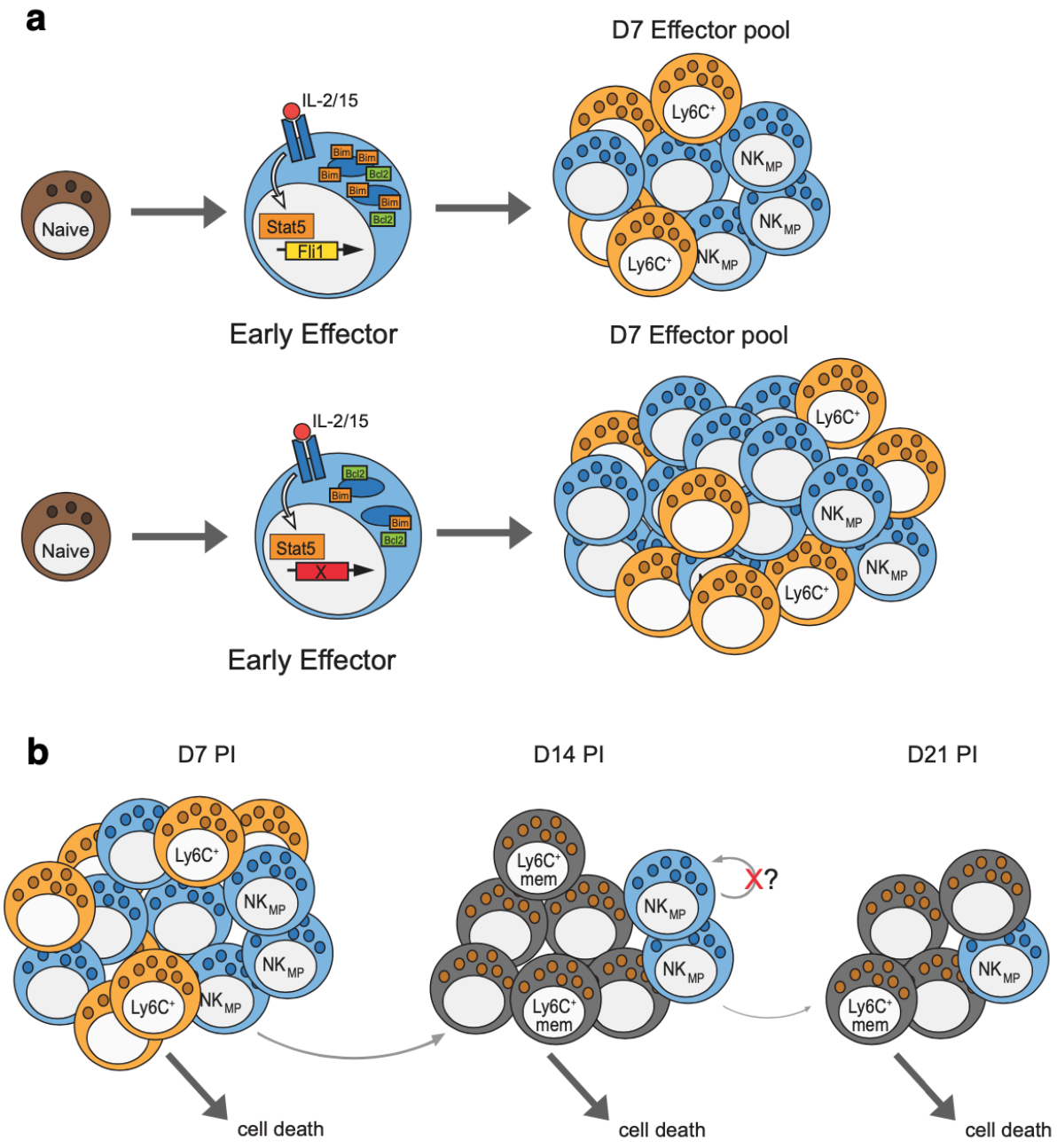

(a) IL-15 stimulated NK cells signal through STAT5 to induce Fli1 expression. During infection, Fli1 increases Bim levels to limit the number of early effector NK cells contributing to the D7 effector pool. In the absence of Fli1, Bim levels are reduced while

BCL2 is unaffected, allowing more early effector NK cells to persist and form MP NK cells. **(b)** In the contraction phase post D7, MP NK cells continually give rise to Ly6C$^+$ memory NK cells. The majority of D7 PI Ly6C$^+$ NK cells undergo cell death, while a small number can become Ly6C$^+$ memory cells. Lacking an stem-like transcriptional program, the pool of MP cells is depleted over time.

Contact for Reagent and Resource Sharing

Further information and requests for resources and reagents should be directed and will be fulfilled by the Lead Contact, Timothy O'Sullivan (tosullivan@mednet.ucla.edu)

Methods

Mice

Mice were bred at UCLA in accordance with the guidelines of the Institutional Animal Care and Use Committee (IACUC). The following mouse strains were used this study: C57BL/6 (CD45.2) (Jackson Labs, #000664), B6.SJL (CD45.1) (Jackson Labs, #002114), *Klra8*$^{-/-}$ (Ly49H-deficient). Experiments were conducted using 6-8 week old age- and gender-matched mice in accordance with approved institutional protocols.

MCMV infection

MCMV (Smith) was serially passaged through BALB/c hosts three times, and then salivary gland viral stocks were prepared with a dounce homogenizer for dissociating the salivary glands of infected mice 3 weeks after infection. Experimental mice in studies were infected with MCMV by i.p. injection of 7.5 x 10^3 plaque-forming units (PFU) in 0.5 mL of PBS. In other experiments, Ly49H$^{-/-}$ mice were intravenously injected with 25,000 sort purified D7 PI Ly49H$^+$ NK cells or PBS as control. 7 days later, recipient mice were infected with MCMV by i.p. injection of 7.5 x 10^3 plaque-forming units (PFU) in 0.5 mL of PBS. Mice were monitored and weighed daily and sacrificed when body weight decreased 10% from initial weight.

Isolation and enrichment of mouse NK cells

Mouse spleens, livers, lungs, lymph nodes, and blood were harvested and prepared into single cell suspensions as described previously[11]. Splenic single cell suspensions were lysed in red blood cell lysis buffer and resuspended in EasySep™ buffer (Stemcell). To avoid depleting Ly6C$^+$ NK cells we developed a custom antibody cocktail as

follows: splenocytes were labeled with 10 µg per spleen of biotin conjugated antibodies against CD3 (17A2), CD19 (6D5), CD8 (53-6.7), CD88 (20/70), Ly6G (1A8), SiglecF (S17007L), TCRβ (H57-597), CD20 (SA275A11), CD172a (P84) and magnetically depleted from total splenocyte suspensions with the use of anti-biotin coupled magnetic beads (Biolegend).

Cell sorting and Adoptive Transfer Experiments

Isolated splenic NK cells were sorted using Aria-H Cytometer. NK cells were sorted to > 95% purity. Approximately 2 × 10^5 enriched NK cells were injected intravenously into mice. In adoptive co-transfer experiments, equal numbers of Ly49H$^+$ NK cells from each population (CD45.1$^+$ and CD45.2$^+$) were injected into recipients 16 hours prior to MCMV infection. In other experiments, TCRβ$^-$CD3$^-$NK1.1$^+$Ly49H$^+$KLRG1$^+$CD45.1$^+$CX$_3$CR1$^+$ and TCRβ$^-$CD3$^-$NK1.1$^+$Ly49H$^+$KLRG1$^+$CD45.2$^+$CX$_3$CR1$^-$ or TCRβ$^-$CD3$^-$NK1.1$^+$Ly49H$^+$KLRG1$^+$Ly6C$^+$ and TCRβ$^-$CD3$^-$NK1.1$^+$Ly49H$^+$KLRG1$^+$Ly6C$^-$ D7 PI NK$_{eff}$ were sorted and then transferred at a 1:1 ratio into naïve or D7 PI Ly49H$^{-/-}$ hosts that had received CD45.1 x CD45.2 Ly49H$^+$ NK cells 7 days prior to MCMV infection. Adoptively transferred cells were recovered by harvesting recipient mouse splenic NK cells, preforming magnetic enrichment, and analysis by flow cytometry at various time points post-transfer.

Guide RNA Design

Synthetic gRNAs were purchased from SYNTHEGO. gRNA sequences were derived from a mouse whole genome CRISPR library described previously[73]. 10 gRNA sequences from this dataset were ranked according to predicted indel percentage and

low off-target score using the inDelphi machine-learning algorithm for each gene target[74]. The top 3-7 guides were validated for high indel percentages by Sanger sequencing and protein knockdown by western blot before utilization in experiments.

Electroporation and cRNP complex formation

gRNAs (Synthego) were diluted to 100 µM (100 pMol/µL) in 1x TE buffer (Sythego). 1.2 uL (120 pMol) of gRNA, 0.9 uL of 100 µM Alt-R® Cas9 Electroporation Enhancer (IDT) and 3.9 uL water were added to a 1.5 mL tube per sample for a total of 6 µL. 1 µL of recombinant Cas9 (20 pMol) (Synthego) was added to 5 µL water in a separate 1.5 mL tube. 6 µL of diluted Cas9 was added to 6 µL of gRNA-enhancer mixture for a total of 12 µL cRNP complex at a 1:3 molar ratio. The cRNP complex was allowed to incubate for at least 10 minutes at room temperature (RT) and electroporated using the Neon Transfection system (Thermo-Fisher) as described previously[56, 75]. Cells were then incubated at 37˚C for either 10 minutes before adoptive transfer or 90 minutes before centrifugation and resuspension in complete media supplemented with 50 ng rmIL-15 for culturing *in vitro*. Cells were cultured *in vitro* for 3 days following electroporation prior to reading out gene editing efficiency by flow cytometry or sanger sequencing.

Ex vivo stimulation of lymphocytes

For plate-bound antibody stimulation experiments, ~5 x 10^5 isolated NK cells were stimulated with 4 mg/mL precoated antibody against NK1.1 (PK136) for 4 hours in complete media containing Brefeldin A (1:1000; BioLegend) and Monensin (2uM; BioLegend). Cells were cultured in media alone as a negative control. In cytokine stimulation experiments, isolated NK cells were incubated with various concentrations of

mouse IL-15 or IL-2, in the presence or absence of 100 uM CAS 285986-31-4 STAT5 inhibitor (Millipore Sigma).

Adoptive transfer cRNP experiments

Adoptive NK cell co-transfer studies were performed by injecting a total of 1 x 10^6 NK cells; *Rosa26* cRNP-edited WT, and gene x cRNP-edited WT NK cells purified from spleens of congenically distinct WT mice (CD45.1, CD45.1.2 or CD45.2) into Ly49H$^{-/-}$ mice 16 hours prior to MCMV infection.

Proliferation assays

CellTrace™ Violet (CTV) stock solution was prepared per the manufacturers' instructions (Thermo) and diluted at 1:1000 in 37C PBS. Isolated NK cells were incubated in 0.5mL of diluted CTVsolution for 10 minutes at 37C. The solution was quenched with 10X the volume of CR-10 media. Cells were then washed and injected i.v. Division, proliferation and expansion indexes were quantified using FlowJo V10 software using the following calculations. Division Index: Total Number of Divisions / The number of cells at start of culture. Proliferation Index: Total Number of Divisions / Cells that went into division. Division Index: Total Number of Divisions / The number of cells at start of culture.

Flow Cytometry

Cells were analyzed for cell-surface markers using fluorophore-conjugated antibodies (BioLegend, eBioscience). Cell surface staining was performed in 1X PBS and intracellular staining was performed by fixing and permeabilizing using the eBioscience Foxp3/Transcription Factor kit for intranuclear proteins or BD Cytofix/Cytoperm kits for

cytokines. Flow cytometry was performed using the Attune NxT Acoustic Focusing cytometer and data were analyzed with FlowJo software (BD). Cell surface and intracellular staining was performed using the following fluorophore-conjugated antibodies: CD45.1 (A20), CD45.2 (104), NK1.1 (PK136), KLRG1 (2F1), TCRβ (H57-597), CD3 (17A2), Ly49H (3D10), IFN-γ (XMG1.2), Ly6C (HK1.4), CD44 (IM7), CD16 (93), Sca-1 (E13-161.7), CX3CR1 (SA011F11), NKG2D (CX5), BCL2 (BCL/10C4), CD11b (M1/70), CD27 (LG.3A10), Bim (C34C5), Ki-67 (16A8), Cytochrome-C (6H2.B4). For mitochondrial dyes, NK cells were enriched from spleens as described above, stained with cell-surface antibodies, and then incubated with various dyes in Hank's balanced salt solution plus Mg and Ca as follows: 100 nM Mitotracker Green (Life Technologies) for 30 min at 37°C to measure mitochondrial mass or 100 nM TMRE (Thermofisher) for 30 min at 37°C to measure mitochondrial membrane potential. BH3 profiling was performed as previously described[76]. Briefly, purified NK cells were resuspended in MEB buffer (150 mM Mannitol 10 mM HEPES-KOH, 50 mM KCl, 0.02 mM EGTA, 0.02 mM EDTA, 0.1 % BSA, 5 mM Succinate). 50µl of cell suspension (1×10^5 cells/well) were plated in wells holding 50 µL MEB buffer containing 0.002% digitonin and BCL2 inhibitor ABT-199. Plates were then incubated at 25°C for 50 min. Cells were then fixed with 4% paraformaldehyde for 10min, followed by neutralization with N2 buffer (1.7M Tris, 1.25M Glycine pH 9.1) for 5min. Samples were stained for 1 hour with 20 µL of staining solution (10% BSA, 2% Tween 20 in PBS) containing anti-cytochrome c (BioLegend). Immediately afterwards, cytochrome c release was quantified using Attune Flow Cytometer.

Single Cell Metabolism assay (SCENITH)

To profile single cell metabolic responses, 95 uL of purified NK cells in complete media were plated at 0.1-0.5x10^6 cells/mL in v-bottom 96-well plates. Experimental triplicates were performed in all conditions. Wells were then treated with Control (DMSO), 2-Deoxy-D-Glucose (DG) final concentration 100mM, Oligomycin (O) final concentration 1 mM, or a sequential combination of DG and O at the final concentrations mentioned. As negative control, the translation initiation inhibitor Harringtonine was added (Harringtonine, 2 mg/mL). Puromycin (final concentration 10 mg/mL) is added immediately after the metabolic inhibitor treatment. After puromycin treatment, cells were washed in cold PBS and stained for surface markers. Intracellular staining of puromycin was achieved using a custom anti-puromycin antibody[27] was performed by incubating cells during 1h at 4°C diluted in permeabilization buffer.

PCR and Sanger Sequencing

DNA from NK cells was isolated using DNeasy Blood and Tissue kits (Qiagen). DNA concentration was measured using the NanoDrop OneC Microvolume UV-Vis Spectrophotometer (Thermo Scientific) and then diluted to 50 ng/µl in water before PCR amplification of cRNP-targeted genomic regions of approximately 500-1000 base pairs. PCR samples from WT and cRNP-edited cells were submitted for Sanger sequencing (GENEWIZ) and then indel percentage was calculated using ICE analysis (SYNTHEGO).

10x Library Preparation, Sequencing, and Alignment

Single cell RNA-sequencing libraries were generated with the Chromium Single Cell 3′ v2 (Day 7) and v3 (Day 14) assay (10X Genomics). Libraries were sequenced using the HighSeq 4000 platform (Illumina) to a depth of approximately 300 million reads per library

with 2x50 read length. Raw reads were aligned to mouse genome (mm10) and cells were called using cellranger count (v3.0.2).

scRNA-seq Cell Clustering

The R package Seurat (v3.1.)[77] was used to cluster the cells. Cells with less than 100 genes detected or more than 10% mitochondrial gene expression were first filtered out as low-quality cells. The gene counts for each cell were divided by the total gene counts for the cell and multiplied by a scale factor 10,000, then natural-log transformation was applied to the counts. The FindVariableFeatures function was used to select variable genes with default parameters. The ScaleData function was used to scale and center the counts in the dataset. Principal component analysis (PCA) was performed on the variable genes, and 20 principal components were used for cell clustering (resolution = 0.5) and uniform manifold approximation and projection (UMAP) dimensional reduction. The cluster markers were found using the FindAllMarkers function. Module scores were calculated using the AddModuleScore function with default parameters. In the comparison between D7 and D14 PI NK cells, the FindIntegrationAnchors and IntegrateData functions were used to find anchors and integrate the D7 and D14 PI datasets, and the other steps were the same as described above.

RNA velocity analysis

To estimate the RNA velocities of single cells, velocyto[48] was used to distinguish unspliced and spliced mRNAs in each sample. The python package scVelo[78] was then used to recover the directed dynamic information by leveraging RNA splicing information.

Specifically, the data was first normalized using the filter_and_normalize function. The first- and second-order moments were computed for velocity estimation using the moments function. The velocity vectors were obtained using the velocity function. The velocities were projected into a lower-dimensional embedding using the velocity_graph function. Finally, the velocities were visualized in the UMAP embedding using the velocity_embedding_stream function. All scVelo functions were used with default parameters.

Pseudo-time trajectory construction

Pseudo-time trajectories were constructed using the R package Monocle[79] (version 2.10.1). The raw counts for cells in the intended cell types were extracted and normalized by the estimateSizeFactors and estimateDispersions functions with the default parameters. Genes with average expression larger than 0.5 and detected in more than 10 cells were retained for further analysis. Variable genes were determined by the differentialGeneTest function with a model against the cell type identities. The top 2,000 variable genes with the lowest adjusted p value were used to order the cells. The orders were determined by the orderCells function, and the trajectory was constructed by the reduceDimension function with default parameters.

Bulk RNA Sequencing

RNA was isolated from the cells using RNeasy Mini kit (Qiagen) and used to generate RNA-seq libraries followed by sequencing using Illumina HighSeq 4000 platform (single end, 50bp). The reads were mapped with STAR[80] (version 2.5.3.a) to the mouse genome

(mm10). The counts for each gene were obtained by using –quantMode GeneCounts commands in STAR, and the other parameters during alignment were set to default. Differential expression analyses were carried out using DESeq2[81] (version 1.24.0) with default parameters. Genes with adjusted p value <0.05 were considered significantly differentially expressed. Sequencing depth normalized counts were used to plot the expression values for individual genes. The T cell bulk RNA-seq datasets were downloaded from GEO (GSE111902),[82] and the same DESeq2 procedure were applied. Genes with the absolute log2 fold change >0.5 and adjusted p value <0.05 in both NK cell and T cell datasets were plotted in Figure 5C. Cytokine stimulated bulk NK RNA-seq datasets were downloaded from GEO (GSE140044)[44].

ATAC-seq analysis

For ATAC-Seq, 50,000 cells per sample were lysed to collect nuclei and treated with Tn5 transposase (Illumina) for 30 minutes at 37°C with gentle agitation. The DNA was isolated with DNA Clean & Concentrator Kit (Zymo) and PCR amplified and barcoded with NEBNext High-Fidelity PCR Mix (New England Biolabs) and unique dual indexes (Illumina). The ATAC-Seq library amplification was confirmed by real-time PCR, and additional barcoding PCR cycles were added as necessary while avoiding overamplification. Amplified ATAC-Seq libraries were purified with DNA Clean & Concentrator Kit (Zymo). The purified libraries were quantified with Kapa Library Quant Kit (KAPA Biosystems) and quality assessed on 4200 TapeStation System (Agilent). The libraries were pooled based on molar concentrations and sequenced on an Illumina HighSeq 4000 platform (paired end, 100bp).

ATAC-seq fastq files were trimmed to remove low-quality reads and adapters using Cutadapt[83] (version 2.3). The reads were aligned to the reference mouse genome (mm10) with bowtie2[84] (version 2.2.9). Peak calling was performed with MACS2[85] (version 2.1.1). The peaks from all samples were merged into a single bed file, peaks from different samples that were closer than 10bp were merged into a single peak. HTseq[86] (version 0.9.1) was used to count the number of reads that overlap each peak per sample. The peak counts were analyzed with DESeq2[81] (version 1.24.0) to identify differentially accessible genomic regions. Peaks with adjusted p value <0.15 were considered significantly differentially accessible. The peak counts were visualized with IGV, version 2.5.0. The differentially accessible peaks were analyzed using the findMotifsGenome.pl function from homer[87] (version 4.9.1) to identify enriched cis-regulatory motifs of transcription factors. The T cell ATAC-seq datasets were downloaded from GEO (GSE111902), the same pipeline described above were used to analyze the datasets. Cytokine stimulated NK cell ATAC-seq datasets were downloaded from GEO (GSE140044) and visualized using the same pipeline described above. Peaks in the T cell ATAC-seq datasets with adjusted p value <0.05 were considered significantly differentially accessible. Significant peaks with the same change directions in the NK and T cell datasets were plotted in Figure 6C.

ChIP-seq analysis

STAT5 ChIP-seq datasets derived from IL-15/IL-2 stimulated splenic NK cells were downloaded from GEO (GSE140044)[44] and visualized using IGV, version 2.5.0.

Western blot

Protein was extracted from enriched primary splenic NK cells using Pierce RIPA buffer (Thermo-Fisher) with Halt protease inhibitor cocktail (Thermo-Fisher) and protein concentration was quantified using the Pierce BCA Protein Assay kit (Thermo-Fisher). Samples were electrophoresed on NuPage Novex 4–12% Bis-Tris Protein Gels, transferred to PVDF membranes, and blocked for one hour at room temperature with 5% w/v nonfat milk in 1X TBS and 0.1% Tween-20. Immunoblots were performed using rabbit anti-Fli1 (Abcam ab133485), rabbit anti-β-actin (Cell Signaling CST4970), and rabbit anti-GAPDH (Millipore Sigma G9545). Proteins were detected using the SuperSignal West Pico PLUS ECL kit (Thermo-Fisher) and visualized using the Azure Biosystems c280 imager. Band density was quantified using ImageJ version 1.53.

Statistical Analyses

For graphs, data are shown as mean ± SEM, and unless otherwise indicated, statistical differences were evaluated using a Student's t test with Welch's correction to assume a non-normal variance in our data distribution. Samples were compared using the Log-rank (Mantel-Cox) test with correction for testing multiple hypotheses. $p < 0.05$ was considered significant. Graphs were produced and statistical analyses were performed using GraphPad Prism.

Data Availability

Sequencing datasets are accessible from GEO with accession number GSE176208

References

1. Biron, C.A., Byron, K.S. & Sullivan, J.L. Severe herpesvirus infections in an adolescent without natural killer cells. *N Engl J Med* **320**, 1731-1735 (1989).

2. Bukowski, J.F., Warner, J.F., Dennert, G. & Welsh, R.M. Adoptive transfer studies demonstrating the antiviral effect of natural killer cells in vivo. *J Exp Med* **161**, 40-52 (1985).

3. Weizman, O.E. *et al.* ILC1 Confer Early Host Protection at Initial Sites of Viral Infection. *Cell* **171**, 795-808 e712 (2017).

4. Riggan, L., Freud, A.G. & O'Sullivan, T.E. True Detective: Unraveling Group 1 Innate Lymphocyte Heterogeneity. *Trends Immunol* **40**, 909-921 (2019).

5. Weizman, O.E. *et al.* Mouse cytomegalovirus-experienced ILC1s acquire a memory response dependent on the viral glycoprotein m12. *Nat Immunol* **20**, 1004-1011 (2019).

6. Sun, J.C., Beilke, J.N. & Lanier, L.L. Adaptive immune features of natural killer cells. *Nature* **457**, 557-561 (2009).

7. Lau, C.M. *et al.* Epigenetic control of innate and adaptive immune memory. *Nat Immunol* **19**, 963-972 (2018).

8. Buchmann, K. Evolution of Innate Immunity: Clues from Invertebrates via Fish to Mammals. *Front Immunol* **5**, 459 (2014).

9. Paludan, S.R., Pradeu, T., Masters, S.L. & Mogensen, T.H. Constitutive immune mechanisms: mediators of host defence and immune regulation. *Nat Rev Immunol* **21**, 137-150 (2021).

10. Kiessling, R., Klein, E. & Wigzell, H. "Natural" killer cells in the mouse. I. Cytotoxic cells with specificity for mouse Moloney leukemia cells. Specificity and distribution according to genotype. *Eur J Immunol* **5**, 112-117 (1975).

11. Cerwenka, A. & Lanier, L.L. Natural killer cell memory in infection, inflammation and cancer. *Nat Rev Immunol* **16**, 112-123 (2016).

12. O'Sullivan, T.E., Sun, J.C. & Lanier, L.L. Natural Killer Cell Memory. *Immunity* **43**, 634-645 (2015).

13. Best, J.A. *et al.* Transcriptional insights into the CD8(+) T cell response to infection and memory T cell formation. *Nat Immunol* **14**, 404-412 (2013).

14. Kaech, S.M. *et al.* Selective expression of the interleukin 7 receptor identifies effector CD8 T cells that give rise to long-lived memory cells. *Nat Immunol* **4**, 1191-1198 (2003).

15. Sarkar, S. *et al.* Functional and genomic profiling of effector CD8 T cell subsets with distinct memory fates. *J Exp Med* **205**, 625-640 (2008).

16. Kaech, S.M., Hemby, S., Kersh, E. & Ahmed, R. Molecular and functional profiling of memory CD8 T cell differentiation. *Cell* **111**, 837-851 (2002).

17. Huster, K.M. *et al.* Selective expression of IL-7 receptor on memory T cells identifies early CD40L-dependent generation of distinct CD8+ memory T cell subsets. *Proc Natl Acad Sci U S A* **101**, 5610-5615 (2004).

18. Schluns, K.S., Kieper, W.C., Jameson, S.C. & Lefrancois, L. Interleukin-7 mediates the homeostasis of naive and memory CD8 T cells in vivo. *Nat Immunol* **1**, 426-432 (2000).

19. Herndler-Brandstetter, D. *et al.* KLRG1(+) Effector CD8(+) T Cells Lose KLRG1, Differentiate into All Memory T Cell Lineages, and Convey Enhanced Protective Immunity. *Immunity* **48**, 716-729 e718 (2018).

20. Crinier, A. *et al.* High-Dimensional Single-Cell Analysis Identifies Organ-Specific Signatures and Conserved NK Cell Subsets in Humans and Mice. *Immunity* **49**, 971-986 e975 (2018).

21. Horowitz, A. *et al.* Genetic and environmental determinants of human NK cell diversity revealed by mass cytometry. *Sci Transl Med* **5**, 208ra145 (2013).

22. Karo, J.M., Schatz, D.G. & Sun, J.C. The RAG recombinase dictates functional heterogeneity and cellular fitness in natural killer cells. *Cell* **159**, 94-107 (2014).

23. Rahim, M.M. *et al.* Expansion and Protection by a Virus-Specific NK Cell Subset Lacking Expression of the Inhibitory NKR-P1B Receptor during Murine Cytomegalovirus Infection. *J Immunol* **197**, 2325-2337 (2016).

24. Kamimura, Y. & Lanier, L.L. Homeostatic control of memory cell progenitors in the natural killer cell lineage. *Cell Rep* **10**, 280-291 (2015).

25. Adams, N.M., Diaz-Salazar, C., Dang, C., Lanier, L.L. & Sun, J.C. Cutting Edge: Heterogeneity in Cell Age Contributes to Functional Diversity of NK Cells. *J Immunol* **206**, 465-470 (2021).

26. Masuya, M. *et al.* Dysregulation of granulocyte, erythrocyte, and NK cell lineages in Fli-1 gene-targeted mice. *Blood* **105**, 95-102 (2005).

27. Narni-Mancinelli, E. *et al.* Fate mapping analysis of lymphoid cells expressing the NKp46 cell surface receptor. *Proc Natl Acad Sci U S A* **108**, 18324-18329 (2011).

28. Simeonov, D.R. & Marson, A. CRISPR-Based Tools in Immunity. *Annu Rev Immunol* **37**, 571-597 (2019).

29. Pickar-Oliver, A. & Gersbach, C.A. The next generation of CRISPR-Cas technologies and applications. *Nat Rev Mol Cell Biol* **20**, 490-507 (2019).

30. Collins, P.L. *et al.* Gene Regulatory Programs Conferring Phenotypic Identities to Human NK Cells. *Cell* **176**, 348-360 e312 (2019).

31. Henning, A.N., Roychoudhuri, R. & Restifo, N.P. Epigenetic control of CD8(+) T cell differentiation. *Nat Rev Immunol* **18**, 340-356 (2018).

32. Youngblood, B., Hale, J.S. & Ahmed, R. T-cell memory differentiation: insights from transcriptional signatures and epigenetics. *Immunology* **139**, 277-284 (2013).

33. Bantug, G.R., Galluzzi, L., Kroemer, G. & Hess, C. The spectrum of T cell metabolism in health and disease. *Nat Rev Immunol* **18**, 19-34 (2018).

34. Chang, J.T., Wherry, E.J. & Goldrath, A.W. Molecular regulation of effector and memory T cell differentiation. *Nat Immunol* **15**, 1104-1115 (2014).

35. Kaech, S.M. & Cui, W. Transcriptional control of effector and memory CD8+ T cell differentiation. *Nat Rev Immunol* **12**, 749-761 (2012).

36. Joshi, N.S. *et al.* Inflammation directs memory precursor and short-lived effector CD8(+) T cell fates via the graded expression of T-bet transcription factor. *Immunity* **27**, 281-295 (2007).

37. Grassmann, S. *et al.* Distinct Surface Expression of Activating Receptor Ly49H Drives Differential Expansion of NK Cell Clones upon Murine Cytomegalovirus Infection. *Immunity* **50**, 1391-1400 e1394 (2019).

38. Arase, H., Mocarski, E.S., Campbell, A.E., Hill, A.B. & Lanier, L.L. Direct recognition of cytomegalovirus by activating and inhibitory NK cell receptors. *Science* **296**, 1323-1326 (2002).

39. Brown, M.G. *et al.* Vital involvement of a natural killer cell activation receptor in resistance to viral infection. *Science* **292**, 934-937 (2001).

40. Artis, D. & Spits, H. The biology of innate lymphoid cells. *Nature* **517**, 293-301 (2015).

41. Vivier, E. *et al.* Innate Lymphoid Cells: 10 Years On. *Cell* **174**, 1054-1066 (2018).

42. Serafini, N., Vosshenrich, C.A. & Di Santo, J.P. Transcriptional regulation of innate lymphoid cell fate. *Nat Rev Immunol* **15**, 415-428 (2015).

43. Nabekura, T., Riggan, L., Hildreth, A.D., O'Sullivan, T.E. & Shibuya, A. Type 1 Innate Lymphoid Cells Protect Mice from Acute Liver Injury via Interferon-gamma Secretion for Upregulating Bcl-xL Expression in Hepatocytes. *Immunity* **52**, 96-108 e109 (2020).

44. Wiedemann, G.M. *et al.* Deconvoluting global cytokine signaling networks in natural killer cells. *Nat Immunol* **22**, 627-638 (2021).

45. Pokrovskii, M. *et al.* Characterization of Transcriptional Regulatory Networks that Promote and Restrict Identities and Functions of Intestinal Innate Lymphoid Cells. *Immunity* **51**, 185-197 e186 (2019).

46. Shih, H.Y. *et al.* Developmental Acquisition of Regulomes Underlies Innate Lymphoid Cell Functionality. *Cell* **165**, 1120-1133 (2016).

47. Min-Oo, G., Bezman, N.A., Madera, S., Sun, J.C. & Lanier, L.L. Proapoptotic Bim regulates antigen-specific NK cell contraction and the generation of the memory NK cell pool after cytomegalovirus infection. *J Exp Med* **211**, 1289-1296 (2014).

48. La Manno, G. *et al.* RNA velocity of single cells. *Nature* **560**, 494-498 (2018).

49. van Helden, M.J. *et al.* Terminal NK cell maturation is controlled by concerted actions of T-bet and Zeb2 and is essential for melanoma rejection. *J Exp Med* **212**, 2015-2025 (2015).

50. Arguello, R.J. *et al.* SCENITH: A Flow Cytometry-Based Method to Functionally Profile Energy Metabolism with Single-Cell Resolution. *Cell Metab* **32**, 1063-1075 e1067 (2020).

51. O'Sullivan, T.E., Johnson, L.R., Kang, H.H. & Sun, J.C. BNIP3- and BNIP3L-Mediated Mitophagy Promotes the Generation of Natural Killer Cell Memory. *Immunity* **43**, 331-342 (2015).

52. Bezman, N.A. *et al.* Molecular definition of the identity and activation of natural killer cells. *Nat Immunol* **13**, 1000-1009 (2012).

53. Min-Oo, G. & Lanier, L.L. Cytomegalovirus generates long-lived antigen-specific NK cells with diminished bystander activation to heterologous infection. *J Exp Med* **211**, 2669-2680 (2014).

54. Johnnidis, J.B. *et al.* Inhibitory signaling sustains a distinct early memory CD8(+) T cell precursor that is resistant to DNA damage. *Sci Immunol* **6** (2021).

55. Viant, C. *et al.* Cell cycle progression dictates the requirement for BCL2 in natural killer cell survival. *J Exp Med* **214**, 491-510 (2017).

56. Riggan, L. *et al.* CRISPR-Cas9 Ribonucleoprotein-Mediated Genomic Editing in Mature Primary Innate Immune Cells. *Cell Rep* **31**, 107651 (2020).

57. Kurtulus, S. *et al.* Bcl-2 allows effector and memory CD8+ T cells to tolerate higher expression of Bim. *J Immunol* **186**, 5729-5737 (2011).

58. Dunkle, A., Dzhagalov, I., Gordy, C. & He, Y.W. Transfer of CD8+ T cell memory using Bcl-2 as a marker. *J Immunol* **190**, 940-947 (2013).

59. Sathe, P. *et al.* Innate immunodeficiency following genetic ablation of Mcl1 in natural killer cells. *Nat Commun* **5**, 4539 (2014).

60. Mujal, A.M., Delconte, R.B. & Sun, J.C. Natural Killer Cells: From Innate to Adaptive Features. *Annu Rev Immunol* **39**, 417-447 (2021).

61. Omilusik, K.D. *et al.* Transcriptional repressor ZEB2 promotes terminal differentiation of CD8+ effector and memory T cell populations during infection. *J Exp Med* **212**, 2027-2039 (2015).

62. Dominguez, C.X. *et al.* The transcription factors ZEB2 and T-bet cooperate to program cytotoxic T cell terminal differentiation in response to LCMV viral infection. *J Exp Med* **212**, 2041-2056 (2015).

63. Omilusik, K.D. *et al.* Sustained Id2 regulation of E proteins is required for terminal differentiation of effector CD8(+) T cells. *J Exp Med* **215**, 773-783 (2018).

64. Delconte, R.B. *et al.* The Helix-Loop-Helix Protein ID2 Governs NK Cell Fate by Tuning Their Sensitivity to Interleukin-15. *Immunity* **44**, 103-115 (2016).

65. Ikawa, T., Fujimoto, S., Kawamoto, H., Katsura, Y. & Yokota, Y. Commitment to natural killer cells requires the helix-loop-helix inhibitor Id2. *Proc Natl Acad Sci U S A* **98**, 5164-5169 (2001).

66. Zook, E.C. *et al.* Transcription factor ID2 prevents E proteins from enforcing a naive T lymphocyte gene program during NK cell development. *Sci Immunol* **3** (2018).

67. Madera, S. *et al.* Cutting Edge: Divergent Requirement of T-Box Transcription Factors in Effector and Memory NK Cells. *J Immunol* **200**, 1977-1981 (2018).

68. Rapp, M. *et al.* Core-binding factor beta and Runx transcription factors promote adaptive natural killer cell responses. *Sci Immunol* **2** (2017).

69. Taveirne, S. *et al.* The transcription factor ETS1 is an important regulator of human NK cell development and terminal differentiation. *Blood* **136**, 288-298 (2020).

70. Grund, E.M., Spyropoulos, D.D., Watson, D.K. & Muise-Helmericks, R.C. Interleukins 2 and 15 regulate Ets1 expression via ERK1/2 and MNK1 in human natural killer cells. *J Biol Chem* **280**, 4772-4778 (2005).

71. Ramirez, K. *et al.* Gene deregulation and chronic activation in natural killer cells deficient in the transcription factor ETS1. *Immunity* **36**, 921-932 (2012).

72. Chen, Z. *et al.* In vivo CD8(+) T cell CRISPR screening reveals control by Fli1 in infection and cancer. *Cell* **184**, 1262-1280 e1222 (2021).

73. Wang, T. *et al.* Gene Essentiality Profiling Reveals Gene Networks and Synthetic Lethal Interactions with Oncogenic Ras. *Cell* **168**, 890-903 e815 (2017).

74. Shen, M.W. *et al.* Predictable and precise template-free CRISPR editing of pathogenic variants. *Nature* **563**, 646-651 (2018).

75. Hildreth, A.D., Riggan, L. & O'Sullivan, T.E. CRISPR-Cas9 Ribonucleoprotein-Mediated Genomic Editing in Primary Innate Immune Cells. *STAR Protoc* **1**, 100113 (2020).

76. Deng, J. *et al.* BH3 profiling identifies three distinct classes of apoptotic blocks to predict response to ABT-737 and conventional chemotherapeutic agents. *Cancer Cell* **12**, 171-185 (2007).

77. Stuart, T. *et al.* Comprehensive Integration of Single-Cell Data. *Cell* **177**, 1888-1902 e1821 (2019).

78. Bergen, V., Lange, M., Peidli, S., Wolf, F.A. & Theis, F.J. Generalizing RNA velocity to transient cell states through dynamical modeling. *Nat Biotechnol* **38**, 1408-1414 (2020).

79. Trapnell, C. *et al.* The dynamics and regulators of cell fate decisions are revealed by pseudotemporal ordering of single cells. *Nat Biotechnol* **32**, 381-386 (2014).

80. Dobin, A. *et al.* STAR: ultrafast universal RNA-seq aligner. *Bioinformatics* **29**, 15-21 (2013).

81. Love, M.I., Huber, W. & Anders, S. Moderated estimation of fold change and dispersion for RNA-seq data with DESeq2. *Genome Biol* **15**, 550 (2014).

82. Yu, B. *et al.* Epigenetic landscapes reveal transcription factors that regulate CD8(+) T cell differentiation. *Nat Immunol* **18**, 573-582 (2017).

83. Kechin, A., Boyarskikh, U., Kel, A. & Filipenko, M. cutPrimers: A New Tool for Accurate Cutting of Primers from Reads of Targeted Next Generation Sequencing. *J Comput Biol* **24**, 1138-1143 (2017).

84. Langmead, B. & Salzberg, S.L. Fast gapped-read alignment with Bowtie 2. *Nat Methods* **9**, 357-359 (2012).

85. Zhang, Y. *et al.* Model-based analysis of ChIP-Seq (MACS). *Genome Biol* **9**, R137 (2008).

86. Anders, S., Pyl, P.T. & Huber, W. HTSeq--a Python framework to work with high-throughput sequencing data. *Bioinformatics* **31**, 166-169 (2015).

87. Heinz, S. *et al.* Simple combinations of lineage-determining transcription factors prime cis-regulatory elements required for macrophage and B cell identities. *Mol Cell* **38**, 576-589 (2010).

88. Wculek, S.K. *et al.* Dendritic cells in cancer immunology and immunotherapy. *Nat Rev Immunol* (2019).

89. Hildner, K. *et al.* Batf3 deficiency reveals a critical role for CD8alpha+ dendritic cells in cytotoxic T cell immunity. *Science* **322**, 1097-1100 (2008).

90. Abram, C.L., Roberge, G.L., Hu, Y. & Lowell, C.A. Comparative analysis of the efficiency and specificity of myeloid-Cre deleting strains using ROSA-EYFP reporter mice. *J Immunol Methods* **408**, 89-100 (2014).

91. Satpathy, A.T. *et al.* Zbtb46 expression distinguishes classical dendritic cells and their committed progenitors from other immune lineages. *J Exp Med* **209**, 1135-1152 (2012).

92. Loschko, J. *et al.* Absence of MHC class II on cDCs results in microbial-dependent intestinal inflammation. *J Exp Med* **213**, 517-534 (2016).

93. Hemmi, H., Hoshino, K. & Kaisho, T. In Vivo Ablation of a Dendritic Cell Subset Expressing the Chemokine Receptor XCR1. *Methods Mol Biol* **1423**, 247-253 (2016).

94. Oliphant, C.J. *et al.* MHCII-mediated dialog between group 2 innate lymphoid cells and CD4(+) T cells potentiates type 2 immunity and promotes parasitic helminth expulsion. *Immunity* **41**, 283-295 (2014).

95. Rankin, L.C. *et al.* Complementarity and redundancy of IL-22-producing innate lymphoid cells. *Nat Immunol* **17**, 179-186 (2016).

96. Shifrut, E. *et al.* Genome-wide CRISPR Screens in Primary Human T Cells Reveal Key Regulators of Immune Function. *Cell* **175**, 1958-1971 e1915 (2018).

97. Farboud, B. *et al.* Enhanced Genome Editing with Cas9 Ribonucleoprotein in Diverse Cells and Organisms. *J Vis Exp* (2018).

98. Wu, C.M. *et al.* Genetic engineering in primary human B cells with CRISPR-Cas9 ribonucleoproteins. *J Immunol Methods* **457**, 33-40 (2018).

99. Seki, A. & Rutz, S. Optimized RNP transfection for highly efficient CRISPR/Cas9-mediated gene knockout in primary T cells. *J Exp Med* **215**, 985-997 (2018).

100. Nabekura, T., Riggan, L., Hildreth, A.D., O'Sullivan, T.E. & Shibuya, A. Type 1 Innate Lymphoid Cells Protect Mice from Acute Liver Injury via Interferon-gamma Secretion for Upregulating Bcl-xL Expression in Hepatocytes. *Immunity* (2019).

101. O'Sullivan, T.E. *et al.* Adipose-Resident Group 1 Innate Lymphoid Cells Promote Obesity-Associated Insulin Resistance. *Immunity* **45**, 428-441 (2016).

102. Fuchs, A. *et al.* Intraepithelial type 1 innate lymphoid cells are a unique subset of IL-12- and IL-15-responsive IFN-gamma-producing cells. *Immunity* **38**, 769-781 (2013).

103. Bernink, J.H. *et al.* Human type 1 innate lymphoid cells accumulate in inflamed mucosal tissues. *Nat Immunol* **14**, 221-229 (2013).

104. Sun, J.C. *et al.* Proinflammatory cytokine signaling required for the generation of natural killer cell memory. *J Exp Med* **209**, 947-954 (2012).

105. Marcus, A. *et al.* Tumor-Derived cGAMP Triggers a STING-Mediated Interferon Response in Non-tumor Cells to Activate the NK Cell Response. *Immunity* **49**, 754-763 e754 (2018).

106. Liu, Y. *et al.* An inhalable nanoparticulate STING agonist synergizes with radiotherapy to confer long-term control of lung metastases. *Nat Commun* **10**, 5108 (2019).

107. Ohta, T. *et al.* Crucial roles of XCR1-expressing dendritic cells and the XCR1-XCL1 chemokine axis in intestinal immune homeostasis. *Sci Rep* **6**, 23505 (2016).

108. Puttur, F. *et al.* Conventional Dendritic Cells Confer Protection against Mouse Cytomegalovirus Infection via TLR9 and MyD88 Signaling. *Cell Rep* **17**, 1113-1127 (2016).

109. Parnas, O. *et al.* A Genome-wide CRISPR Screen in Primary Immune Cells to Dissect Regulatory Networks. *Cell* **162**, 675-686 (2015).

110. Theisen, D.J. *et al.* WDFY4 is required for cross-presentation in response to viral and tumor antigens. *Science* **362**, 694-699 (2018).

111. Kim, S., Kim, D., Cho, S.W., Kim, J. & Kim, J.S. Highly efficient RNA-guided genome editing in human cells via delivery of purified Cas9 ribonucleoproteins. *Genome Res* **24**, 1012-1019 (2014).

112. Ramakrishna, S. *et al.* Gene disruption by cell-penetrating peptide-mediated delivery of Cas9 protein and guide RNA. *Genome Res* **24**, 1020-1027 (2014).

113. Pikovskaya, O. *et al.* Cutting Edge: Eomesodermin Is Sufficient To Direct Type 1 Innate Lymphocyte Development into the Conventional NK Lineage. *J Immunol* **196**, 1449-1454 (2016).

114. Pahl, J. & Cerwenka, A. Tricking the balance: NK cells in anti-cancer immunity. *Immunobiology* **222**, 11-20 (2017).

115. Fu, B. *et al.* Natural Killer Cells Promote Fetal Development through the Secretion of Growth-Promoting Factors. *Immunity* **47**, 1100-1113 e1106 (2017).

116. Wensveen, F.M. *et al.* NK cells link obesity-induced adipose stress to inflammation and insulin resistance. *Nat Immunol* **16**, 376-385 (2015).

117. Loschko, J. *et al.* Inducible targeting of cDCs and their subsets in vivo. *J Immunol Methods* **434**, 32-38 (2016).

118. Esterhazy, D. *et al.* Classical dendritic cells are required for dietary antigen-mediated induction of peripheral T(reg) cells and tolerance. *Nat Immunol* **17**, 545-555 (2016).

119. Mayer, C.T. *et al.* Selective and efficient generation of functional Batf3-dependent CD103+ dendritic cells from mouse bone marrow. *Blood* **124**, 3081-3091 (2014).

120. Van der Meulen, J., Speleman, F. & Van Vlierberghe, P. The H3K27me3 demethylase UTX in normal development and disease. *Epigenetics* **9**, 658-668 (2014).

121. Chiossone, L. *et al.* Maturation of mouse NK cells is a 4-stage developmental program. *Blood* **113**, 5488-5496 (2009).

122. Pfefferle, A. *et al.* Deciphering Natural Killer Cell Homeostasis. *Front Immunol* **11**, 812 (2020).

123. Huntington, N.D. *et al.* Interleukin 15-mediated survival of natural killer cells is determined by interactions among Bim, Noxa and Mcl-1. *Nat Immunol* **8**, 856-863 (2007).

124. Wang, C. *et al.* UTX regulates mesoderm differentiation of embryonic stem cells independent of H3K27 demethylase activity. *Proc Natl Acad Sci U S A* **109**, 15324-15329 (2012).

125. Miller, S.A., Mohn, S.E. & Weinmann, A.S. Jmjd3 and UTX play a demethylase-independent role in chromatin remodeling to regulate T-box family member-dependent gene expression. *Mol Cell* **40**, 594-605 (2010).

126. Huang, D.W. *et al.* DAVID Bioinformatics Resources: expanded annotation database and novel algorithms to better extract biology from large gene lists. *Nucleic Acids Res* **35**, W169-175 (2007).

127. Townsend, M.J. *et al.* T-bet regulates the terminal maturation and homeostasis of NK and Valpha14i NKT cells. *Immunity* **20**, 477-494 (2004).

128. Holmes, T.D. *et al.* The transcription factor Bcl11b promotes both canonical and adaptive NK cell differentiation. *Sci Immunol* **6** (2021).

129. Geiger, T.L. *et al.* Nfil3 is crucial for development of innate lymphoid cells and host protection against intestinal pathogens. *J Exp Med* **211**, 1723-1731 (2014).

130. Deng, Y. *et al.* Transcription factor Foxo1 is a negative regulator of natural killer cell maturation and function. *Immunity* **42**, 457-470 (2015).

131. Delconte, R.B. *et al.* CIS is a potent checkpoint in NK cell-mediated tumor immunity. *Nat Immunol* **17**, 816-824 (2016).

132. Jeevan-Raj, B. *et al.* The Transcription Factor Tcf1 Contributes to Normal NK Cell Development and Function by Limiting the Expression of Granzymes. *Cell Rep* **20**, 613-626 (2017).

133. O'Sullivan, T.E. *et al.* Atg5 Is Essential for the Development and Survival of Innate Lymphocytes. *Cell Rep* **15**, 1910-1919 (2016).

134. Nausch, N. *et al.* Cutting edge: the AP-1 subunit JunB determines NK cell-mediated target cell killing by regulation of the NKG2D-ligand RAE-1epsilon. *J Immunol* **176**, 7-11 (2006).

135. Adams, N.M. *et al.* Transcription Factor IRF8 Orchestrates the Adaptive Natural Killer Cell Response. *Immunity* **48**, 1172-1182 e1176 (2018).

136. Geary, C.D. *et al.* Non-redundant ISGF3 Components Promote NK Cell Survival in an Auto-regulatory Manner during Viral Infection. *Cell Rep* **24**, 1949-1957 e1946 (2018).

137. Wiedemann, G.M. *et al.* Divergent Role for STAT5 in the Adaptive Responses of Natural Killer Cells. *Cell Rep* **33**, 108498 (2020).

138. Pomeroy, C., Delong, D., Clabots, C., Riciputi, P. & Filice, G.A. Role of interferon-gamma in murine cytomegalovirus infection. *J Lab Clin Med* **132**, 124-133 (1998).

139. Mitchell, J.E. *et al.* UTX promotes CD8(+) T cell-mediated antiviral defenses but reduces T cell durability. *Cell Rep* **35**, 108966 (2021).

140. Cook, K.D. *et al.* T Follicular Helper Cell-Dependent Clearance of a Persistent Virus Infection Requires T Cell Expression of the Histone Demethylase UTX. *Immunity* **43**, 703-714 (2015).

141. Beyaz, S. *et al.* The histone demethylase UTX regulates the lineage-specific epigenetic program of invariant natural killer T cells. *Nat Immunol* **18**, 184-195 (2017).

142. Maj, T. *et al.* Oxidative stress controls regulatory T cell apoptosis and suppressor activity and PD-L1-blockade resistance in tumor. *Nat Immunol* **18**, 1332-1341 (2017).

143. Cribbs, A. *et al.* Inhibition of histone H3K27 demethylases selectively modulates inflammatory phenotypes of natural killer cells. *J Biol Chem* **293**, 2422-2437 (2018).

144. Kruidenier, L. *et al.* A selective jumonji H3K27 demethylase inhibitor modulates the proinflammatory macrophage response. *Nature* **488**, 404-408 (2012).

145. van der Heiden, M. *et al.* Differential effects of Cytomegalovirus carriage on the immune phenotype of middle-aged males and females. *Sci Rep* **6**, 26892 (2016).

146. Ahmed, F., Jo, D.H. & Lee, S.H. Can Natural Killer Cells Be a Principal Player in Anti-SARS-CoV-2 Immunity? *Front Immunol* **11**, 586765 (2020).

147. Riggan, L., Shah, S. & O'Sullivan, T.E. Arrested development: suppression of NK cell function in the tumor microenvironment. *Clin Transl Immunology* **10**, e1238 (2021).

Chapter 3:

CRISPR Cas9 ribonucleoprotein-mediated genomic editing in primary innate immune cells

CRISPR Cas9 ribonucleoprotein-mediated genomic editing in primary innate immune cells

Luke Riggan[1,2,#], Andrew D. Hildreth[1,2,#], Marion Rolot[1], Yung-Yu Wong[1], William Satyadi[1], Ryan Sun[1], Christopher Huerta[1], and Timothy E. O'Sullivan[1,2,*]

[1]Department of Microbiology, Immunology, and Molecular Genetics, David Geffen School of Medicine at UCLA, Los Angeles, CA 90095
[2]Molecular Biology Institute, University of California, Los Angeles, Los Angeles, CA 90095, USA
[#]These authors contributed equally to this work
[*]Corresponding Author

Correspondence:

Timothy E. O'Sullivan, PhD
David Geffen School of Medicine at UCLA
615 Charles E. Young Drive South, BSRB 245F
Los Angeles, CA 90095
Phone: 310-825-4454
Email: tosullivan@mednet.ucla.edu

Abstract

CRISPR (clustered, regularly interspaced, short palindromic repeats) genome engineering has become a powerful tool to functionally investigate the complex mechanisms of immune system regulation. While decades of work have aimed to genetically reprogram innate immunity, current approaches are often inefficient or nonspecific, limiting their use in innate immune cells *in vivo*. Here, we describe an optimized strategy for non-viral CRISPR-Cas9 ribonucleoprotein (cRNP) genomic editing of primary innate lymphocytes (ILCs) and myeloid lineage cells that results in an almost complete loss of single or double target gene expression from a single electroporation. Furthermore, we describe *in vivo* adoptive transfer mouse models that can be utilized to screen for gene function during viral infection using cRNP-edited naïve NK cells and bone marrow-derived dendritic cell precursors. Using these methods, we demonstrate that $XCR1^{+}$ conventional dendritic cells (cDC1) are sufficient and necessary for host protection to mouse cytomegalovirus (MCMV) in a MyD88-dependent manner. This scalable method will enhance target gene discovery and offer a specific and simplified approach to gene editing in the innate immune system.

Introduction

The mammalian immune system consists of both tissue-resident and circulating immune cells. Tissue-resident innate immune cells, such as dendritic cells (DCs), can produce a wide-variety of effector molecules that can directly or indirectly limit pathogen spread and tumor growth in tissue microenvironments [3, 88, 89]. Innate lymphoid cells (ILCs) are tissue-resident cells that produce both proinflammatory and regulatory cytokines in response to local injury, inflammation, pathogen infection, or commensal microbiota perturbation [41]. However, persistent inflammatory signals can also lead to unrestrained activation of innate immunity that is associated with inflammatory pathologies such as Crohn's disease (CD), chronic obstructive pulmonary disease (COPD), Type II diabetes mellitus (T2D), and systemic lupus erythematosus (SLE) [4, 41]. Although understanding and harnessing the cellular and molecular mechanisms that regulate the innate immune system hold promise for the treatment of several inflammatory disorders, a mechanistic understanding of the mammalian innate immune system has been limited by suboptimal cell lineage gene targeting strategies.

Current models to specifically manipulate gene expression in the mouse innate immune system have been confounded by non-lineage specific Cre mouse transgenic lines. For example, *LysM*^{Cre}, *Csf1r*^{Cre}, and *Cx3cr1*^{Cre} mice (commonly used to target macrophage populations) contain overlapping expression profiles in several other myeloid lineage cells based on previous fate mapping studies [90], making a Cre-transgenic line specific for macrophages currently impossible. Furthermore, mouse transgenic Cre lines used to selectively target dendritic cells *in vivo*, such as *Itgax*^{Cre} and *Zbtb46*^{Cre}, express the transgene in dendritic cells, macrophages, and NK cells (*Itgax*) [90], or

conventional type 1 (cDC1) and type 2 (cDC2) dendritic cells, as well as endothelial cells (*Zbtb46*) [91, 92]. While *Xcr1*^{Cre} mice can be used to selectively target and ablate cDC1 [93], there are no current tools to specifically target gene expression in cDC2 *in vivo*. In the ILC lineage, *Ncr1*^{Cre} mice induce gene deletion in natural killer (NK) cells, type 1 innate lymphoid cells (ILC1), and a subset of ILC3 [27]. While genetic strategies exist for ablation of each individual ILC lineage *in vivo* [3, 94, 95], there are currently no tools available for specific genetic manipulation in primary ILCs without off-target effects in other cell types or potential cell-extrinsic effects derived from whole body knockout (KO) mice. Thus, the prevalent issue of non-specific gene targeting of innate immune cells significantly limits the precise mechanistic understanding of the innate immune system in models of host defense and disease *in vivo*.

Recent advances in CRISPR-Cas9 genome editing provide and alternative gene manipulation tool that can be used on enriched primary immune cells [28]. Cas9 is a DNA endonuclease that can bind to a complementary region of the genome through its associated guide RNA (gRNA) to generate double strand breaks in the DNA that result in insertions and/or deletions (indels) in coding regions of proteins to permanently suppress their expression [29]. Specifically, viral and non-viral based strategies have been used to manipulate gene expression in purified primary human and mouse adaptive lymphocytes by lentiviral or retroviral overexpression of Cas9 and gRNA sequences, or electroporation of a Cas9: gRNA ribonucleoprotein complex (cRNP) [28, 96-99]. While these approaches have been used to elucidate novel gene function in mammalian adaptive lymphcytes, whether CRISPR-Cas9 gene editing techniques can be used to delete gene expression in primary innate immune cells *in vivo* is currently not well understood. Here, we describe

an optimized strategy for non-viral cRNP genomic editing of primary mouse innate immune cells. Optimal voltage parameters were determined for maximal Cas9 protein electroporation efficiency and viability of primary innate leukocytes. Using these optimized conditions, we were able to achieve high KO efficiency of cell surface proteins, intracellular signaling proteins, and transcription factors in innate immune cells using cRNP complexes. Furthermore, we describe two *in vivo* adoptive transfer models using cRNP-edited naïve NK cells and dendritic cell precursors to reveal mechanistic details of antiviral gene function in these cell types during mouse cytomegalovirus (MCMV) infection. This general gene editing strategy may be further adapted to other primary immune cell types and *in vivo* transfer models to investigate protective or pathologic biological processes in the mammalian innate immune system.

Results

Optimized cRNP electroporation of primary splenic innate immune cells

To determine the optimized electroporation efficiencies for Cas9 in primary leukocytes, mouse splenocytes were electroporated using the Neon transfection system. Because we determined that primary leukocytes display maximal viability at an electroporation pulse width of 1 x 20ms (data not shown), we first tested a range of voltages to optimize the maximal frequency of intracellular $Cas9^+$ leukocytes following electroporation. While freshly isolated splenic NK and T cells had lower electroporation efficiencies of Cas9 with increasing voltage, overnight activation with interleukin (IL)-15 *in vitro* increased the frequency of intracellular $Cas9^+$ cells to ~80% in both NK and T cells at all voltages tested (**Fig. 1a and Extended Data Fig. 1a,b**). In contrast, freshly isolated splenic macrophages and conventional type 1 (cDC1) and 2 (cDC2) dendritic cells displayed similar frequencies of intracellular $Cas9^+$ cells following electroporation when compared to splenocytes stimulated with M-CSF or FLT3-L overnight at all voltages tested (**Fig. 1b and Extended Data Fig. 1c**). Furthermore, increased concentrations of Cas9 present in the electroporation buffer decreased the frequency of intracellular $Cas9^+$ lymphocytes, with a much more severe reduction in NK cells (~40% reduction) than $CD4^+$ and $CD8^+$ T cells (~20% reduction) at a constant voltage (**Fig. 1c**). However, splenic macrophages, cDC1, and cDC2 did not display a similar dose dependent decrease in the frequency of intracellular $Cas9^+$ cells, suggesting that splenic myeloid lineages have an increased capacity of intracellular Cas9 delivery following electroporation at a constant voltage (**Fig. 1d**). Although our results suggested that splenocytes could be reliably used to measure intracellular Cas9 following electroporation in all leukocyte populations tested, it remained

possible that these results may not precisely reflect the response of purified leukocytes. However, purified NK cells displayed a similar frequency of intracellular Cas9$^+$ cells as NK cells from splenocytes, suggesting that the presence of other leukocytes in a splenocyte single cell suspension does not inhibit intracellular Cas9 uptake following electroporation (**Extended Data Fig. 1d**). These results reveal cell-intrinsic differences in resting and cytokine stimulated leukocyte electroporation efficiencies of Cas9 that need to be optimized for each cell type and condition of interest.

Efficient cRNP-mediated gene editing in primary circulating and tissue-resident innate immune cells *ex vivo*

Group 1 ILCs consist of circulating NK cells and tissue-resident ILC1 that confer host protection during viral infection and liver injury [3, 4, 100], while also contributing to tissue pathology during intestinal inflammation and obesity [101-103]. However, there are currently no genetic tools to selectively ablate gene expression in NK cells or ILC1 [4]. In order to achieve specific gene deletion in group 1 ILCs, we first purified splenic NK cells and found that electroporation at 1900V led to the highest frequency of viable intracellular Cas9$^+$ NK cells (**Fig. 2a**). These results were not influenced by NK cell maturation, because all developmental stages of splenic NK cells displayed similar frequencies of intracellular Cas9$^+$ cells (**Extended Data Fig. 2b**). We next determined that electroporation of purified IL-15 pre-activated splenic NK cells in the presence of 40pMol Cas9 : 120pMol gRNA *Klrb1c* (NK1.1) cRNP complex yielded the highest KO efficiency (~90%) (**Fig. 2b-e**). Purified IL-15 pre-activated NK cells and ILC1 from the liver also displayed high frequencies of NK1.1$^-$ cells (~80%) using the same conditions, suggesting that cRNP

gene editing is not limited to specific group 1 ILCs or lymphocytes from distinct tissues (**Fig. 2f**). However, we observed that gene KO efficiency in primary NK cells is highly dependent on the individual guide RNA (gRNA) used and the type of recombinant Cas9. We found that poor efficiency guides targeting similar *Klrbc1* exons could be pooled together in separate cRNP complexes within a single electroporation to achieve similar KO efficiencies as the highest efficiency cRNP complex, similar to a previous report in primary T cells [99] (**Extended Data Fig. 2b,c**). Furthermore, we observed that different lymphocyte populations could achieve varying levels of KO efficiency using the same *Thy1.2* (CD90) cRNP complex (**Fig. 2g**). Together, these results suggest that cell lineage-intrinsic differences as well as gRNA editing efficiency contribute to overall KO efficiency following cRNP electroporation in primary lymphocytes.

Given our results with group 1 ILCs, we next tested a range of voltages and Cas9 concentrations that would lead to optimized cRNP-mediated gene editing in myeloid lineage cells. Bone marrow derived macrophages (BMDM) and cDC1 (BMDC1) did not differ in the frequency of intracellular $Cas9^+$ cells following electroporation at all voltages tested, similar to splenic macrophages and dendritic cells (**Fig. 3a and Fig. 1b**). However, higher voltages sequentially decreased the viability of both BMDM and BMDC1, suggesting that electroporation at 1900V was optimal (**Fig. 3b**). Indeed, electroporation of $CD11b^+$ BMDM or $CD11c^+$ BMDC1 with 40pMol Cas9 : 120pMol gRNA *Itgam* cRNP complex or *Itgax* cRNP complex lead to (~90% KO, CD11b) and (~95% KO, CD11c) in BMDM and BMDC1 respectively (**Fig. 3c,d**). Although slightly higher KO efficiencies were achieved with a higher concentration of Cas9 and gRNA cRNP complex, this reduced cell viability in BMDM and BMDC1, suggesting that a 40pMol Cas9 : 120pMol gRNA cRNP

complex and electroporation at 1900V was ideal for maximal gene deletion efficiency and viability for both cell types (**Fig. 3d,e**). These results were corroborated by high efficiency gene KOs of CD11c and CD11b in primary splenic dendritic cells and macrophages respectively (**Fig. 3f**). To test whether multiple cRNP complexes could be complexed together in a single electroporation to generate double KO innate immune cells, we electroporated IL-15 pre-activated purified splenic NK cells in the presence of *Klrb1c* and *Thy1.2* cRNP complexes. 3 days post activation with IL-15 *in vitro*, we observed that ~55% of NK cells were NK1.1^{-}CD90^{-} (**Fig. 4a,b**). Similarly, ~77% of bone marrow-derived macrophages electroporated in the presence of CD11b and *β2M* cRNP complexes and stimulated with interferon (IFN)-γ were CD11b^{-}MHCI^{-} (**Fig. 4c,d**). Together, these results suggest that our cRNP gene editing method can be used to efficiently create single and double KO primary innate leukocytes.

cRNP editing in NK cells and cDC1 for *in vitro* functional assays

To demonstrate the utility of this gene editing approach *in vitro*, we chose to target the transcription factor *Stat4*, which is essential for IL-12-mediated IFN-γ production in primary NK cells [3, 104]. Similar to *Stat4*$^{-/-}$ NK cells, *Stat4* cRNP-edited NK cells displayed a significant decrease in IFN-γ production following stimulation with IL-12 *ex vivo* when compared to a control *Rosa26* cRNP (WT NTC) NK cells (**Fig. 5a-c**). Previous studies have suggested that tumor-intrinsic production of the cyclic dinucleotide 2'3'-cGAMP can activate dendritic cells to mediate anti-tumor immunity in a type I interferon-dependent manner [105, 106]. However, whether cGAMP can also stimulate the production of other anti-tumor cytokines in cDC1 is not well understood. Using bone marrow-derived dendritic cell

precursors from *Il12p40*^{YFP} reporter mice, we observed that stimulation with the cyclic dinucleotide 2'3'-cGAMP significantly increased the frequency of YFP^{+} BMDC1 (**Fig. 5d-f**). IL-12 production by BMDC1 required *Tmem173* (STING) signaling, because *Tmem173* cRNP-edited BMDC1 displayed similar frequencies of YFP^{+} cells when compared to unstimulated controls (**Fig. 5e,f**). These results were unlikely due to cRNP-extrinsic effects on cDC1 activation or maturation, because resting *Rosa26* cRNP-edited (NTC) cDC1 displayed a similar phenotype and background YFP^{+} frequency as resting unedited controls (**Extended Data Fig. 3a,b**). Thus, our gene editing system revealed that cDC1 robustly produced IL-12 in response to extracellular cGAMP in a STING dependent manner *in vitro*.

Adoptively transferred cRNP-edited primary innate immune cells can be used to elucidate gene function *in vivo*

While previous studies have used cRNP gene editing in adaptive immune cells to elucidate gene function during *in vitro* functional assays [96, 99], there are currently no models to assay the function of cRNP-edited genes in innate immune cells *in vivo*. To address this issue, we modified an adoptive transfer system whereby congenically distinct Ly49H^{+} NK cells can be transferred to Ly49H$^{-/-}$ hosts to generate effector and memory NK cells following MCMV infection [6] (**Fig. 6a**). Specifically, IL-15 pre-activated splenic Ly49H^{+} NK cells were electroporated in the presence of either *Rosa26* cRNP (NTC) or *Stat4* cRNP complexes and adoptively transferred into Ly49H$^{-/-}$ mice at a 1:1 ratio. Following MCMV infection of recipient mice, we observed that *Stat4* cRNP-edited NK cells failed to expand on D7 post-infection (P.I.) and generated significantly fewer memory NK

cells on D28 P.I., similar to a previous study [104] (**Fig. 6b,c**). The expansion phenotype of *Stat4* cRNP-edited NK cells was not due to off-target effects or influence from congenic mouse strains, as *Stat4* cRNP-edited NK cells failed to expand to a similar extent as co-transferred congenically distinct *Stat4*$^{-/-}$ NK cells (**Fig. 6d and Extended Data Fig. 4a,b**). These results suggest that adoptively transferred cRNP-edited primary NK cells can reliably be used to assay gene function during NK cell effector and memory responses to MCMV *in vivo*.

Previous studies have shown that the transcription factor *Batf3* is essential for cDC1 development and protection against viral infection and tumor development [89]. However, *Batf3* is expressed in CCR6^{+} ILC3, cDC2, and macrophage subsets *in vivo* (Immgen), and the functional contribution of *Batf3* in these subsets is not well understood *in vivo*. Thus, the precise contribution of cDC1 during host protection during viral infection is not well defined. To determine the role of cDC1 during viral infection, we used XCR1$^{Cre/+}$ x LsLDTA (hereafter referred to as cDC1$^{-/-}$) mice that specifically ablate XCR1^{+} cDC1 [93, 107]. While XCR1$^{+/+}$ x LsLDTA (hereafter referred to as WT) littermates were protected against MCMV challenge, all cDC1$^{-/-}$ mice rapidly succumbed to MCMV infection by D7 P.I., indicating an early essential contribution of cDC1 to host protection following MCMV infection (**Fig. 6e**). In order to generate an *in vivo* transfer model for cRNP-edited cDC1, we tested whether D9 *in vitro* cultured BMDC precursors could generate mature cDC1 in cDC1$^{-/-}$ mice. Following adoptive transfer of congenically distinct BMDC, we observed that XCR1^{+}CD11b^{-} cDC1 reconstituted cDC1$^{-/-}$ mice in peripheral organs, albeit to a lesser extent than endogenous cDC1 present in WT littermate controls (**Extended Data Fig. 5**). Because CD11c^{+} cell-intrinsic MyD88 expression has been

shown to be essential for host protection during viral infection [108], we then tested whether cDC1-intrinsic MyD88 signaling was sufficient for host protection during MCMV infection (**Fig. 6f**). While adoptively transferred NTC cRNP-edited BMDC were sufficient to rescue $cDC1^{-/-}$ mice, MyD88 cRNP-edited cDC precursors failed to rescue $cDC1^{-/-}$ mice in a similar manner as untransferred control $cDC1^{-/-}$ mice (**Fig. 6g**). These results suggest that cDC1-intrinsic MyD88 signaling is sufficient for host protection to MCMV. Thus, these adoptive transfer models of cRNP-edited primary innate immune cells can be used and modified in future studies to reliably elucidate gene function in the innate immune system *in vivo.*

Discussion

Using the Neon electroporation system, we define the conditions necessary for electroporation of cRNP complexes in naïve and cytokine-activated mouse leukocytes. It is important to note that we detected minimal nuclear localized Cas9 in leukocytes two hours post-electroporation (data not shown), suggesting that our optimized conditions are specific to cytoplasmic incorporation of Cas9 in leukocytes at this timepoint. Irrespective of these findings, we demonstrate that cytoplasmic Cas9 can be used to optimize cRNP gene KO efficiencies and cell viability by varying electroporation voltage conditions. This degree of customization may prove to be more beneficial to optimize new immune cell types rather than by using proprietary pulse codes from other electroporation platforms. We observed cell type specific differences in Cas9 electroporation efficiencies and KO frequencies using set electroporation voltages and concentrations of Cas9 : gRNA cRNP complexes. These results may be due to stochastic variations in the epigenetic state of each cell lineage that may impact editing efficiency at a given genomic loci, or cell-intrinsic differences in cell surface protein turnover following *in vitro* culture with specific activating cytokines. Future studies will be necessary to determine the mechanisms behind cell type specific electroporation and cRNP-editing efficiencies. Furthermore, utilization of gRNA sequences derived from recent whole genome based CRISPR-Cas9 KO libraries [73] suggests that many gRNAs have low KO efficiencies for certain genes tested (e.g. *Klrb1c*) when used as a cRNP complex to edit electroporated primary lymphocytes. Thus, whole genome based CRISPR screens in primary T cells may not accurately reflect KO efficiencies in primary innate immune cells and need to be verified independently with validated gRNA sequences in a cell type-specific manner. Together, our results reveal

important cell type specific differences that will need to be considered when performing cRNP-based gene editing in primary immune cells.

Although viral-based strategies have been used to elucidate novel gene regulatory networks in mouse bone marrow-derived dendritic cells [109, 110], these approaches require the use of transgenic Cas9 mouse strains and lentiviral or retroviral transduction (which induce cell death during selection of the CRISPR gRNA pool to achieve low multiplicity of infection). Because it is not well understood how the overall frequency of random mutagenic effects from stochastic viral integration into the host genome or high levels of cell death present in these cultures might affect native signaling pathways of CRSPR Cas9-edited dendritic cells *in vitro*, viral vector-based gene editing strategies may come with several caveats. Similarly, overexpression of both Cas9 and gRNA sequences could lead to prolonged gene editing activity of Cas9, leading to an increased chance of off-target effects [111, 112]. Our optimized cRNP genome editing approach in innate immune cells improves on viral based strategies by limiting cell death due to high efficiency gene deletion without the need for selection, and minimizes Cas9 off-target activity due to the rapid intracellular degradation of cRNP complexes [111, 112]. Furthermore, future studies coupling whole transcriptome sequencing with validated high indel-inducing cRNPs will eliminate the need for *in vitro* or *in vivo* whole genome CRISPR screens that would be otherwise impossible in rare innate immune cells, such as tissue-resident ILCs. Therefore, our studies provide a framework for efficient and practical gene editing that eliminates several key caveats from previous CRISPR gene editing approaches in innate immune cells.

Our study describes the use of two *in vivo* adoptive transfer models that can be used to elucidate the molecular mechanisms of memory NK cell formation and cDC1 responses to viral infection. However, cRNP-edited primary NK cells and bone marrow derived cDC precursors could be used in several additional *in vivo* models. For instance, *Ncr1*^{Cre} x *Eomes*$^{fl/fl}$ mice selectively lack circulating NK cells [113], and could be used with adoptively transferred cRNP-edited NK cells to precisely understand the gene regulatory networks induced during anti-tumor responses, obesity, and fetal development [114-116]. In addition, we observed congenically distinct cDC2 in peripheral organs of WT mice following adoptive transfer of D9 BMDC i.v. (data not shown). Adoptive transfer of D9 BMDC into cDC2-deficient mice, such as *Zbtb46*^{Cre} x *Irf4*$^{fl/fl}$ [117], could potentially be used to elucidate cDC2-specific gene regulatory networks *in vivo.* Furthermore, mouse models of inducible monocyte-macrophage deletion, such as *Lyz2*^{Cre} x *Csf1r*$^{LsL\text{-}DTR}$ [118], might also be able to be reconstituted with cRNP-edited bone marrow derived macrophages to elucidate macrophage specific gene networks *in vivo*, although future work will be necessary to confirm these proposed models. Together, a wide variety of *in vivo* models of lineage-specific ablation can be coupled with cRNP-edited primary innate immune cells to overcome previous experimental limitations of gene deletion in specific innate immune lineages *in vivo*.

Our finding that XCR1^{+} cDC1 are sufficient and necessary to protect against MCMV infection is supported by previous studies demonstrating *Batf3* and *Irf8*-dependent cDC1 are essential for host protection during viral infection [3, 89]. However, our results expand on these previous findings because the roles of *Batf3* and *Irf8* in cDC2 are not well defined and could not be previously excluded during host responses to viral infection.

Similarly, recent studies have suggested that TLR7/9 signaling through MyD88 in $CD11c^+$ cells is required for host protection against MCMV [108]. Because CD11c is expressed in TLR7/9-expressing macrophages, cDC1, and cDC2 [90] Immgen), our results using cRNP-edited cells suggest that cDC1 expression of MyD88 is sufficient for host protection to MCMV. MyD88 signaling likely acts upstream of IL-12 production in cDC1, which is essential for group 1 ILC production of IFN-γ to suppress viral replication and confer host protection at initial sites of infection [3]. Thus, cRNP-mediated gene editing serves as a useful approach to rapidly elucidate gene function in the innate immune system *in vivo*. This general gene editing strategy may be further adapted in future studies to other primary immune cell types and *in vivo* transfer models to investigate protective or pathologic biological processes in the mammalian innate immune system.

Acknowledgements

We thank members of the O'Sullivan, Lanier, Fregoso, and Sun labs for helpful discussion. A.D.H was supported by the Ruth L. Kirschstein National Research Service Award AI007323. T.E.O. was supported by the NIH (P30DK063491, AI145997).

The authors declare no financial conflicts of interest.

Author Contributions

L.R., A.D.H., and T.E.O. designed the study; A.D.H., L.R., M.R., Y.W., W.S., C.H., and R.S. performed the experiments; T.E.O., L.R., and A.D.H. wrote the manuscript.

Competing Interests Statement

The authors declare no competing interests.

Figure 1. Optimized electroporation of Cas9 in mouse splenic leukocytes.

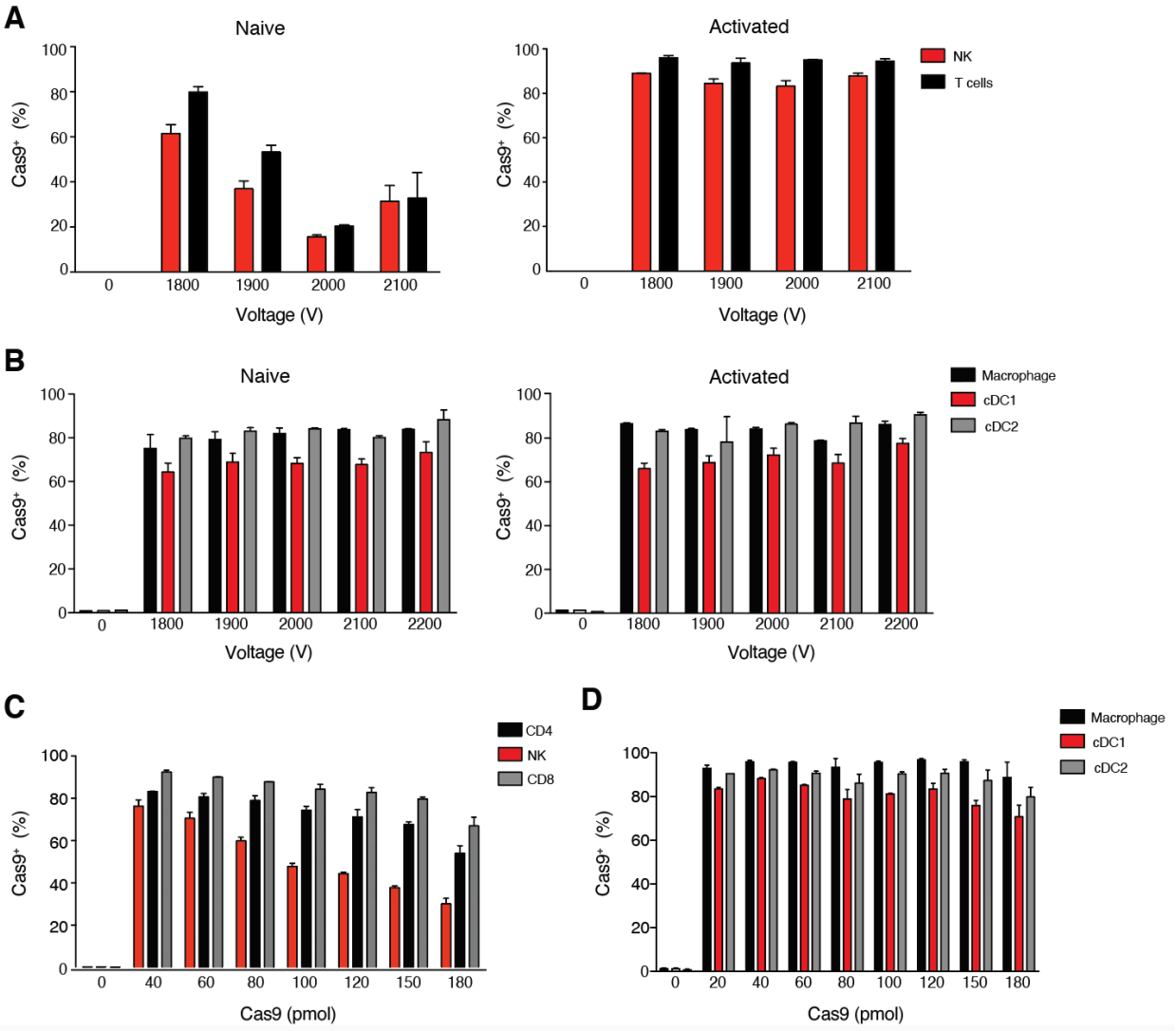

(**A-B**) Mouse splenocytes were either freshly harvested (naïve) or cultured for 16 hours with mouse IL-15 (activated NK and T cells), FLT3-L (activated cDC1, cDC2), or M-CSF (activated macrophage) in complete media and subsequently electroporated in the presence of 40pMol Cas9 protein. Frequency of intracellular Cas9$^+$ naïve and activated (**A**) NK (TCRβ$^-$CD3$^-$NK1.1$^+$), T cells (TCRβ$^+$CD3$^+$NK1.1$^-$), (**B**) macrophages (TCRβ$^-$CD3$^-$NK1.1$^-$CD64$^+$CD11b$^+$), cDC1 (TCRβ$^-$CD3$^-$NK1.1$^-$CD64$^-$CD11b$^-$XCR1$^+$), and cDC2 (TCRβ$^-$CD3$^-$NK1.1$^-$CD64$^-$CD11b$^+$XCR1$^-$) following electroporation at the indicated

voltages (**C-D**) Splenocytes were either freshly harvested (macrophage, cDC1, cDC2) or cultured for 16 hours with mouse IL-15 (NK, $CD4^+$, $CD8^+$ T cells) and subsequently electroporated in the presence of various amounts of Cas9 protein. Frequency of intracellular $Cas9^+$ (**C**) activated NK, $CD4^+$ T ($TCR\beta^+CD3^+CD4^+NK1.1^-$), $CD8^+$ T cells ($TCR\beta^+CD3^+CD8^+NK1.1^-$), (**D**) naïve macrophages, cDC1, and cDC2 following electroporation at 1900V in the presence of the indicated concentration of Cas9 protein. Data are representative of 2 independent experiments of 3 mice per group.

Figure 2. Efficient cRNP complex-mediated gene deletion in primary mouse group 1 ILC's.

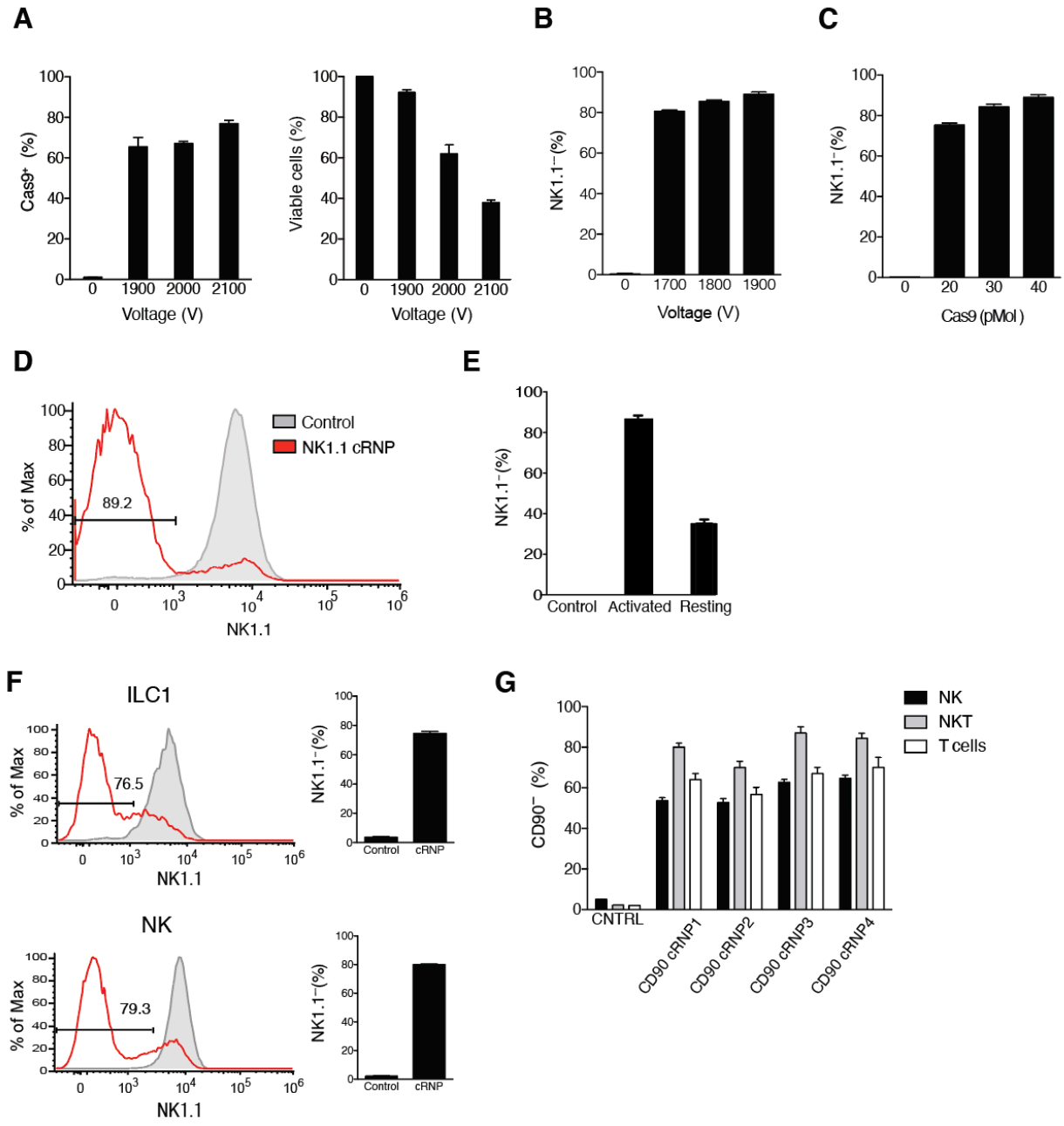

(A-E) Purified splenic NK cells were cultured for 16 hours with mouse IL-15 in complete media or freshly isolated before electroporation. **(A)** Frequency of intracellular Cas9^{+} NK cells and percent viable NK cells 2 hours following electroporation of 5 x 10^{5} IL-15 pre-activated NK cells each at the indicated voltages compared to un-electroporated controls.

(**B-C**) Percentage of NK1.1^{-} IL-15 pre-activated NK cells 3 days after electroporation of with 40 pMol Cas9 : 120 pMol gRNA *Klrb1c* cRNP complex compared to un-electroporated controls with (**B)** varying voltages or **(C)** concentrations of Cas9 in the *Klrb1c* cRNP complex. **(D)** Representative histogram of NK1.1 expression and (**E**) Percentage of NK1.1^{-} NK cells 3 days after electroporation of 5 x 10^5 IL-15 pre-activated activated or freshly isolated naive cells compared to un-electroporated controls. **(F)** Representative histograms and frequency of NK1.1 expression 3 days after electroporation of 2.5 x 10^5 IL-15 pre-activated purified liver NK cells (TCRβ^{-}CD3^{-} NK1.1^{+}CD49b^{+}CD200r^{-}) or ILC1 (TCRβ^{-}CD3^{-}NK1.1^{+}CD49b^{-}CD200r^{+}) with 40 pMol Cas9 : 120pMol gRNA *Klrb1c* cRNP complex compared to un-electroporated controls. **(G)** Percentage of indicated CD90^{-} cells 3 days after electroporation of 2.5 x 10^5 IL-15 pre-activated activated liver NK, NKT (TCRβ^{+}CD3^{+}NK1.1^{+}) and T cells with various 40 pMol Cas9:120pMol gRNA *Thy1.2* cRNP complexes compared to un-electroporated controls. Data are representative of 3 independent experiments of 3 mice per group.

Figure 3. High efficiency gene deletion of primary and bone marrow-derived myeloid cells using cRNP complexes.

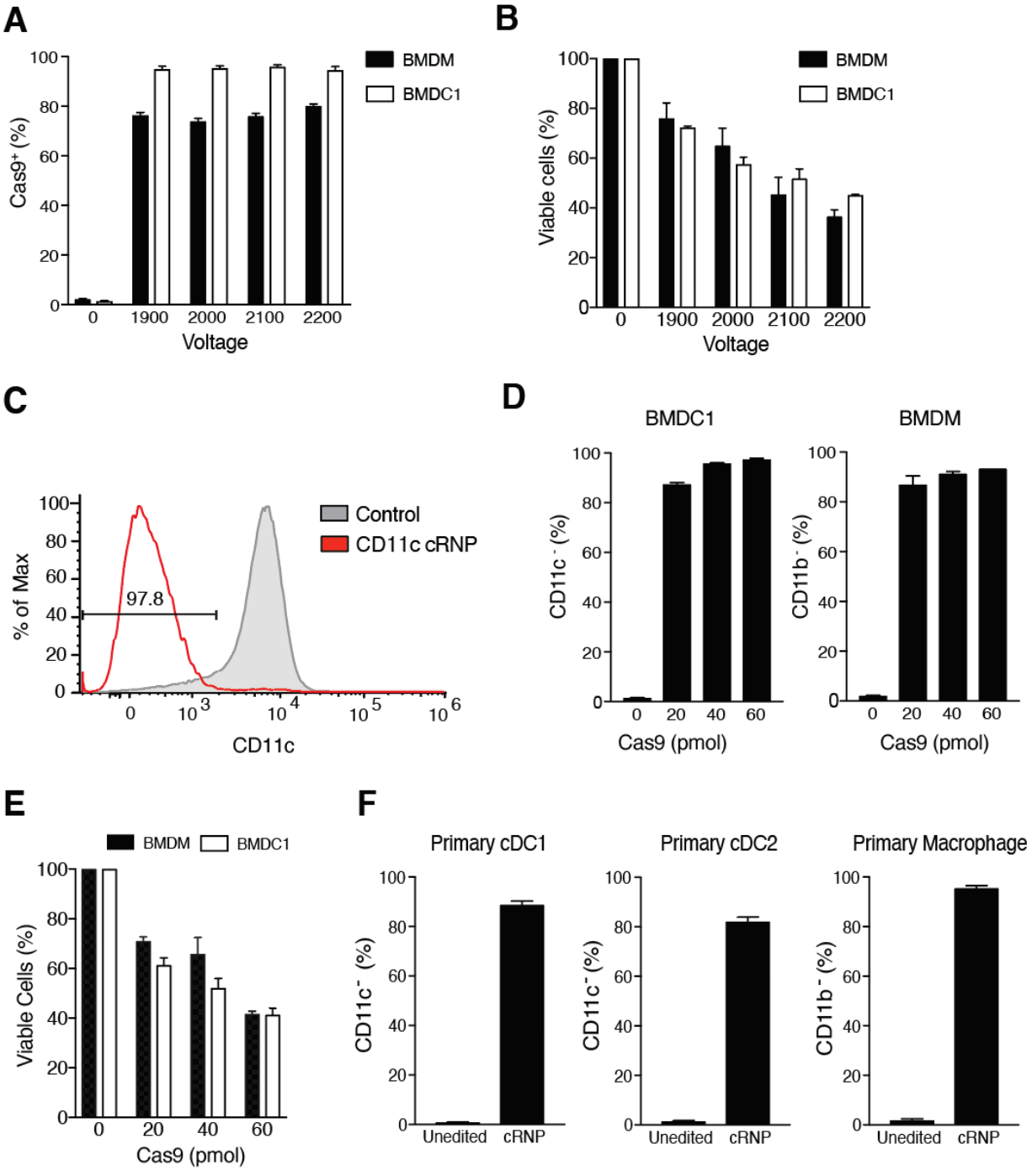

(A) Frequency of intracellular Cas9⁺ bone marrow-derived macrophage (BMDM) or bone marrow-derived cDC1 (BMDC1) 2 hours post-electroporation with 40pMol Cas9. **(B)**

Percent of viable BMDM or BMDC1 4 or 6 days, respectively, after electroporation of 1 x 10^6 cells at indicated voltages with or without Cas9. **(C-F)** BMDC or BMDM were electroporated at 1900V in the presence of 40pMol Cas9 : 120pMol gRNA unless indicated otherwise. **(C)** Representative histogram of CD11c expression 6 days after electroporation of 1 x 10^6 BMDC1. **(D)** Percent of $CD11c^-$ BMDC1 and $CD11b^-$ BMDM and (**E**) viable cells 4 or 6 days, respectively, post electroporation of 1 x 10^6 cells at the indicated concentrations of Cas9 present in cRNP complex. **(F)** Frequencies of primary splenic $CD11c^-$ cDC1, cDC2 and $CD11b^-$ macrophages 4 days post electroporation. Data are representative of 3 independent experiments or 3 mice per group.

Figure 4. cRNP complex-mediated double gene ablation in ILCs and myeloid cells.

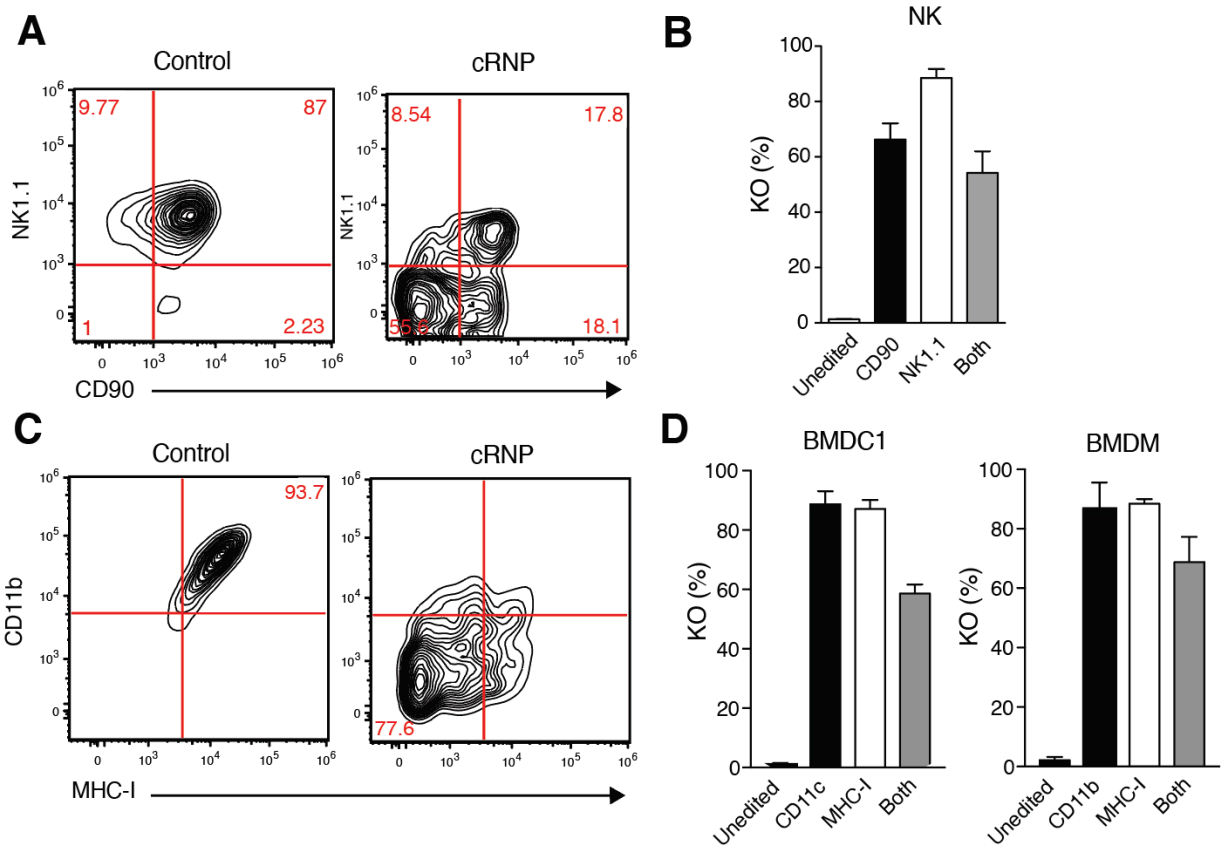

(A-D) NK cells, BMDC and BMDM were electroporated at 1900V in the presence of 40pMol Cas9 : 120pMol gRNA cRNP1 and 40pMol Cas9 : 120pMol gRNA cRNP2 complexes **(A)** Representative flow plots of NK cell NK1.1 and CD90 expression 3 days after electroporation of 5 x 10^5 cells (right) or control un-electroporated cells (left). **(B)** Percent of NK1.1$^-$, CD90$^-$ or NK1.1$^-$ and CD90$^-$ ("Both") NK cells **(C-D)** BMDM and BMDC1 were stimulated with 20ng/mL IFN-γ for 48h *in vitro* **(C)** Representative flow plots of BMDM CD11b and MHC-I expression 4 days after electroporation of 1 x 10^6 cells (right) or control un-electroporated cells (left). **(D)** Percent of CD11c$^-$, MHC-I$^-$, or CD11c$^-$ and MHC-I$^-$ ("Both") BMDC1 cells 6 days after electroporation of 1 x 10^6 cells (left). Percent of

CD11b^{-}, MHC-I^{-}, or CD11b^{-} and MHC-I^{-} (“Both”) BMDM cells depicted in (C) (right). Data are representative of 2 independent experiments of 3 mice per group.

Figure 5. cRNP-edited innate immune cells are functionally deficient *in vitro*

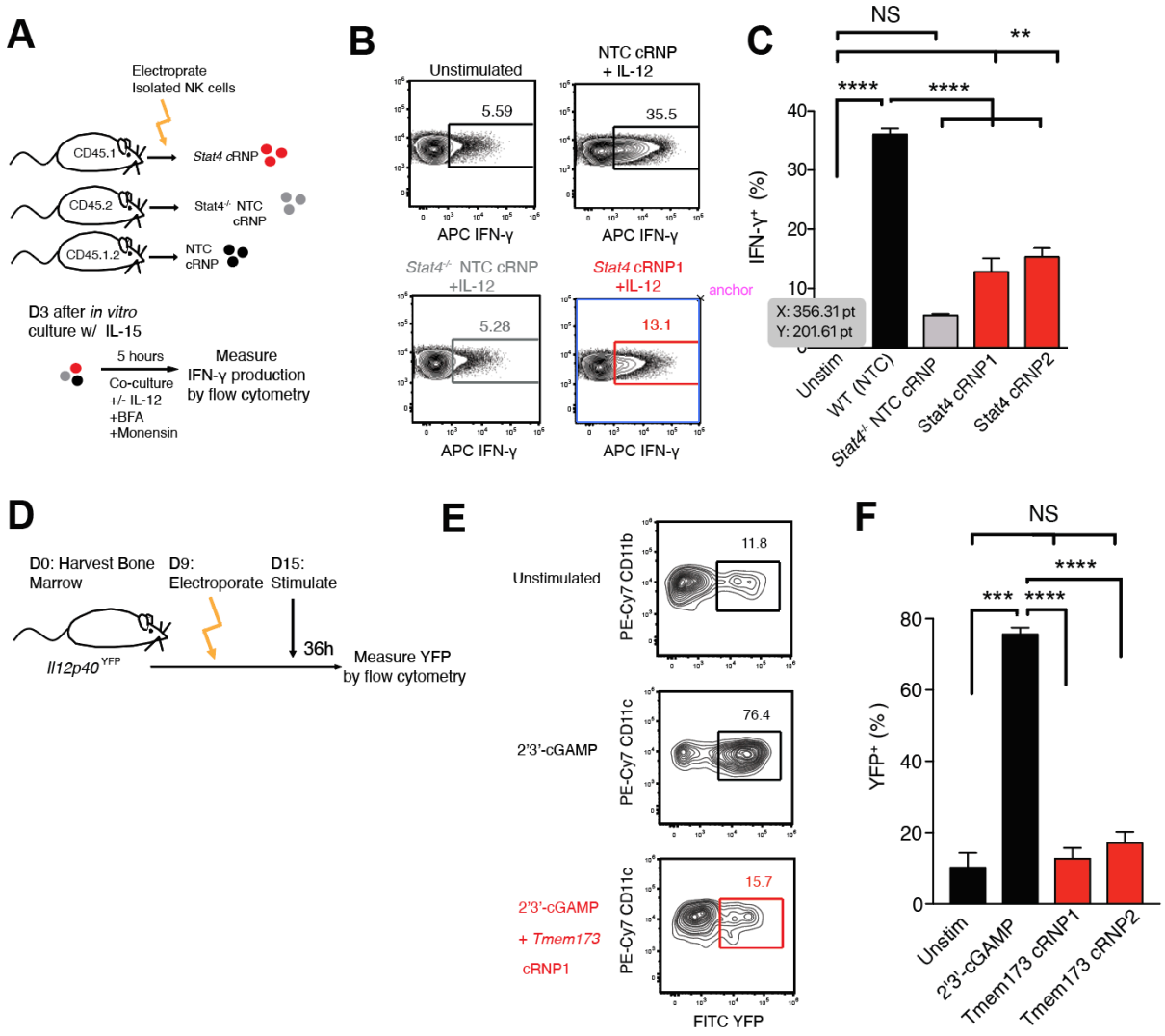

(A-C) Briefly, congenically distinct purified NK cells from WT (CD45.1, CD45.1 x CD45.2) or *Stat4*$^{-/-}$ (CD45.2) mice were electroporated at 1900V in the presence of either *Rosa26* cRNP (NTC) or *Stat4* cRNP complexes, mixed and equal ratios, and cultured in vitro with IL-15 for 3 days before stimulation with our without IL-12 in the presence of brefeldin A and monensin (**A**) Schematic of experiment **(B)** Representative flow plots of intracellular IFN-γ expression in IL-12 stimulated NTC cRNP-edited, *Stat4* cRNP-edited NK cells, and NTC cRNP-edited *Stat4*$^{-/-}$ NK cells 5 hours following stimulation **(C)** Percentage of IFN-

γ^{+} cells for indicated experimental groups **(D-F)** Briefly, *Il12p40*^{YFP} D9 BMDC were either electroporated in the presence or absence of *Tmem173* cRNP complexes and cultured for an additional 6 days in DC medium before stimulation with DC media (unstim) or DC media containing 2'3'-cGAMP for 36 hours. (**D**) Schematic of experiment. **(E)** Representative flow plots of cDC1 YFP production from unstimulated, 2'3'-cGAMP stimulated, and *Tmem173* cRNP-edited + 2'3'-cGAMP stimulated conditions. **(F)** Percentage of YFP^{+} cDC1 shown for indicated conditions. Data are representative of 2 independent experiments of 3 mice per group. Samples were compared using an unpaired, two-tailed Student's t test with Welch's correction, and data are presented as the mean ± SEM (**p < 0.01,***p < 0.001, ****p < 0.0001).

Figure 6. cRNP-edited innate immune cells can be used to elucidate antiviral gene function *in vivo*

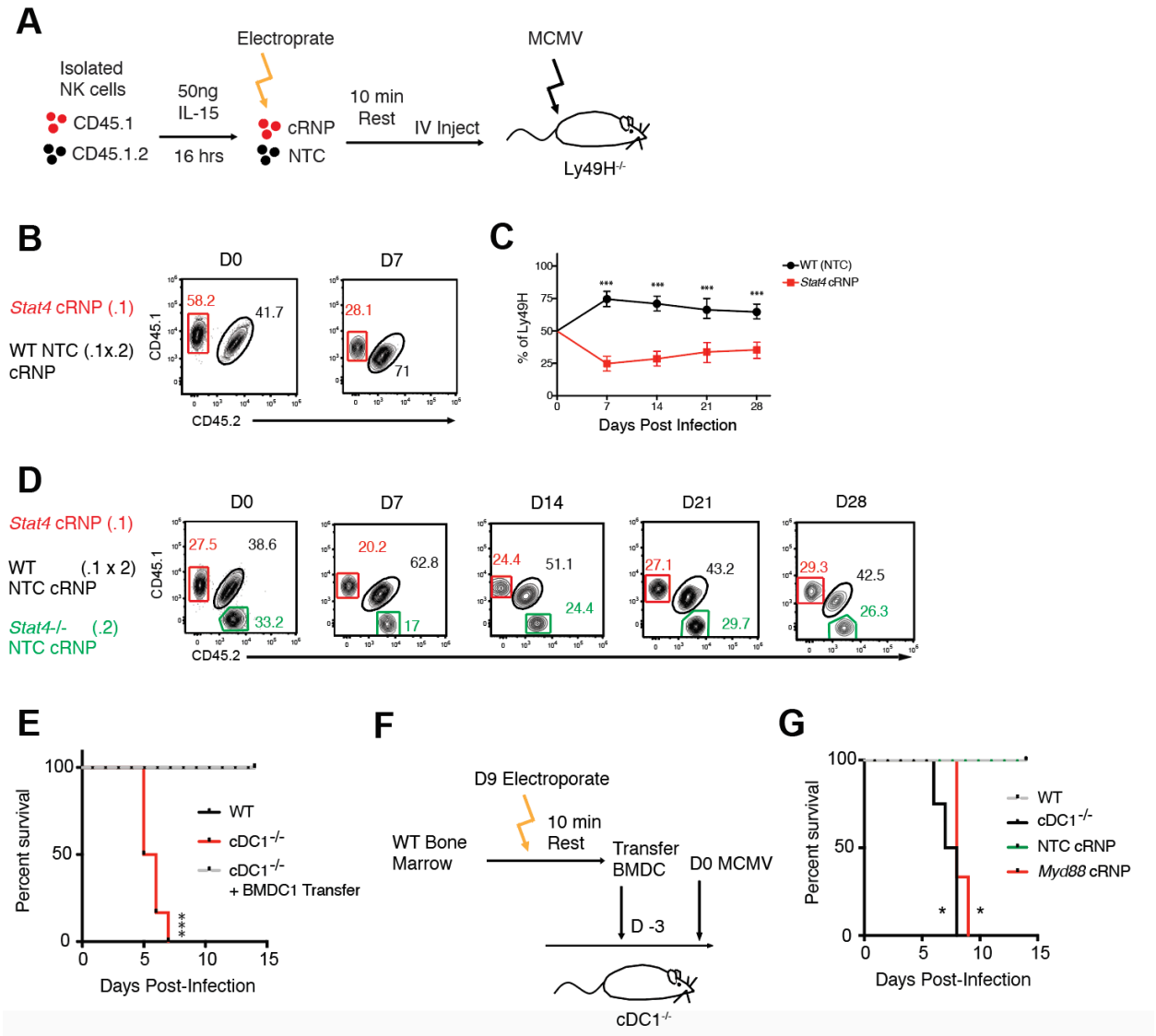

(A-C) IL-15 pre-activated splenic WT Ly49H$^+$ NK cells were electroporated in the presence of either *Rosa26* cRNP (NTC) (CD45.1 x CD45.2) or *Stat4* cRNP complexes (CD45.1) and adoptively transferred i.v. into Ly49H-deficient recipients at a 1:1 ratio. Recipient mice were infected i.p with MCMV 16 hours after adoptive transfer. (**A**) Schematic of experiment. **(B)** Representative flow plots of indicated Ly49H$^+$ NK cells pre-injection (left) and at D7 P.I. (right). **(C)** Quantification of adoptively transferred Ly49H$^+$

Rosa26 cRNP (NTC) or *Stat4* cRNP-edited NK cells in the blood of recipient mice at various timepoints P.I. (**D**) IL-15 pre-activated splenic WT Ly49H^{+} NK cells or Stat4$^{-/-}$ (CD45.2) were electroporated in the presence of either *Rosa26* cRNP (NTC) (CD45.1 x CD45.2) or *Stat4* cRNP complexes (CD45.1) and adoptively transferred i.v. into Ly49H-deficient recipients at a 1:1:1 ratio and subsequently infected with MCMV. Representative flow plots of blood Ly49H^{+} NK cells pre-injection and at indicated days P.I. (**E**) WT or cDC1$^{-/-}$ mice were infected with MCMV i.p. Kaplan-Meier survival curves of each indicated cohort. **(F,G)** Briefly, 1 x 10^{7} D9 BMDC were electroporated in the presence of either *Rosa26* cRNP (NTC) or *Myd88* cRNP complexes and transferred into recipient cDC1$^{-/-}$ mice 3 days before MCMV infection. **(F)** Schematic of experiment. **(G)** Kaplan-Meier survival curves of each indicated cohort. Data are representative of 2 independent experiments of n = 3-4 mice per group (*$p < 0.05$, ***$p < 0.001$).

Extended Data Figure 1. Optimization of electroporation conditions for Cas9 in primary leukocytes

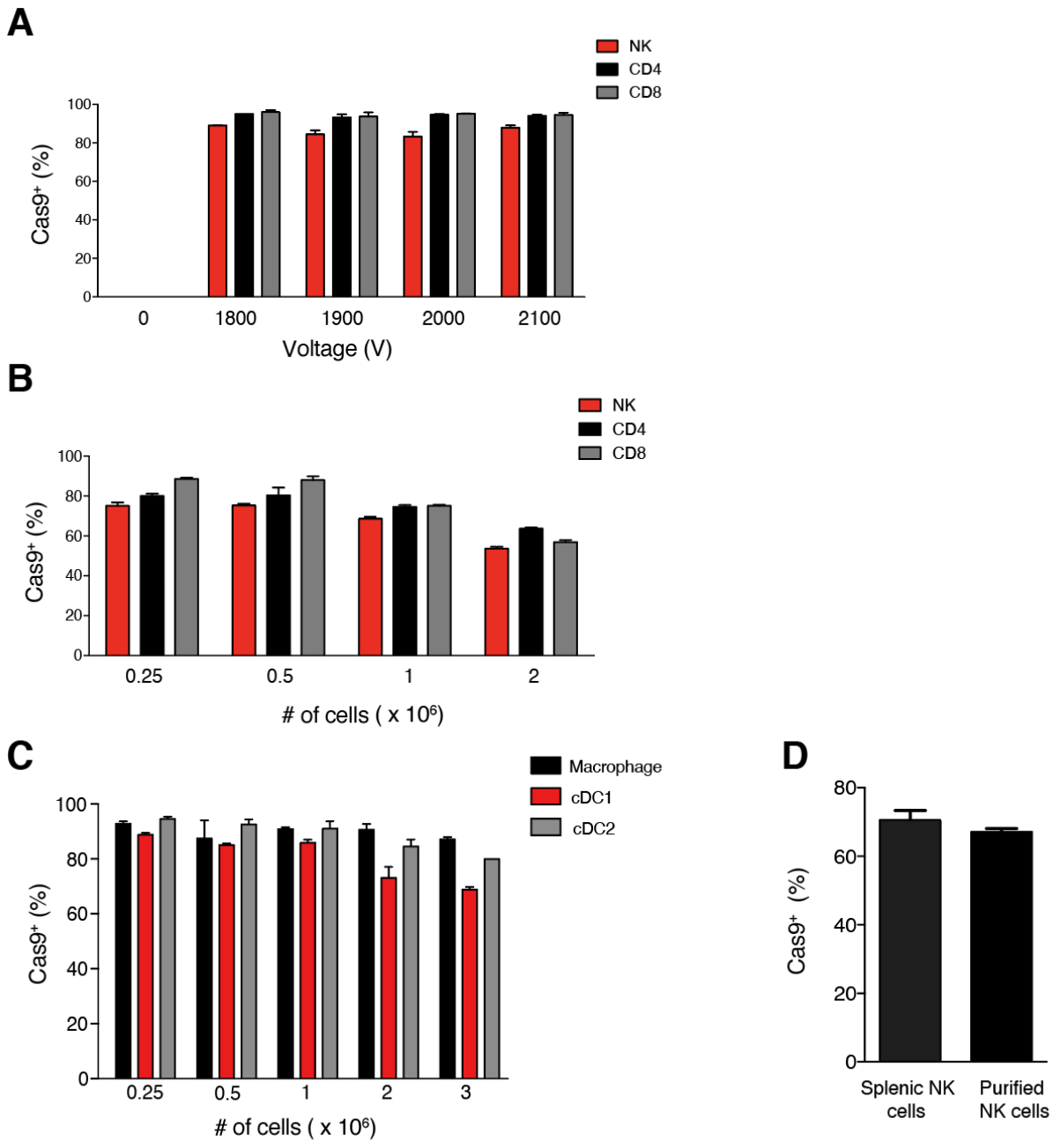

(A-D) Mouse splenocytes were either freshly harvested (naïve) or cultured for 16 hours with mouse IL-15 (activated NK and T cells) in complete media and subsequently electroporated in the presence of 40pMol Cas9 protein. **(A)** Frequency of

intracellular Cas9$^+$ activated primary NK, CD4$^+$ T, and CD8$^+$ T cells following electroporation at the indicated voltages. Frequency of intracellular Cas9$^+$ **(B)** activated NK, CD4$^+$ T, and CD8$^+$ T cells or **(C)** naive splenic macrophages, cDC1, and cDC2 following electroporation at the indicated cell numbers. **(D)** Frequency of intracellular Cas9$^+$ NK cells following electroporation of bulk splenocytes or purified NK cells. Data are representative of 2 independent experiments of 3 mice per group.

Extended Data Figure 2. Optimization of cRNP-mediated gene editing in primary NK cells.

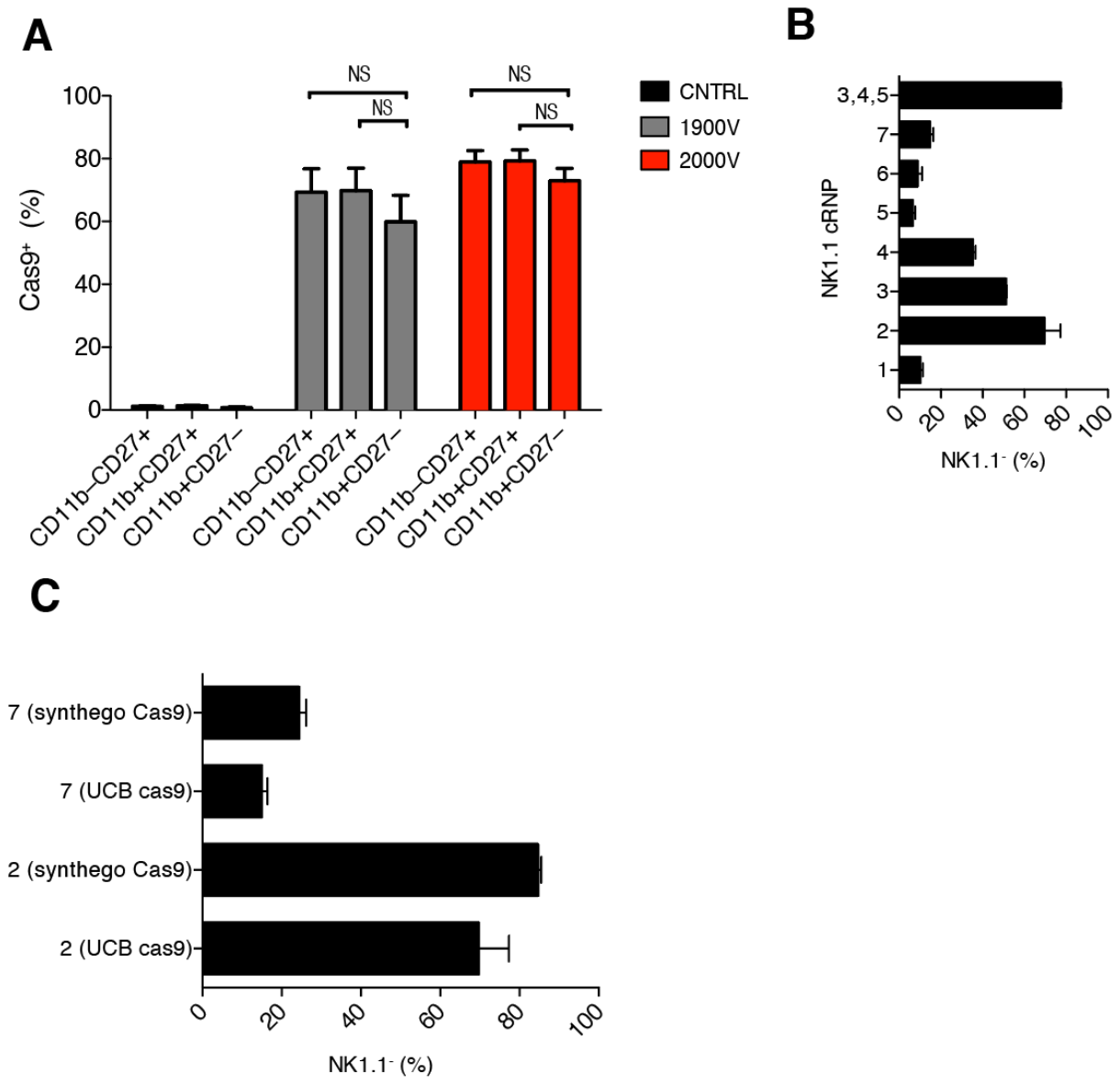

(A-C) Purified splenic NK cells were cultured for 16 hours with rmIL-15 in complete media. **(A)** Frequency of intracellular $Cas9^+$ activated NK cell subpopulations after electroporation at the indicated voltages. **(B)** Percent of $NK1.1^-$ NK cells 3 days after electroporation of 5 x 10^5 activated NK cells in the presence of various NK1.1 cRNP complexes. **(C)** Percent of $NK1.1^-$ NK cells 3 days after electroporation of 5 x 10^5 activated

NK cells in the presence of selected guides and Cas9 from different manufacturers. Data are representative of 2 independent experiments of 3-5 mice per group. Samples were compared using an unpaired, two-tailed Student's t test with Welch's correction, and data are presented as the mean ± SEM.

Extended Data Figure 3. cRNP-editing of BMDC1 does not cause phenotypic defects or spontaneous activation

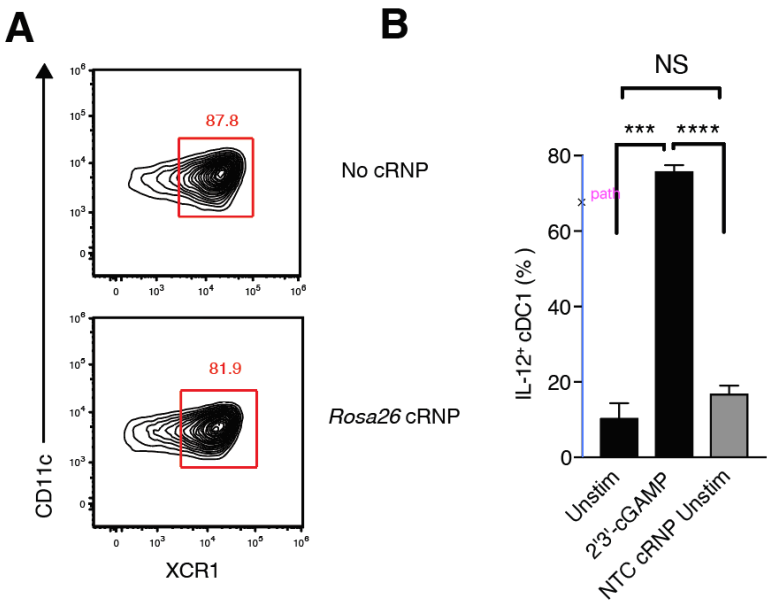

Briefly, *Il12p40*^{YFP} D9 BMDC were either electroporated in the presence or absence of *Rosa26* cRNP complexes and cultured for an additional 6 days in DC medium before stimulation with DC media (unstim) or DC media containing 2'3'-cGAMP for 36 hours. **(A)** Representative flow plots of un-edited or *Rosa26* cRNP-edited BMDC1 phenotypes. **(B)** Percentage of IL-12^{+} cDC1 shown for indicated conditions. Data are representative of 2 independent experiments of 3 mice per group. Samples were compared using an unpaired, two-tailed Student's t test with Welch's correction, and data are presented as the mean ± SEM (*$p < 0.05$, **$p < 0.01$,***$p < 0.001$, ****$p < 0.0001$).

Extended Data Figure 4. Adoptively transferred Ly49H$^+$ *Rosa26* (NTC) cRNP-edited NK cells do not display differences during MCMV infection (A-B)

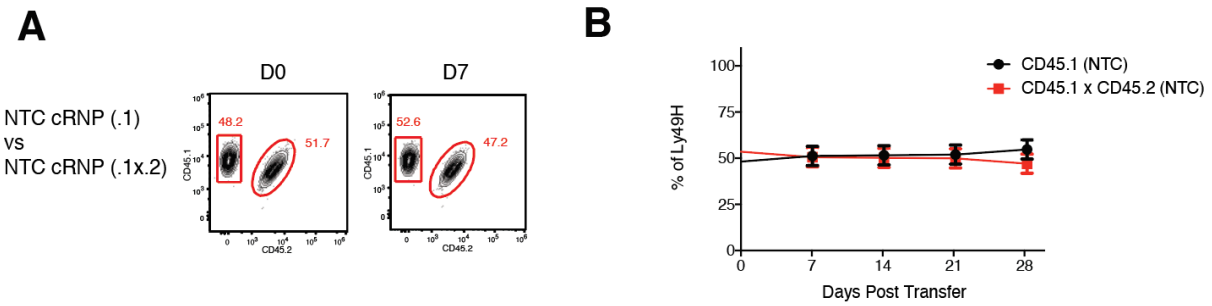

IL-15 pre-activated congenically distinct NK cells were electroporated in the presence of *Rosa26* NTC cRNP before being transferred i.v. into Ly49H-deficient recipients at a 1:1 ratio. **(A)** Representative flow plots of NTC cRNP-edited NK cells pre-injection (left) and from blood Ly49H$^+$ NK cells D7 P.I. with MCMV (right). **(B)** Frequencies of indicated blood Ly49H$^+$ NK cells at indicated days PI. Data are representative of 2 independent experiments of 3 mice per group.

Extended Data Figure 5. Reconstitution of cDC1$^{-/-}$ mice with congenically distinct BMDC.

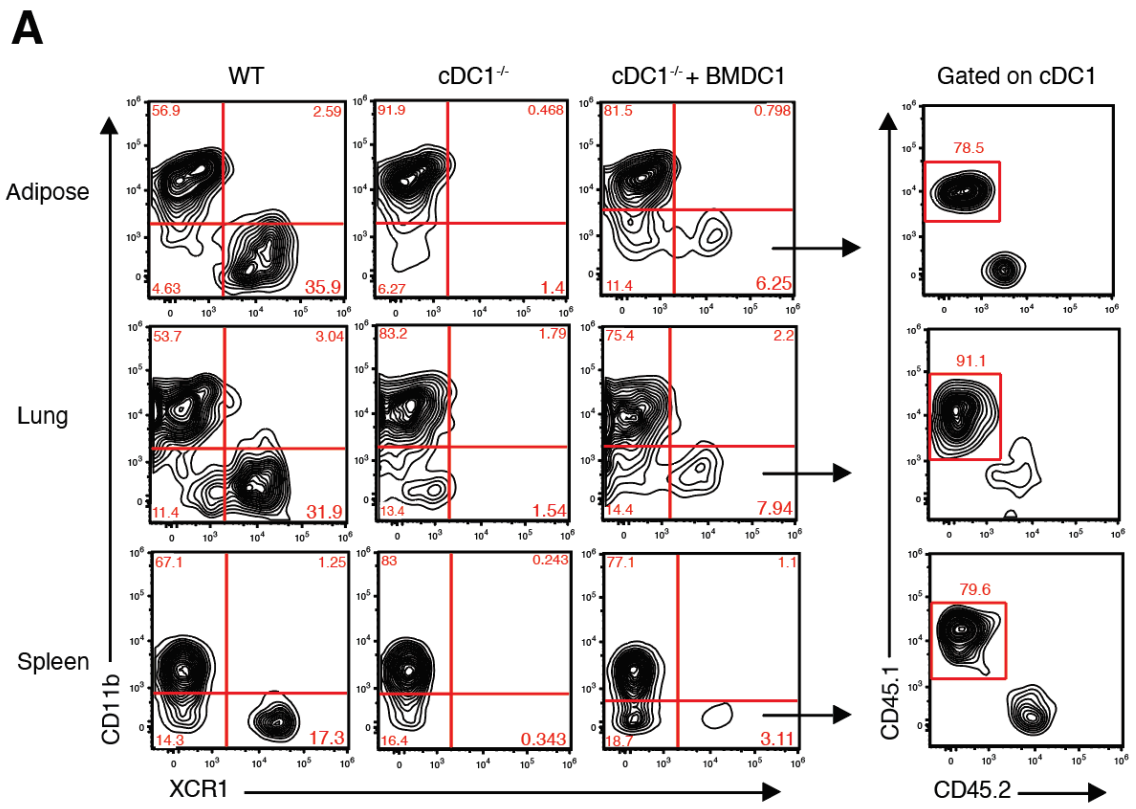

(A) Representative flow plots showing conventional dendritic cell populations from the adipose tissue, spleen, and lungs of WT, cDC1$^{-/-}$, and cDC1$^{-/-}$ mice reconstituted with 1 x 10^7 CD45.1 D9 BMDC. Tissues were isolated and analyzed 4 days after transfer. Data are representative of 2 independent experiments of 3 mice per group.

Methods

Mice

Mice were bred at UCLA in accordance with the guidelines of the institutional Animal Care and Use Committee (IACUC). The following mouse strains were used this study: C57BL/6 (CD45.2) (Jackson Labs, #000664), B6.SJL (CD45.1) (Jackson Labs, #002114), *Klra8*$^{-/-}$ (Ly49H-deficient), *Il12b*$^{tm1.1Lky}$*/J (Il12p40*^{YFP}*), Xcr1-Cre* [93], *Rosa26-LSL-DTA*, and *Stat4*$^{-/-}$. Experiments were conducted using 6-8 week old age- and gender-matched mice in accordance with approved institutional protocols.

Viruses and In vivo Infection Models

MCMV (Smith) was serially passaged through BALB/c hosts three times, and then salivary gland viral stocks were prepared with a dounce homogenizer for dissociating the salivary glands of infected mice 3 weeks after infection. Experimental mice in studies were infected with MCMV by i.p. injection of 7.5 x 10^3 plaque-forming units (PFU) in 0.5 mL of PBS.

Isolation of mouse leukocytes

Mouse spleens, livers, lungs, adipose tissue and bone marrow were harvested and prepared into single cell suspensions as described previously [3, 101]. For purified NK and ILC1 isolation, liver or splenic single cell suspensions were resuspended in EasySep™ buffer (Stemcell) and processed using the EasySep™ Mouse NK Cell Isolation Kit according to the manufacturers protocol. Isolated cells were then cultured in CR-10 (RMPI 1640 + 25 mM HEPES + 10% FBS, 1% L-glutamine, 1% 200 mM sodium pyruvate, 1%

MEM-NEAA, 1% penicillin-streptomycin, 0.5% sodium bicarbonate, 0.01% 55 mM 2-mercaptoethanol) supplemented with 50ng rmIL-15 (Peprotech).

In vitro bone marrow-derived macrophages and cDC1 culture

To generate bone marrow derived macrophages and dendritic cells, bone marrow leukocytes were resuspended at $1.5x10^7$ cells/10mL in DC media (RMPI 1640 + 25mM HEPES + 10% FBS, 1% L-glutamine, 1% 200mM sodium pyruvate, 1% MEM-NEAA, 1% penicillin-streptomycin, 0.5% sodium bicarbonate, 0.01% 55 mM 2-mercaptoethanol supplemented with 200 ng/mL FLT3-L and 50 ng/mL GM-CSF) or macrophage media (DMEM + 10%FBS, 1% L-glutamine, 1% penicillin-streptomycin, 0.5% sodium pyruvate, supplemented with 50 ng/ml M-CSF and then plated in 10cm non-TC treated culture dishes (Corning). BMDC were cultured for 9 days in DC media with an additional 5 mL of DC media added on D5. Media was changed on D9 and BMDC1 were used for experiments on D15 as described previously [119]. BMDM are cultured for 7 days in macrophage media, with a media change on D3.

Guide RNA Design

Synthetic gRNAs were purchased from SYNTHEGO. gRNA sequences were derived from a mouse whole genome CRISPR library described previously [73]. 10 gRNA sequences from this dataset were ranked according to predicted indel percentage and low off-target score using the inDelphi machine-learning algorithm for each gene target [74]. The top 3-7 guides were validated for high indel percentages by sanger sequencing before utilization in experiments.

cRNP complex formation

gRNAs (Synthego) were diluted to 100μM (100 pMol/μL) in 1x TE buffer. 1.2uL (120 pMol) of gRNA, 0.9uL of 100μM Alt-R® Cas9 Electroporation Enhancer (IDT) and 3.9 uL water were added to a 1.5mL tube per sample for a total of 6μL. 2μL of recombinant Cas9 (Synthego or QB3 Macrolab) was added to 4μL water in a separate 1.5mL tube. 6μL of diluted Cas9 was added to 6μL of gRNA-enhancer mixture for a total of 12μL cRNP complex at a 1:3 molar ratio. The cRNP complex was allowed to incubate for at least 10 minutes at room temperature (RT). For double KO experiments, 3μL of diluted Cas9 was added to 3μL of each gRNA-enhancer mixture at a 1:3 molar ratio and complexed separately at RT.

Electroporation

cRNP complexes and 5 x 10^5 - 3 x 10^6 leukocytes resuspended in 100μL of Buffer T were mixed and electroporated using the Neon Transfection system (Thermo-Fisher) at pulse code (20ms x 1 pulse) using 100ul Neon tips (Thermo-Fisher) at various voltages (1800-2200V). Immediately following electroporation, cells were slowly pipetted into 1.5mL Eppendorf tubes containing pre-warmed culture media (CR-10 with 50ng rmIL-15 for NK cells, DC media, or Macrophage media) and inverted several times to dilute the T buffer. Cells were then incubated at 37^0C for 90 minutes before centrifugation and resuspension in cell specific media before culturing *in vitro*. Cells were cultured *in vitro* for 3-6 days following electroporation prior to reading out gene editing efficiency by flow cytometry or sanger sequencing.

Adoptive transfer experiments

BMDC were cultured until D9 and then 1 x 10^7 cells were transferred i.v. into recipient cDC1$^{-/-}$ mice 3 days before MCMV infection. In other experiments, BMDC were cultured *in vitro* until D9, electroporated and then rested for 10 minutes and 5 x 10^6 cells were transferred into cDC1$^{-/-}$ recipient mice 3 days before MCMV infection. Adoptive NK cell co-transfer studies were performed by injecting a total of 1 x 10^6 NK cells; *Rosa26* cRNP-edited *Stat4*$^{-/-}$, *Rosa26* cRNP-edited WT, and *Stat4* cRNP-edited WT NK cells purified from spleens of congenically distinct WT mice (CD45.1, CD45.1.2 or CD45.2) into *Klra8*$^{-/-}$ mice 16 hours prior to MCMV infection.

Flow Cytometry

Cells were analyzed for cell-surface markers using fluorophore-conjugated antibodies (BioLegend, eBioscience,). Cell surface staining was performed in 1x PBS and intracellular staining was performed using the eBioscience Foxp3/Transcription Factor Kit. Flow cytometry was performed using the Attune NxT and data were analyzed with FlowJo software (Tree Star). Cell surface and intracellular staining was performed using the following fluorophore-conjugated antibodies: CD45.1 (A20), CD45.2 (104), NK1.1 (PK136), CD49b (DX5), KLRG1 (2F1), TCRβ (H57-597), CD3 (17A2), Ly49H (3D10), CD200r1 (OX-110), CD8α (53–6.7), CD4 (GK1.5), IFN-γ (XMG1.2), I-A/I-E (M5/114.15.2), CD19 (ID3), CD11c (N418), CD11b (M1/70), CD64 (X54-5/7.1), XCR1 (Zet), Ly6G (1A8), and Cas9 (7A9-3A3 Cell Signaling Technology).

Ex vivo stimulation of lymphocytes

~5 x 10^5 NK cells were stimulated for 5 hours in CR-10 containing 50ng/mL rmIL-15, Brefeldin A (1:1000; BioLegend) and Monensin (2uM; BioLegend) with or without recombinant mouse IL-12 (20 ng/ml; Peprotech). ~1 x 10^6 BMDC1 were stimulated for 36h in DC media with or without 2'3'-cGAMP (5 µg/mL; InvovGen). Cells were cultured in media alone as a negative control.

PCR and Sanger Sequencing:

DNA from primary leukocytes was isolated using the DNeasy Blood and Tissue kits (Qiagen). DNA concentration was measured using the NanoDrop OneC Microvolume UV-Vis Spectrophotometer (Thermo Scientific) and then diluted to 50 ng/µl in water before PCR amplification of cRNP-targeted genomic regions of approximately 500-1000 base paris. PCR samples from WT and cRNP-edited cells were submitted for sanger sequencing (GENEWIZ) and then indel percentage was calculated using ICE analysis (SYNTHEGO) (see Supplementary Table 1).

Statistical analyses

For graphs, data are shown as mean ± SEM, and unless otherwise indicated, statistical differences were evaluated using a Student's t test with Welch's correction to a assume a non-normal variance in our data distribution. $p < 0.05$ was considered significant. Graphs were produced and statistical analyses were performed using GraphPad Prism.

Data Availability

The data that support the findings of this study are available from the corresponding author upon request.

References

1. Wculek, S.K. *et al.* Dendritic cells in cancer immunology and immunotherapy. *Nat Rev Immunol* (2019).
2. Hildner, K. *et al.* Batf3 deficiency reveals a critical role for CD8alpha+ dendritic cells in cytotoxic T cell immunity. *Science* **322**, 1097-1100 (2008).
3. Weizman, O.E. *et al.* ILC1 Confer Early Host Protection at Initial Sites of Viral Infection. *Cell* **171**, 795-808 e712 (2017).
4. Vivier, E. *et al.* Innate Lymphoid Cells: 10 Years On. *Cell* **174**, 1054-1066 (2018).
5. Riggan, L., Freud, A.G. & O'Sullivan, T.E. True Detective: Unraveling Group 1 Innate Lymphocyte Heterogeneity. *Trends Immunol* **40**, 909-921 (2019).
6. Abram, C.L., Roberge, G.L., Hu, Y. & Lowell, C.A. Comparative analysis of the efficiency and specificity of myeloid-Cre deleting strains using ROSA-EYFP reporter mice. *J Immunol Methods* **408**, 89-100 (2014).
7. Satpathy, A.T. *et al.* Zbtb46 expression distinguishes classical dendritic cells and their committed progenitors from other immune lineages. *J Exp Med* **209**, 1135-1152 (2012).
8. Loschko, J. *et al.* Absence of MHC class II on cDCs results in microbial-dependent intestinal inflammation. *J Exp Med* **213**, 517-534 (2016).
9. Hemmi, H., Hoshino, K. & Kaisho, T. In Vivo Ablation of a Dendritic Cell Subset Expressing the Chemokine Receptor XCR1. *Methods Mol Biol* **1423**, 247-253 (2016).
10. Narni-Mancinelli, E. *et al.* Fate mapping analysis of lymphoid cells expressing the NKp46 cell surface receptor. *Proc Natl Acad Sci U S A* **108**, 18324-18329 (2011).
11. Oliphant, C.J. *et al.* MHCII-mediated dialog between group 2 innate lymphoid cells and CD4(+) T cells potentiates type 2 immunity and promotes parasitic helminth expulsion. *Immunity* **41**, 283-295 (2014)
12. Rankin, L.C. *et al.* Complementarity and redundancy of IL-22-producing innate lymphoid cells. *Nat Immunol* **17**, 179-186 (2016).

13. Simeonov, D.R. & Marson, A. CRISPR-Based Tools in Immunity. *Annu Rev Immunol* **37**, 571-597 (2019).
14. Pickar-Oliver, A. & Gersbach, C.A. The next generation of CRISPR-Cas technologies and applications. *Nat Rev Mol Cell Biol* **20**, 490-507 (2019).
15. Shifrut, E. *et al.* Genome-wide CRISPR Screens in Primary Human T Cells Reveal Key Regulators of Immune Function. *Cell* **175**, 1958-1971 e1915 (2018)
16. Farboud, B. *et al.* Enhanced Genome Editing with Cas9 Ribonucleoprotein in Diverse Cells and Organisms. *J Vis Exp* (2018).
17. Wu, C.M. *et al.* Genetic engineering in primary human B cells with CRISPR-Cas9 ribonucleoproteins. *J Immunol Methods* **457**, 33-40 (2018).
18. Seki, A. & Rutz, S. Optimized RNP transfection for highly efficient CRISPR/Cas9-mediated gene knockout in primary T cells. *J Exp Med* **215**, 985-997 (2018).
19. Nabekura, T., Riggan, L., Hildreth, A.D., O'Sullivan, T.E. & Shibuya, A. Type 1 Innate Lymphoid Cells Protect Mice from Acute Liver Injury via Interferon-gamma Secretion for Upregulating Bcl-xL Expression in Hepatocytes. *Immunity* (2019).
20. O'Sullivan, T.E. *et al.* Adipose-Resident Group 1 Innate Lymphoid Cells Promote Obesity-Associated Insulin Resistance. *Immunity* **45**, 428-441 (2016).
21. Fuchs, A. *et al.* Intraepithelial type 1 innate lymphoid cells are a unique subset of IL-12- and IL-15-responsive IFN-gamma-producing cells. *Immunity* **38**, 769-781 (2013).
22. Bernink, J.H. *et al.* Human type 1 innate lymphoid cells accumulate in inflamed mucosal tissues. *Nat Immunol* **14**, 221-229 (2013).
23. Sun, J.C. *et al.* Proinflammatory cytokine signaling required for the generation of natural killer cell memory. *J Exp Med* **209**, 947-954 (2012).

24. Marcus, A. *et al.* Tumor-Derived cGAMP Triggers a STING-Mediated Interferon Response in Non-tumor Cells to Activate the NK Cell Response. *Immunity* **49**, 754-763 e754 (2018)

25. Liu, Y. *et al.* An inhalable nanoparticulate STING agonist synergizes with radiotherapy to confer long-term control of lung metastases. *Nat Commun* **10**, 5108 (2019).

26. Sun, J.C., Beilke, J.N. & Lanier, L.L. Adaptive immune features of natural killer cells. *Nature* **457**, 557-561 (2009).

27. Ohta, T. *et al.* Crucial roles of XCR1-expressing dendritic cells and the XCR1-XCL1 chemokine axis in intestinal immune homeostasis. *Sci Rep* **6**, 23505 (2016).

28. Puttur, F. *et al.* Conventional Dendritic Cells Confer Protection against Mouse Cytomegalovirus Infection via TLR9 and MyD88 Signaling. *Cell Rep* **17**, 1113-1127 (2016).

29. Wang, T. *et al.* Gene Essentiality Profiling Reveals Gene Networks and Synthetic Lethal Interactions with Oncogenic Ras. *Cell* **168**, 890-903 e815 (2017).

30. Parnas, O. *et al.* A Genome-wide CRISPR Screen in Primary Immune Cells to Dissect Regulatory Networks. *Cell* **162**, 675-686 (2015).

31. Theisen, D.J. *et al.* WDFY4 is required for cross-presentation in response to viral and tumor antigens. *Science* **362**, 694-699 (2018).

32. Kim, S., Kim, D., Cho, S.W., Kim, J. & Kim, J.S. Highly efficient RNA-guided genome editing in human cells via delivery of purified Cas9 ribonucleoproteins. *Genome Res* **24**, 1012-1019 (2014).

33. Ramakrishna, S. *et al.* Gene disruption by cell-penetrating peptide-mediated delivery of Cas9 protein and guide RNA. *Genome Res* **24**, 1020-1027 (2014).

34. Pikovskaya, O. *et al.* Cutting Edge: Eomesodermin Is Sufficient To Direct Type 1 Innate Lymphocyte Development into the Conventional NK Lineage. *J Immunol* **196**, 1449-1454 (2016).

35. Pahl, J. & Cerwenka, A. Tricking the balance: NK cells in anti-cancer immunity. *Immunobiology* **222**, 11-20 (2017).

36. Fu, B. *et al.* Natural Killer Cells Promote Fetal Development through the Secretion of Growth-Promoting Factors. *Immunity* **47**, 1100-1113 e1106 (2017).

37. Wensveen, F.M. *et al.* NK cells link obesity-induced adipose stress to inflammation and insulin resistance. *Nat Immunol* **16**, 376-385 (2015).

38. Loschko, J. *et al.* Inducible targeting of cDCs and their subsets in vivo. *J Immunol Methods* **434**, 32-38 (2016).

39. Esterhazy, D. *et al.* Classical dendritic cells are required for dietary antigen-mediated induction of peripheral T(reg) cells and tolerance. *Nat Immunol* **17**, 545-555 (2016).

40. Mayer, C.T. *et al.* Selective and efficient generation of functional Batf3-dependent CD103+ dendritic cells from mouse bone marrow. *Blood* **124**, 3081-3091 (2014).

41. Shen, M.W. *et al.* Predictable and precise template-free CRISPR editing of pathogenic variants. *Nature* **563**, 646-651 (2018).

Chapter 4:
UTX regulates the epigenetic programs of NK cell development and anti-viral effector function

UTX regulates the epigenetic programs of NK cell development and anti-viral effector function

Mandy I. Cheng[1,2,$], Luke Riggan[1,2,$], Feiyang Ma[3,4], Rana Yakhshi Tafti[1], Scott Chin[1], Matteo Pellegrini[3,4], Timothy E. O'Sullivan[1,2,*] and Maureen A. Su[1,2,5,*]

[1]Department of Microbiology, Immunology, and Molecular Genetics, David Geffen School of Medicine at UCLA, Los Angeles, CA 90095
[2]Molecular Biology Institute, University of California, Los Angeles, Los Angeles, CA 90095, USA
[3]Department of Molecular, Cell, and Developmental Biology, University of California, Los Angeles, California, USA.
[4]Institute for Genomics and Proteomics, University of California, Los Angeles, California, USA.
[5]Department of Pediatrics, David Geffen School of Medicine at UCLA, Los Angeles, CA 90095
[$]These authors contributed equally
[*]Corresponding Authors

Correspondence:

Timothy E. O'Sullivan, PhD
David Geffen School of Medicine at UCLA
615 Charles E. Young Drive South, BSRB 245F
Los Angeles, CA 90095
Phone: 310-825-4454
Email: tosullivan@mednet.ucla.edu

Maureen A. Su, MD
David Geffen School of Medicine at UCLA
615 Charles E. Young Drive South, BSRB 290C
Los Angeles, CA 90095
Phone: 310-825-2130
Email: masu@mednet.ucla.edu

Abstract

Natural killer cells are circulating type 1 innate lymphocytes that protect against viral infection and cancer. While it is now clear that NK cells display distinct epigenetic states during development and activation, the factors that control the epigenetic programming of NK cells during these processes are not well understood. Here, we show that the H3K27me3 histone demethylase UTX epigentically regulates NK cells in a cell-intrinsic and demethylase-independent manner by regulating the chromatin accessibility of gene loci involved in homeostasis and effector function. As a consequence, mice with NK cell-specific UTX deficiency displayed an increase in peripheral immature NK cell cells that express higher levels of Bcl-2. Furthermore, UTX-deficient NK cells produce lower amounts of interferon (IFN)-γ and granzyme B following MCMV infection, resulting in increased mortality. These findings reveal UTX as an essential regulator of NK cell homeostatic and effector epigenetic programs.

Introduction

Innate lymphoid cells (ILCs) are rapid producers of both proinflammatory and regulatory cytokines in response to local injury, inflammation, pathogen infection, or commensal microbiota perturbation[40-42]. The ability of ILCs to quickly respond to tissue stress and inflammation underpins their critical role in regulating tissue homeostasis and repair during infection or injury[3, 43]. Recent evidence suggests that ILCs contain developmentally imprinted open chromatin landscapes of stimulation-responsive elements (regulomes) that underpin their rapid responsiveness to environmental stimuli[7, 44-46]. However, the factors that maintain the "poised" epigenetic state of these elements during development and homeostasis are not well understood.

Natural Killer (NK) cells are cytotoxic group 1 innate lymphocytes that protect against viral infection and cancer formation through production of cytotoxic molecules (i.e. granzyme B) and cytokines such as interferon (IFN)-γ[4, 11]. While previous work has identified distinct transcriptional and epigenetic states of mouse and human NK cells during development and viral infection[6,7, 30], the factors that control the epigenetic landscape of NK cells during these processes remain unclear. Here, we identify ubiquitously transcribed tetratricopeptide repeat, X chromosome (UTX; also known as *Kdm6a*) as a critical regulator of the NK cell regulome. Analysis of mice with NK cell-specific deletion of UTX revealed increased peripheral immature NK numbers with a defect in effector responses to mouse cytomegalovirus (MCMV) infection. Assay for transposase-accessible chromatin using sequencing (ATAC-seq) along with bulk RNA sequencing (RNA-seq) identified UTX-mediated changes in chromatin accessibility at

several gene loci involved in NK cell development, homeostasis, and effector function. Together, these results identify UTX as a critical epigenetic regulator of NK cells in mice.

Results

UTX regulates NK cell development

NK cells undergo dynamic chromatin remodeling during development and in response to viral infection[6,7]. However, the epigenetic regulators that are responsible for these genome-wide chromatin changes are unknown. To address these questions, we analyzed transcriptomes of naïve and activated NK cells following MCMV infection using previously published datasets[7]. This analysis revealed dynamic regulation of multiple epigenetic regulators, including the H3K27me3 demethylase *Kdm6a* (UTX) (data not shown)[120]. Flow cytometric analysis of UTX protein levels in NK cells during MCMV confirmed increased UTX levels on Day 4 (D4) post-infection (PI) compared to uninfected controls (D0), suggesting that UTX may regulate NK cell anti-viral function (**Extended Data Fig. 1a**). To test this possibility, we generated mice with conditional deletion of UTX in NK cells (*Kdm6a*$^{fl/fl}$ x *Ncr1*^{Cre}, referred to as UTX^{NKD} hereafter), and confirmed reduced UTX protein levels in UTX^{NKD} NK cells by flow cytometry (**Extended Data Fig. 1b,c**).

Analysis of naïve UTX^{NKD} mice revealed a significant increase in the percentage and absolute numbers of NK cells in all peripheral organs tested (**Fig. 1a-c**). To determine whether these results were due to altered development of peripheral NK cells, we analyzed CD27 and CD11b expression, which can be used to identify 4 stages of NK cell maturation in mice[121]. Percentages and absolute numbers of immature CD27^{-}CD11b^{-} NK cells were increased, while more mature CD27^{+}CD11b^{+} NK cells were decreased in the spleen of UTX^{NKD} mice (**Fig. 1d,e**). However, the absolute numbers of terminally differentiated mature CD27^{-}CD11b^{+} NK cells were increased in UTX^{NKD} mice, suggesting

that NK cell maturation is not influenced by loss of UTX. (**Fig. 1e,f**). To determine whether the developmental changes observed in NK cells from UTX^{NKD} mice were cell-intrinsic, we produced mixed bone marrow chimeric (mBMC) mice, where congenically-distinct WT ($CD45.1^+$) and UTX^{NKD} ($CD45.2^+$) cells developed in the same host environment. Indeed, we observed an increased percentage of immature $CD27^-CD11b^-$ NK cells and a decreased percentage of more mature $CD27^+CD11b^+$ NK cells derived from UTX^{NKD} bone marrow **(Fig. 1g)**. Together, these data indicate that UTX may control NK cell fitness at distinct stages of development.

UTX regulates NK cell homeostasis and effector function

NK cell homeostasis is balanced by proliferation in response to homeostatic cytokines and cell-intrinsic apoptosis following terminal differentiation[122, 123]. We therefore investigated whether the observed increase in NK cells present in UTX^{NKD} mice may reflect a hyper-proliferative state of UTX-deficient NK cells. In contrast to this hypothesis, UTX^{NKD} mice displayed decreased percentages of $Ki67^+$ splenic NK cells at all maturation stages (**Fig. 2a,b**). Similarly, UTX-deficient NK cells displayed less CFSE-dilution in response to IL-15 *ex vivo*, suggesting that the increased number of NK cells present in UTX^{NKD} mice was not due to enhanced proliferative capacity (**Fig. 2c-e**). Previous studies have shown that the mitochondrial-associated pro-survival molecule Bcl-2 antagonizes the pro-apoptotic molecule Bim to promote NK cell survival during homeostasis[15,55]. To test whether altered Bcl-2 or Bim levels could account for increased numbers of NK cells, we analyzed intracellular levels of Bcl-2 and Bim in splenic NK cells harvested from

UTX^{NKD} mice and littermate controls. We found that while UTX-deficient NK cells displayed a modest increase in intracellular Bim levels, Bcl-2 levels were significantly increased (**Fig. 2f-h**). This resulted in higher observed Bcl-2:Bim ratios across all maturation stages, excluding terminally differentiated CD27^{-}CD11b^{+} NK cells (**Fig. 2i,j**). Thus, UTX regulates NK cell development and homeostasis through reduction of Bcl-2 levels to restrict the fitness of immature NK cells.

To investigate whether UTX influences other NK cell functions *in vivo*, we challenged WT and UTX^{NKD} mice with MCMV. In spite of increased peripheral NK cell numbers, we observed that UTX^{NKD} mice rapidly succumbed to a sublethal dose of murine cytomegalovirus (MCMV) while all littermate controls survived, indicating that UTX may also regulate NK cell effector function (**Fig. 3a**). To determine whether UTX-deficient NK cells displayed a cell-intrinsic defect in effector molecule production, WT (CD45.1^{+}):UTX^{NKD} (CD45.2^{+}) mBMC mice were infected with MCMV. Indeed, UTX-deficient splenic NK cells displayed a marked defect in IFN-γ and granzyme B production on D1.5 PI (**Fig. 3b**). Similarly, intracellular staining revealed a significant defect in IFN-γ production in UTX-deficient NK cells following stimulation with IL-12 and IL-18 (**Fig. 3c,d**), indicating that UTX-deficient NK cell effector responses are defective in response to proinflammatory cytokines produced during viral infection. Because NK cell development is perturbed by the loss of UTX in a cell-intrinsic manner, the observed defect in anti-viral effector responses in total NK cells may represent an overabundance of immature NK cells with reduced effector capacity. To investigate this possibility, we analyzed NK cell maturation stages in the spleen of MCMV-infected WT (CD45.1^{+}):UTX^{NKD} (CD45.2^{+}) mBMC mice. While UTX-deficient mature CD27^{-}CD11b^{-} NK cells displayed reductions in

IFN-γ and granzyme B production on a per-cell basis in the spleen of infected mice, immature $CD27^{-}CD11b^{-}$ NK cells did not reduce IFN-γ production and increased granzyme B levels compared to WT controls (**Fig. 3e,f**). Together, these results suggest that UTX regulates the anti-viral effector response in a maturation-stage specific manner during MCMV infection.

UTX regulates NK cell developmental and effector gene expression through control of chromatin accessibility

As a histone demethylase, UTX may control NK cell development and effector gene expression programs by catalyzing the removal of a methyl group from H3K27me3 (a repressive histone mark) to poise chromatin for active gene expression[120]. To test this possibility, we used mice that express a catalytically inactive UTX (UTX "demethylase-dead" or UTX^{DMD}), with H1146A and E1148A point mutations in the UTX catalytic domain[124]. However, we observed that UTX^{DMD} and WT controls displayed similar frequencies and absolute numbers of splenic NK cells (**Fig. 4a-c**). Moreover, UTX^{DMD} and WT NK cells displayed similar proportions of NK cell maturation subsets in contrast to NK cells derived from UTX^{NKD} mice (**Fig. 4d,e**). To confirm whether this phenotype was not influenced by loss of UTX demethylase activity in other cell types, we generated mBMC mice in which WT and UTX^{DMD} NK cells developed in the same host. Analysis of splenic NK cells revealed similar NK subset frequencies between WT and UTX^{DMD} NK cells (**Fig. 4f**), suggesting that loss of NK cell-intrinsic UTX demethylase activity is inconsequential for NK cell development. To investigate whether UTX demethylase activity influences NK cell effector function, we stimulated WT, UTX^{NKD} and UTX^{DMD} NK cells with IL-12 and IL-

18 *ex vivo*. While UTX^{NKD} NK cells displayed a loss of IFN-γ production following proinflammatory cytokine stimulation, we did not observe a difference between WT and UTX^{DMD} NK cells, suggesting UTX demethylase activity is also dispensable for optimal NK cell effector function (**Fig. 4g)**.

Previous studies have shown that UTX can interact with the SWI/SNF complex to mediate general chromatin remodeling in a demethylase-independent manner[125]. To test this possibility, we performed Assay for Transposase-Accessible Chromatin using sequencing (ATAC-seq) on sort-purified WT (CD45.1^{+}) and UTX-deficient (CD45.2^{+}) NK cells from WT:UTX^{NKD} mBMC mice. ATAC-seq revealed 4230 significant peaks with decreased accessibility and 2143 with increased accessibility in UTX^{NKD} compared to WT NK cells (**Fig. 5a, Supplementary Table 1**). DAVID gene ontology analysis[126] identified differentially accessible peaks associated with apoptotic and proliferative pathways (**Extended Data Fig. 2a**). Furthermore, DA peaks were found in genes associated with NK cell development (*Tbx21, Atg5, Foxo3, Bcl11b, Ets1, Hhex, Nfil3, Tcf7, Zeb2)*, homeostasis (*Runx2, Runx1, Bcl2),* effector response (*Ifng*, *Ccl5*, *Csf2*, *Gzmm*, *Il10)*, cytokine signaling (*Cish, Jak1, Jak2, Nfkb1, Socs3, Socs5*, *Il12rb2*, *Il2ra*, *Stat5b*, *Stat4)* and maturation (*Thy1, Ly6c2, Klrg1, Cx3cr1)*[49, 68, 69, 104, 127-133] **(Fig. 5b, Extended Data Fig. 2b**). HOMER (Hypergeometric Optimization of Motif Enrichment) transcription factor motif analysis of DA peaks revealed decreased accessibility in motifs bound by AP-1 and JunB, transcription factors important for cytokine responsiveness; BATF, which is required for peripheral NK cell homeostasis; as well as ETS1 and RUNX1, which are important in driving gene programs necessary for NK cell development (**Fig. 5c**)[68, 69, 71, 134]. These data suggest that UTX regulates the chromatin accessibility of several genes

known to influence NK cell development, homeostasis and effector responses, while also controlling genome-wide accessibility of transcription factor binding sites of transcription factors implicated in these processes.

To determine if the observed chromatin accessibility changes impact gene expression, transcriptomic analysis was performed using RNA sequencing on sort-purified WT (CD45.1$^+$) and UTX^{NKD} (CD45.2$^+$) NK cells from WT:UTX^{NKD} mBMC mice. RNA sequencing revealed 397 significant downregulated genes and 246 upregulated genes in UTX^{NKD} compared to WT NK cells (**Fig. 5d, Supplementary Table 2**). In accordance with changes in chromatin accessibility, *Thy1, Ly6c2, Ldha, Nfil3, Socs3, Tcf7 and Ifng* transcripts were decreased in UTX^{NKD} NK cells, while *Bcl2* transcripts were increased (**Fig. 5e**). Flow cytometric analysis confirmed a significant decrease in CD90 (*Thy1*) and Ly6C (*Ly6c2*) in UTX-deficient NK cells (**Fig. 5f,g**). Together, these findings suggest UTX regulates the accessibility and expression of genes associated with NK cell development and effector function.

UTX regulates the chromatin landscape of NK cells during development and inflammation

NK cells undergo dramatic epigenetic remodeling in response to proinflammatory cytokines produced during viral infection[7, 44]. However, whether UTX mediates inflammation-induced changes to the NK cell regulome was unknown. To determine this, ATAC-seq was performed on NK cells sorted from WT:UTX^{NKD} mBMC mice on D1.5 after MCMV infection. Analysis of this dataset revealed 4,026 differentially accessible gene loci

in UTX^{NKD} vs. WT NK cells (**Fig. 6a, Supplementary Table 3**). While gene ontology analysis of gene regions with decreased accessibility in UTX^{NKD} revealed similar pathways to steady state (e.g., apoptotic processes and regulation of cell proliferation), additional pathways involved in inflammation and effector responses (e.g., natural killer cell mediated cytotoxicity, Jak-STAT signaling pathway) were identified (**Fig. 6b**). Specifically, UTX deficiency in NK cells on D1.5 PI was associated with decreased accessibility at distinct peaks located in the *Ifng*, *Gzmb*, and *Il2ra* loci (**Fig. 6c, Extended Data Fig. 3a**). The decrease in accessibility at the *Gzmb* locus in UTX-deficient NK cells was observed during inflammation (D1.5), but not at steady state (D0). Similarly, distinct peaks in a p300 and H3K27ac-bound putative enhancer region in proximity to a T-bet-bound region in the *Ifng* locus displayed decreased accessibility in UTX-deficient NK cells specifically during viral-induced inflammation (**Extended Data Fig. 3b,c**). Furthermore, HOMER analysis revealed decreased accessibility of motifs bound by transcription factors involved in anti-viral responses (NFkB, IRF8, STAT4), inflammatory cytokine responsiveness (STAT1 and STAT5), and NK cell effector function (Eomes, T-bet) (**Fig. 6d**)[7, 44, 104, 135-137]. These results suggest UTX mediates distinct inflammation-induced epigenetic modifications in NK cells in addition to its role during development. In support of this hypothesis, principal component analysis (PCA) of both D0 and D1.5 PI WT and UTX-deficient NK cells revealed distinct epigenetic and transcriptional landscapes, with 648 genes associated with differentially accessibility and 422 genes differentially expressed that were unique to D1.5 PI (**Fig. 6e-h, Supplementary Table 4**). Transcriptomic analysis of differentially accessible genes revealed transcripts that were differentially expressed at D0 only (*Ifng, Ldha, Nfil3, Socs3*), shared between D0 and

D1.5 PI (*Bcl2*, *Ccl5*, *Ly6c2*, *Tcf7*, *Thy1*, *Jak1*), and D1.5 PI only (*Csf2, Il12rb2, Stat4, Tfeb*) (**Extended Data Fig. 4a-c**). Thus, while UTX controls transcription of certain effector genes (e.g., *Ifng*) prior to infection, it also is required for normal expression of distinct effector genes during viral-induced inflammation (e.g., *Csf2, Il12rb2, Stat4*).

Distinct changes in chromatin accessibility and gene expression suggest that UTX may have different roles in different NK cell maturational stages. Indeed, our data suggest that UTX differentially regulates IFN-γ protein production at different NK cell maturational stages **(Fig. 3e).** However, it is unknown whether expression of UTX during NK cell development is sufficient to epigenetically prime effector loci, or whether continuous expression of UTX in NK cells is required to maintain optimal effector programs. To explore these questions, we developed a mouse model in which UTX expression can be inducibly deleted by tamoxifen administration immediately prior to MCMV infection (*Kdm6a*$^{fl/fl}$ x *Rosa26*^{CreERT2}, referred to as iUTX$^{-/-}$ hereafter). To control for cell-extrinsic effects of UTX deletion, mBMC mice were generated with bone marrow from WT (CD45.1^{+}) and iUTX$^{-/-}$ (CD45.2^{+}), and UTX deletion in NK cells was confirmed by flow cytometry (**Extended Data Fig. 5a,b**). Similar to results in UTX^{NKD} mice, we observed a decrease in the percentage and MFI of IFN-γ in iUTX$^{-/-}$ NK cells compared to WT controls on D1.5 PI (**Fig. 6i,j**). Furthermore, there was a positive correlation ($p=0.0138$, $r^2 = 0.814$) between UTX expression levels and IFN-γ production (**Fig. 6k**). Together, these findings suggest a model in which UTX is required continuously as a central regulator of the NK cell regulome to produce rapid and robust anti-viral effector responses (**Extended Data Fig. 6**).

Discussion

In this study, we identify UTX as a critical epigenetic regulator of NK cell development and anti-viral immunity. NK cell-specific deletion of UTX was associated with loss of IFN-γ and granzyme B production following MCMV infection, resulting in increased mortality of UTX^{NKD} mice. These findings demonstrate a key role for UTX in controlling NK cell effector responses during viral infection. Indeed, inducible deletion of UTX 3 days prior to MCMV infection was sufficient to attenuate NK cell IFN-γ production, suggesting that continuous UTX expression is required for optimal NK cell effector function. Our data indicate that UTX also regulates gene expression associated with NK cell development and homeostasis. UTX promotes the expression of *Thy1* and *Ly6c2,* and controls NK cell fitness by suppressing *Bcl2* expression. Together, these findings identify UTX as a critical regulator of NK cell-mediated anti-viral immunity and demonstrate specific roles for UTX in priming specific epigentici states in NK cells.

NK cell-mediated effector functions during viral infection include cytokine production (IFN-γ) and cytotoxicity mediated by Granzyme B production[138]. Our results suggest that UTX poises the chromatin landscape of NK cells at rest to quickly respond to viral challenge by increasing accessibility of effector loci such as *Ifng.* As a consequence, significant decreases in IFN-γ protein levels were detected at D1.5 PI in UTX-deficient NK cells. However, *Ifng* transcript levels were not differentially expressed at D1.5 PI despite lower IFN-γ protein levels at this timepoint. One possibility is that UTX may function post-transcriptionally in promoting IFN-γ production in NK cells. In $CD8^+$ T cells, UTX regulates the expression of inhibitory receptors without significantly impacting transcript levels, implicating a possible post-transcriptional role for UTX in controlling

effector programs in cytotoxic lymphocytes[139]. These results support a model in which UTX plays a dual role during viral infection to drive a rapid and robust IFN-γ response: i) UTX regulates chromatin accessibility at the *Ifng* locus at steady-state and ii) alters IFN-γ expression at the post-transcriptional level during inflammation. Alternatively, it is also possible that UTX's regulation of IFN-γ production is NK cell subset-specific. In support of this hypothesis, we identified maturation subset-specific changes in IFN-γ and granzyme B levels in NK cells during viral infection. Further studies on sorted NK cell subsets by CD27 and CD11b expression will be required to delineate potential subset-specific roles of UTX in controlling effector gene expression.

Our findings indicate UTX restricts NK cell numbers at steady state, since NK cells are increased with UTX deficiency. Previous studies reported UTX deletion results in moderate ($CD8^+$ and $CD4^+$ T cells) or severe (iNKT) decreases in peripheral cell numbers[139-141]. Interestingly, T cell-specific UTX-deficiency is associated with $CD8^+$ T cell accumulation during viral infection. Thus, it is possible that UTX-mediated gene programs that inhibit $CD8^+$ T cell numbers during inflammation are shared by NK cells at rest[139]. Indeed, increased Bcl2 expression was noted in both UTX-deficient NK cells and UTX-deficient $CD8^+$ T cells, suggesting that UTX down-regulates this anti-apoptotic factor in both of these immune cell lineages. In contrast, UTX may also epighenetically regulate lymphocyte homepstasis and effector function in distinct cell-type specific mechanisms. In iNKT cells, UTX has been reported to control cell fate through direct control of expression of JunB, a transcription factor important in iNKT development[141]. However, our studies using HOMER motif analysis revealed UTX deficiency in NK cells results in decreased accessibility of JunB, suggesting in UTX may be acting with JunB to control

expression of JunB target genes. Furthermore, In $CD4^+$ T cells, UTX forms multiprotein complexes with Brg1, T-bet and Eomes to drive Th1 IFN-γ production[19]. Our results identified a putative enhancer region in the *Ifng* gene locus bound by p300 and H3K27ac, and in proximity to a T-bet-bound site that has decreased in accessibility in UTX-deficient NK cells during viral infection. Moreover, HOMER motif analysis showed decreased accessibility of T-bet and Eomes binding sites in UTX-deficient NK cells, indicating UTX may be form complexes with T-bet, Eomes, and p300 in NK cells. These findings suggest UTX may associate with distinct multiprotein complexes in a cell-type specific manner. However, further studies are needed to identify multiprotein complexes important in NK cell- mediated anti-viral responses.

Our findings demonstrate that UTX's H3K27 demethylase activity is dispensable for NK cell development and effector function. In $CD8^+$ T cells, UTX binds to enhancer and TSS of effector genes to promote effector gene programs in a demethylase-independent manner[139]. In contrast, demethylase activity in iNKT cells is required for development and function and H3K27 methylation correlated with gene programs important for $CD4^+$ T follicular helper cell development[140, 142]. Thus, while UTX has conserved protein interactions within multiple immune cell types, our study reveals NK cell-type specific roles UTX plays in order to fine tune inflammatory responses. A previous study treated human NK cells with a small molecule inhibitor of H3K27me3 demethylases (GSK-J4) and found reduced cytokine expression (IFN-γ, TNF-α, GM-CSF, and IL-10) in response to *in vitro* stimulation[143]. However, GSK-J4 is not a specific tool for studying UTX-mediated mechanisms because it also inhibits Jmjd3, another H3K27me3 demethylase as well as non-specifically upon other histone demethylases[144], thus further

studies using more specific genetic modification strategies are needed to understand the impact of UTX regulation in human NK cells.

NK cells are critical for control of CMV infection in humans since NK cell-deficient individuals develop disseminated herpesvirus infections[1, 145]. Sex differences in immune response to multiple viruses have been reported, including immune responses to CMV[145]. As an X-linked gene that escapes inactivation, UTX is expressed from two copies of the X chromosome in females but only one copy of the X chromosome in males. Thus, it is possible that sex differences in anti-viral immunity may be due to differences in UTX expression, although this will need to be explored in future studies. UTX deficiency has also been associated with Kabuki Syndrome and Turner Syndrome, two human conditions associated with immune dysregulation and increased infections. Our findings suggest the possibility that UTX deficiency in human NK cells may contribute to decreased viral immunosurveillance observed in these patients, although future work will be needed to support this hypothesis.

Acknowledgements

We thank members of the O'Sullivan and Su labs for helpful discussion. We thank the UCLA Technology Center for Genomics and Bioinformatics for RNA sequencing library preparation and the Cedars Sinai Applied Genomics, Computation, and Translational Core Facility for ATAC sequencing library preparation. T.E.O. is supported by the NIH (AI145997) and UC CRCC (CRN-20-637105). M.A.S. is supported by the NIH (NS107851, AI143894, DK119445) Department of Defense (USAMRAA PR200530), and National Organization of Rare Diseases. M.I.C. is supported by Ruth L. Kirschstein National Research Service Awards (GM007185 and AI007323), and Whitcome Fellowship from the Molecular Biology Institute at UCLA. L.R. is supported by the Warsaw fellowship from the MIMG department at UCLA.

The authors declare no financial conflicts of interest.

Author Contributions

L.R., M.I. C., M.A.S. and T.E.O. designed the study; L.R., M.I.C., and S.C. performed the experiments; F.M., M.I.C., R.T.Y. and M.P. performed bioinformatics analysis; T.E.O., M.I.C., M.A.S. and L.R. wrote the manuscript.

Competing Interests Statement

The authors declare no competing interests.

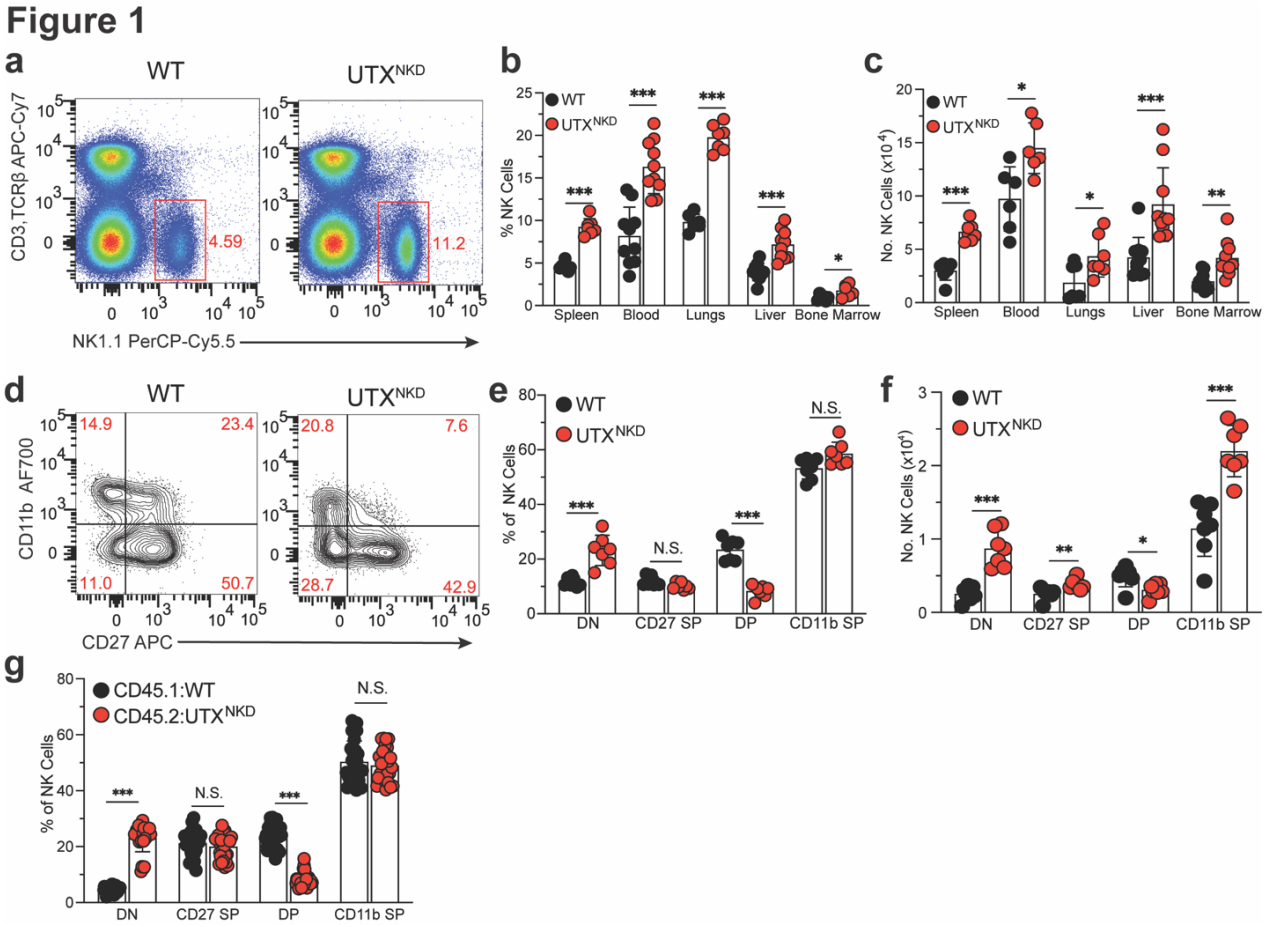

Figure 1: UTX controls peripheral NK cell development. a) Representative flow cytometry plots of splenocytes from WT and UTX^{NKD} mice, gated on NK cells (CD3,TCRβ^{-} NK1.1^{+}). **b)** Percentage and **c)** absolute numbers of NK cells isolated from the spleen, blood, lungs, liver, and bone marrow of WT and UTX^{NKD} mice (n=6-10). **d)** Representative flow cytometry plots from WT and UTX^{NKD} splenic NK cells, gated on maturation subsets based on CD11b and CD27 expression (DN: CD27^{-}CD11b^{-}; CD27 SP: CD27^{+}CD11b^{-}; DP: CD27^{+}CD11b^{+}; CD11b SP: CD27^{-}CD11b^{+}). **e)** Percentage and **f)** absolute numbers of each indicated NK subset (n=7). **g)** Percentage of peripheral blood NK cell maturation subsets (DN, CD27 SP, DP, and CD11b SP) from WT:UTX^{NKD} mBMC mice (n=28). Data are representative of 2-3 independent experiments. Samples were compared using two-

tailed Student's t test with Welch's correction, assuming unequal SD, and data points are presented as individual mice with the mean ± SEM (N.S., Not Significant; *, $p < 0.05$; **, $p < 0.01$; ***, $p < 0.001$).

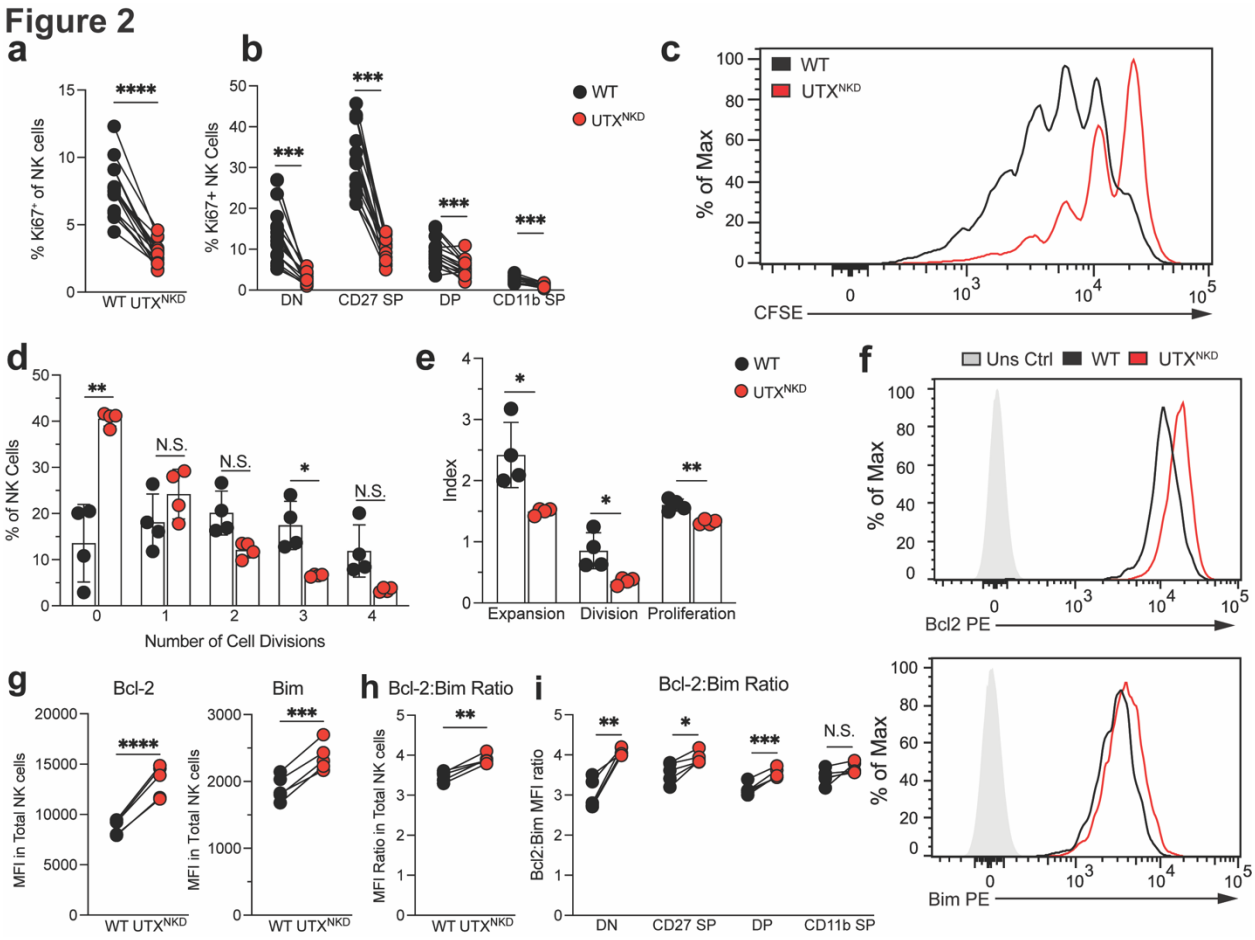

Figure 2: UTX regulates NK cell proliferation and apoptosis. a-b) Peripheral blood NK cells from WT:UTX^{NKD} mBMC peripheral blood were analyzed for percent Ki67^{+} in **a)** total NK cells (TCRβ^{-}CD3^{-}NK1.1^{+}) and **b)** NK cell subpopulations (DN, CD27SP, DP, and CD11b) (n=28 recipient mice). **c)** Representative flow cytometry plot, **d)** quantification of cell divisions, and **e)** quantification of CFSE expansion, division and proliferation indexes of CFSE-labeled splenic NK cells from WT:UTX^{NKD} mBMC mice stimulated *ex vivo* with IL-15 (50 ng/mL) for 4 days. **f)** Representative flow cytometry plot for Bcl-2 (top) and Bim (bottom) of total peripheral blood NK cells from WT:UTX^{NKD} mBMC mice. **g)** Bcl-2 and Bim MFI, and h) Bcl-2/Bim MFI Ratio from flow cytometric analysis of total peripheral blood NK cells from WT:UTX^{NKD} mBMC mice. i) Bcl-2/Bim MFI Ratio of NK cell

subpopulations. Data represent 2-3 independent experiments. Samples were compared using two-tailed Student's t test with Welch's correction, assuming unequal SD, and data points are presented as individual mice with the mean ± SEM (N.S., Not Significant; *, $p < 0.05$; **, $p < 0.01$; ***, $p < 0.001$; ****, $p < 0.0001$).

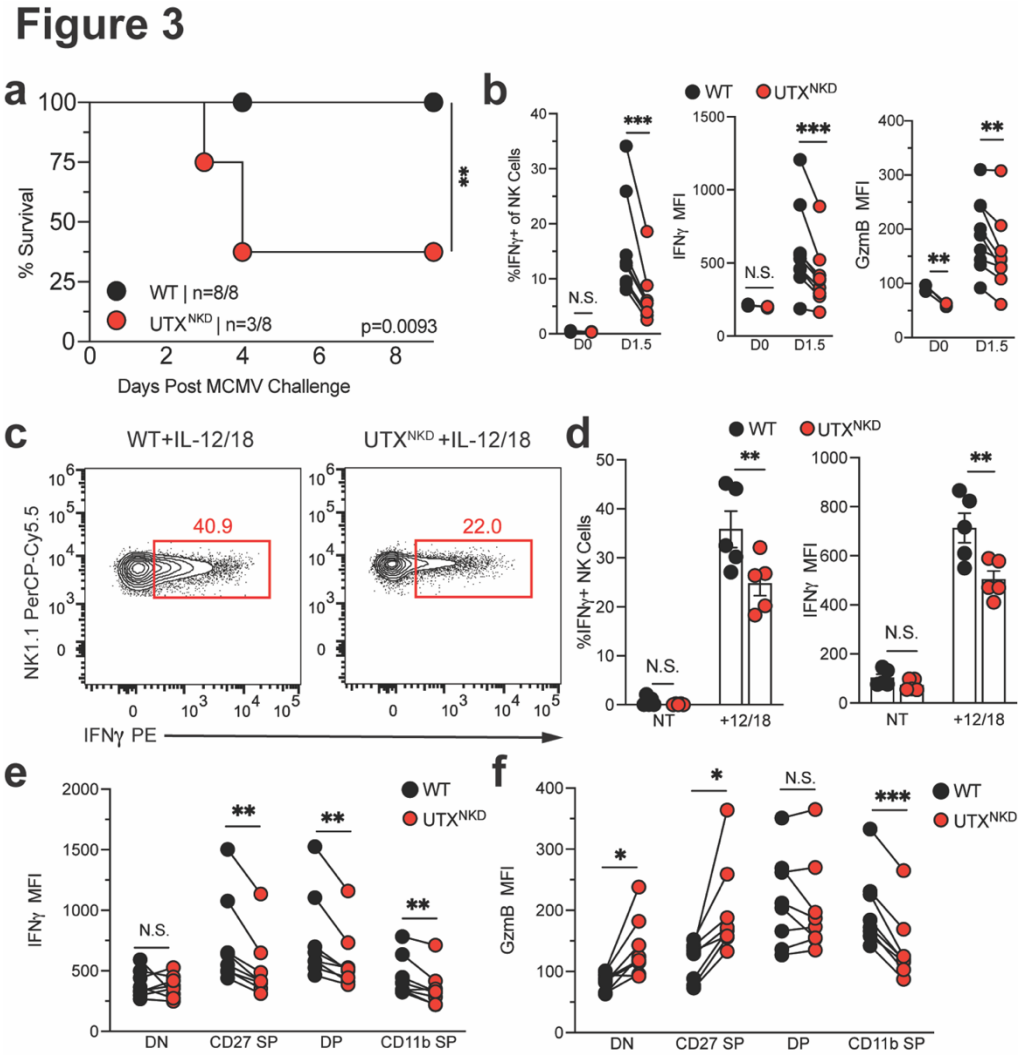

Figure 3: UTX is required for NK cell anti-viral immunity. **a)** Kaplan-Meier survival curves of WT and UTX^{NKD} mice infected with MCMV (n=8 per genotype). Mantel-Cox test (**, p=0.0093). **b)** Flow cytometric analysis of percent IFN-γ^{+}, IFN-γ MFI, and GzmB MFI in splenic NK cells from uninfected (D0) or D1.5 PI of WT:UTX^{NKD} mBMC mice (n=7). **c)** Representative flow cytometry plot and **d)** percent IFN-γ^{+} and IFN-γ MFI of WT and UTX^{NKD} splenic NK cells stimulated with IL-12/IL-18 for 5 hours *ex vivo* (n=5). **e)** IFN-γ and **f)** GzmB MFI of NK cell subpopulations from WT:UTX^{NKD} mBMC splenic NK cells (n=7). Data are representative of 2-3 independent experiments. Samples were compared using two-tailed Student's t test with Welch's correction, assuming unequal SD, and data

points are presented as individual mice with the mean ± SEM (N.S., Not Significant; *, p <0.05; **, p <0.01; ***, p<0.001).

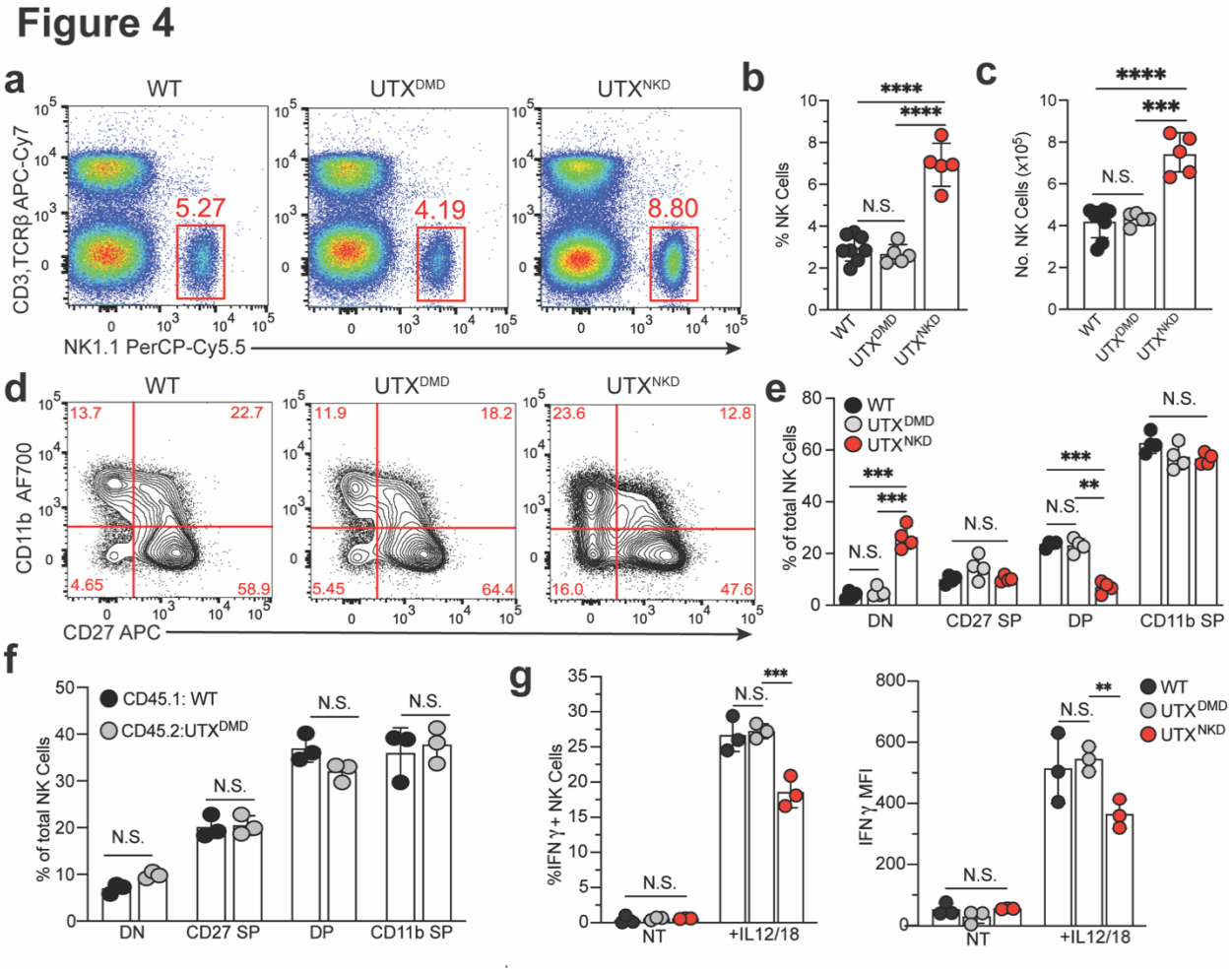

Figure 4: UTX regulates NK cell development and effector function in a demethylase-independent manner. a) Representative flow plots and **b)** percentage and **c)** absolute numbers of NK cells (CD3,TCRβ$^-$ NK1.1$^+$) in spleens from WT, UTX^{DMD}, and UTX^{NKD} mice. **d)** Representative flow plots of CD11b and CD27 expression and **e)** % of each maturation subset in splenic NK cells from WT, UTX^{DMD}, UTX^{NKD} mice. **f)** % of each maturation subset in splenic NK cells from WT:UTX^{DMD} mBMCs (n=3). **g)** Percent IFN-γ$^+$ and IFN-γ MFI in NK cells from WT, UTX^{DMD}, and UTX^{NKD} mice stimulated with IL-12 and IL-18 for 5 hours *ex vivo.* Data are representative of 2-3 independent experiments. Samples were compared using two-tailed Student's t test with Welch's correction,

assuming unequal SD, and data points are presented as individual mice with the mean ± SEM (N.S., Not Significant; *, $p < 0.05$; **, $p < 0.01$; ***, $p < 0.001$; ****, $p < 0.0001$).

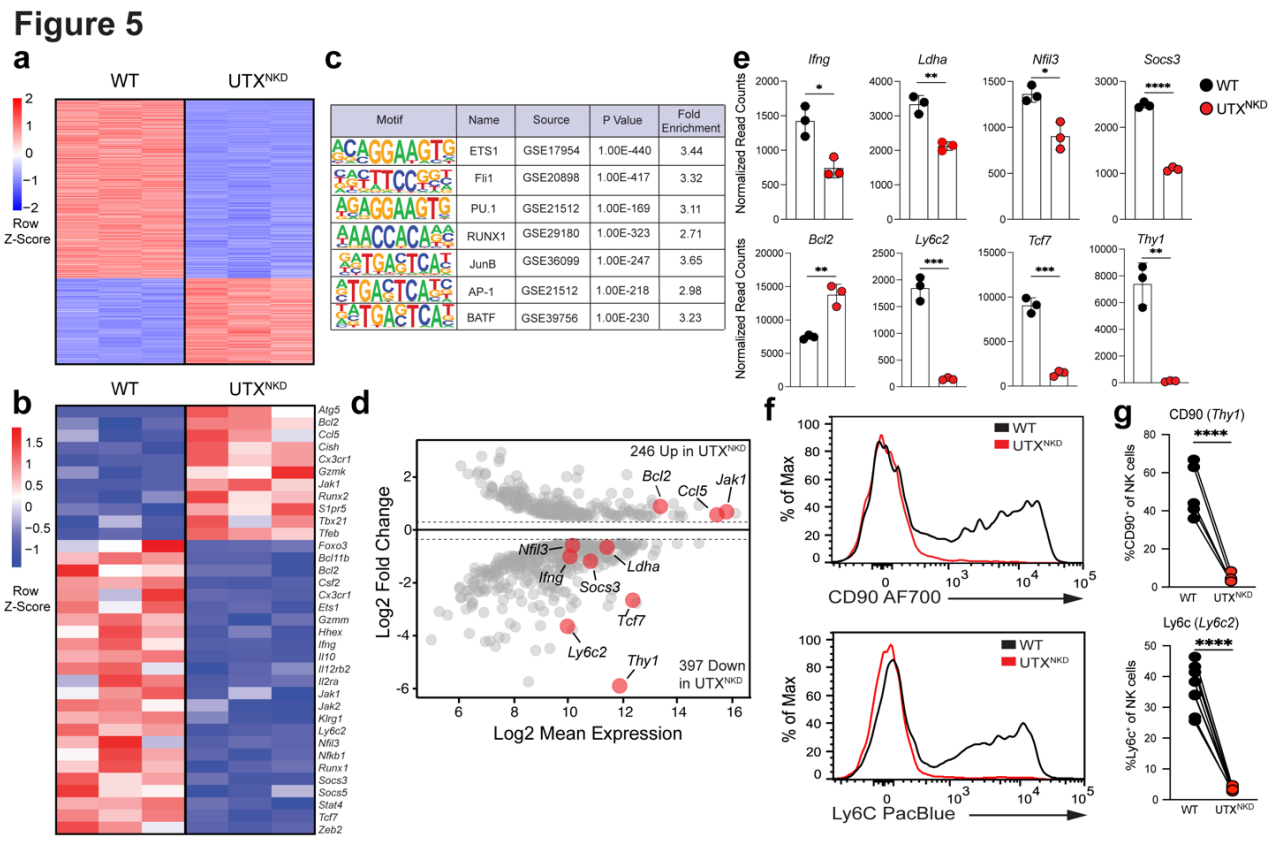

Figure 5: UTX regulates NK cell developmental and effector gene expression through control of chromatin accessibility. a) Heatmap of differentially accessible peaks identified by ATAC-seq of splenic NK cells from WT:UTX^{NKD} mBMC mice**. b)** Heatmap of differentially expressed transcripts identified by RNA-seq of splenic NK cells from WT:UTX^{NKD} mBMC mice. **c)** HOMER motif analysis displaying transcription factor binding sites with decreased accessibility in UTX^{NKD} compared to WT NK cells. **d)** Volcano plot highlighting selected differentially expressed genes (FDR and adjusted p-value < 0.05). Y-axis depicts Log2 FC and x-axis depicts Log2 mean expression. Shown are all expressed genes (TPM>5) comparing transcripts which are up in UTX^{NKD} (top) versus down in UTX^{NKD} cells (bottom). **e)** Normalized read counts of selected genes shown in **(b)**. **f)** Representative flow cytometry for CD90 (*Thy1*) and Ly6C (*Ly6c2*) and **g)** %CD90^{+}, and %Ly6C^{+} in peripheral blood NK cells from WT:UTX^{NKD} mBMC mice (n=5-

7). Data are representative of 2-3 independent experiments. Samples were compared using two-tailed Student's t test with Welch's correction, assuming unequal SD, and data points are presented as individual mice with the mean ± SEM (*, $p < 0.05$; **, $p < 0.01$; ***, $p < 0.001$; ****, $p < 0.0001$). All genes displayed in heatmaps met the following threshold of significance: FDR > 0.05, $p < 0.05$, and Log2FC > 0.05.

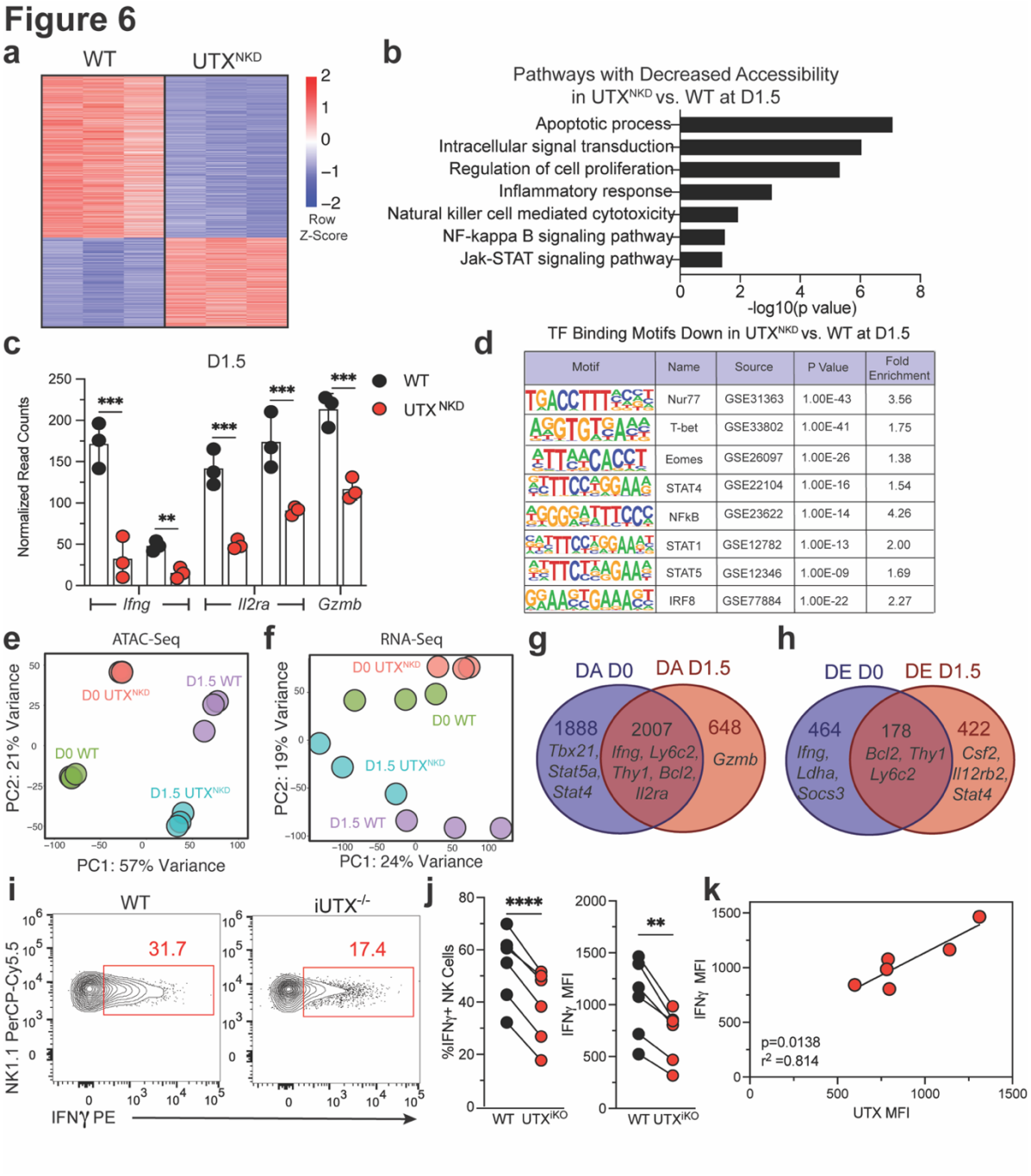

Figure 6: UTX regulates NK effector gene accessibility through chromatin remodeling at distinct loci during inflammation. a) Heatmap of differentially accessible peaks by ATAC-seq of splenic NK cells from WT:UTX^{NKD} mBMC mice D1.5 PI. All genes displayed in heatmap met the following threshold of significance: FDR >

0.05, p < 0.05, and Log2FC ± 0.05. **b)** Gene Ontology pathway analysis of gene regions with decreased accessibility in UTX^{NKD} vs. WT NK cells at D1.5 PI (adjusted p-value < 0.05). **c)** Normalized read counts of accessibility at peaks located in the *Ifng*, *Il2ra*, and *Gzmb* loci at D1.5 PI. **d)** HOMER motif analysis displaying TF binding sites with decreased accessibility in UTX^{NKD} vs. WT NK cells at D1.5 PI. **e,f)** Principal component analysis (PCA) of epigenetic (ATAC-seq) **e)** and transcriptional (RNA-seq) **f)** changes in WT and UTX^{NKD} NK cells at D0 and D1.5 PI. Venn diagrams illustrating unique and overlapping differentially accessible (DA) peaks from ATAC-seq **g)** and differentially expressed (DE) genes from RNA-seq **h).** Numbers represent DA peaks or DE genes specific to NK cells at D0 only (blue), at D1.5 PI only (red), or shared (overlap). **i)** Representative flow cytometry plot and **j)** %IFN-γ^+ and IFN-γ MFI of splenic NK cells from WT:$iUTX^{-/-}$ mBMC (n=6). Data are representative of 2-3 independent experiments. Two-tailed Student's t-test with Welch's correction, assuming unequal SD was performed, and data points depict individual mice with the mean ± SEM (**, p<0.01; ***, p<0.001; ****, p<0.0001). **k)** Correlation of IFN-γ vs. UTX MFI in splenic NK cells (n=6). Two-tailed correlation of XY data performed. Pearson's r^2 =0.8144, and p = 0.0138.

Methods

Mice

Mice were bred at UCLA in accordance with the guidelines of the institutional Animal Care and Use Committee (IACUC). The following mouse strains were used in this study: C57BL/6 (CD45.2) (Jackson Labs, #000664), B6.SJL (CD45.1) (Jackson Labs, #002114), *Rosa26*^{ERT2Cre}, *Ncr1*^{Cre}, *Utx*$^{fl/fl}$, UTX demethylase dead (UTX^{DMD}) which harbors two point mutations at H1146A and E1148A (a gift from Kai Ge). UTX is located on the X chromosome and escapes inactivation, it is expressed from 2 chromosomal copies in females but only one in males. Thus, to control for the number of UTX copies, experiments were conducted using 6-8 week old age-matched females in accordance with approved institutional protocols. Mixed bone marrow chimeric (mBMC) mice were generated by depleting host CD45.1 x CD45.2 mice by intraperitoneal (i.p.) injection of busulfan (1mg/mL) at 20mg/kg for 3 consecutive days, which were then reconstituted 24 hours later with various mixtures of bone marrow cells from WT (CD45.1) and knockout (CD45.2) donor mice.

MCMV infection

MCMV (Smith) was serially passaged through BALB/c hosts three times, and then salivary gland viral stocks were prepared with a dounce homogenizer for dissociating the salivary glands of infected mice 3 weeks after infection. Experimental mice in studies were infected with MCMV by i.p. injection of 7.5 x 10^3 plaque-forming units (PFU) in 0.5 mL of PBS. Mice were monitored and weighed daily and sacrificed when body weight dropped over 20% from initial weight.

Isolation and enrichment of mouse NK cells

Mouse spleens, livers, lungs, lymph nodes, and blood were harvested and prepared into single cell suspensions as described previously[3]. Splenic single cell suspensions were lysed in red blood cell lysis buffer and resuspended in EasySep™ buffer (Stemcell). To avoid depleting $Ly6C^+$ NK cells we developed a custom antibody cocktail as follows: splenocytes were labeled with 10 µg per spleen of biotin conjugated antibodies against CD3 (17A2), CD19 (6D5), CD8 (53-6.7), CD88 (20/70), Ly6G (1A8), SiglecF (S17007L), TCRβ (H57-597), CD20 (SA275A11), CD172a (P84) and magnetically depleted from total splenocyte suspensions with the use of anti-biotin coupled magnetic beads (Biolegend).

Ex vivo stimulation of lymphocytes

~5 x 10^5 NK cells were stimulated for 5 hours in CR-10 (RPMI 1640 + 25 mM HEPES + 10% FBS, 1% L-glutamine, 1% 200 mM sodium pyruvate, 1% MEM-NEAA, 1% penicillin-streptomycin, 0.5% sodium bicarbonate, 0.01% 55 mM 2-mercaptoethanol) , Brefeldin A (1:1000; BioLegend) and Monensin (2uM; BioLegend) with or without recombinant mouse IL-12 (20 ng/ml; Peprotech) and recombinant mouse IL-18 (10ng/ml; Peprotech) for 5 hours. Cells were cultured in CR-10 media alone as a negative control (No Treatment or NT).

Proliferation assays

CellTrace™ CFSE (Thermo) stock solution was prepared per the manufacturers' instructions and diluted at 1:10,000 in 37C PBS. Isolated NK cells were incubated in 0.5mL of diluted CFSE solution for 5 minutes at 37C. The solution was quenched with

10X the volume of CR-10 media. Cells were then washed and plated at 50 ng rmIL-15 (Peprotech) and cultured for 4 days to assess proliferation.

Flow Cytometry and Cell Sorting

Cells were analyzed for cell-surface markers using fluorophore-conjugated antibodies (BioLegend, eBioscience). Cell surface staining was performed in FACS Buffer (2% FBS and 2 mM EDTA in PBS) and intracellular staining was performed by fixing and permeabilizing using the eBioscience Foxp3/Transcription Factor kit for intranuclear proteins or BD Cytofix/Cytoperm kits for cytokines. Flow cytometry was performed using the Attune NxT Acoustic Focusing cytometer and data were analyzed with FlowJo software (TreeStar). Cell surface and intracellular staining was performed using the following fluorophore-conjugated antibodies: CD45.1 (A20), CD45.2 (104), NK1.1 (PK136), TCRβ (H57-597), CD3 (17A2), Ly49H (3D10), IFN-γ (XMG1.2), Ly6C (HK1.4), BCL2 (BCL/10C4), CD11b (M1/70), CD27 (LG.3A10), CD25 (PC61), Granzyme B (GB11), UTX (N2C1 - GeneTex), Goat anti-rabbit H&L (Abcam - ab6717), BIM (c34c5), CD90 (30-H12), Ki-67 (16A8). Isolated splenic NK cells were sorted using Aria-H Cytometer to > 95% purity.

RNA-seq and ATAC-seq library construction and analysis

RNA was isolated from the cells using RNeasy Mini kit (Qiagen) and used to generate RNA-seq libraries followed by sequencing using Illumina HighSeq 4000 platform (single end, 50bp). The reads were mapped with HISAT2 (version 2.2.1) to the mouse genome

(mm10). The counts for each gene were obtained by HtSeq[86], in print, online at doi:10.1093/bioinformatics/btu638). Differential expression analyses were carried out using DESeq2[81] (version 1.24.0) with default parameters. Genes with adjusted p value <0.05 were considered significantly differentially expressed. Sequencing depth normalized counts were used to plot the expression values for individual genes.

ATAC-seq libraries were produced by the Applied Genomics, Computation, and Translational Core Facility at Cedars Sinai in the following manner: 50,000 cells per sample were lysed to collect nuclei and treated with Tn5 transposase (Illumina) for 30 minutes at 37°C with gentle agitation. The DNA was isolated with DNA Clean & Concentrator Kit (Zymo) and PCR amplified and barcoded with NEBNext High-Fidelity PCR Mix (New England Biolabs) and unique dual indexes (Illumina). The ATAC-Seq library amplification was confirmed by real-time PCR, and additional barcoding PCR cycles were added as necessary while avoiding overamplification. Amplified ATAC-Seq libraries were purified with DNA Clean & Concentrator Kit (Zymo). The purified libraries were quantified with Kapa Library Quant Kit (KAPA Biosystems) and quality assessed on 4200 TapeStation System (Agilent). The libraries were pooled based on molar concentrations and sequenced on an Illumina HighSeq 4000 platform (paired end, 100bp).

ATAC-seq fastq files were trimmed to remove low-quality reads and adapters using Cutadapt[83] (version 2.3). The reads were aligned to the reference mouse genome (mm10) with bowtie2[84] (version 2.2.9). Peak calling was performed with MACS2[85] (version 2.1.1). The peaks from all samples were merged into a single bed file, peaks from different samples that were closer than 10bp were merged into a single peak. HTseq[86] (version

0.9.1) was used to count the number of reads that overlap each peak per sample. The peak counts were analyzed with DESeq2[81] (version 1.24.0) to identify differentially accessible genomic regions. Peaks with adjusted p-value < 0.05 were considered significantly differentially accessible. The peak counts were visualized with IGV, version 2.5.0. The differentially accessible peaks were analyzed using the findMotifsGenome.pl function from homer[87] (version 4.9.1) to identify enriched cis-regulatory motifs of transcription factors.

Statistical Analyses

For graphs, data are shown as mean ± SEM, and unless otherwise indicated, statistical differences were evaluated using a Student's t-test with Welch's correction to assume a non-normal variance in our data distribution. Samples were compared using the Log-rank (Mantel-Cox) test with correction for testing multiple hypotheses. A p-value < 0.05 was considered significant. Graphs were produced and statistical analyses were performed using GraphPad Prism.

Data Availability

Sequencing datasets are accessible from GEO with accession number GSE185065.

References

1. Artis, D. & Spits, H. The biology of innate lymphoid cells. *Nature* **517**, 293-301 (2015).
2. Vivier, E. *et al.* Innate Lymphoid Cells: 10 Years On. *Cell* **174**, 1054-1066 (2018).
3. Serafini, N., Vosshenrich, C.A. & Di Santo, J.P. Transcriptional regulation of innate lymphoid cell fate. *Nat Rev Immunol* **15**, 415-428 (2015)
4. Nabekura, T., Riggan, L., Hildreth, A.D., O'Sullivan, T.E. & Shibuya, A. Type 1 Innate Lymphoid Cells Protect Mice from Acute Liver Injury via Interferon-gamma Secretion for Upregulating Bcl-xL Expression in Hepatocytes. *Immunity* **52**, 96-108 e109 (2020).
5. Weizman, O.E. *et al.* ILC1 Confer Early Host Protection at Initial Sites of Viral Infection. *Cell* **171**, 795-808 e712 (2017).
6. Wiedemann, G.M. *et al.* Deconvoluting global cytokine signaling networks in natural killer cells. *Nat Immunol* **22**, 627-638 (2021).
7. Lau, C.M. *et al.* Epigenetic control of innate and adaptive immune memory. *Nat Immunol* **19**, 963-972 (2018).
8. Pokrovskii, M. *et al.* Characterization of Transcriptional Regulatory Networks that Promote and Restrict Identities and Functions of Intestinal Innate Lymphoid Cells. *Immunity* **51**, 185-197 e186 (2019).
9. Shih, H.Y. *et al.* Developmental Acquisition of Regulomes Underlies Innate Lymphoid Cell Functionality. *Cell* **165**, 1120-1133 (2016).
10. Riggan, L., Freud, A.G. & O'Sullivan, T.E. True Detective: Unraveling Group 1 Innate Lymphocyte Heterogeneity. *Trends Immunol* **40**, 909-921 (2019).

11. Cerwenka, A. & Lanier, L.L. Natural killer cell memory in infection, inflammation and cancer. *Nat Rev Immunol* **16**, 112-123 (2016).

12. Collins, P.L. *et al.* Gene Regulatory Programs Conferring Phenotypic Identities to Human NK Cells. *Cell* **176**, 348-360 e312 (2019).

13. Van der Meulen, J., Speleman, F. & Van Vlierberghe, P. The H3K27me3 demethylase UTX in normal development and disease. *Epigenetics* **9**, 658-668 (2014).

14. Chiossone, L. *et al.* Maturation of mouse NK cells is a 4-stage developmental program. *Blood* **113**, 5488-5496 (2009).

15. Pfefferle, A. *et al.* Deciphering Natural Killer Cell Homeostasis. *Front Immunol* **11**, 812 (2020).

16. Huntington, N.D. *et al.* Interleukin 15-mediated survival of natural killer cells is determined by interactions among Bim, Noxa and Mcl-1. *Nat Immunol* **8**, 856-863 (2007).

17. Viant, C. *et al.* Cell cycle progression dictates the requirement for BCL2 in natural killer cell survival. *J Exp Med* **214**, 491-510 (2017).

18. Wang, C. *et al.* UTX regulates mesoderm differentiation of embryonic stem cells independent of H3K27 demethylase activity. *Proc Natl Acad Sci U S A* **109**, 15324-15329 (2012).

19. Miller, S.A., Mohn, S.E. & Weinmann, A.S. Jmjd3 and UTX play a demethylase-independent role in chromatin remodeling to regulate T-box family member-dependent gene expression. *Mol Cell* **40**, 594-605 (2010).

20. Huang, D.W. *et al.* DAVID Bioinformatics Resources: expanded annotation database and novel algorithms to better extract biology from large gene lists. *Nucleic Acids Res* **35**, W169-175 (2007).
21. Taveirne, S. *et al.* The transcription factor ETS1 is an important regulator of human NK cell development and terminal differentiation. *Blood* **136**, 288-298 (2020).
22. Townsend, M.J. *et al.* T-bet regulates the terminal maturation and homeostasis of NK and Valpha14i NKT cells. *Immunity* **20**, 477-494 (2004).
23. Holmes, T.D. *et al.* The transcription factor Bcl11b promotes both canonical and adaptive NK cell differentiation. *Sci Immunol* **6** (2021).
24. Geiger, T.L. *et al.* Nfil3 is crucial for development of innate lymphoid cells and host protection against intestinal pathogens. *J Exp Med* **211**, 1723-1731 (2014).
25. Deng, Y. *et al.* Transcription factor Foxo1 is a negative regulator of natural killer cell maturation and function. *Immunity* **42**, 457-470 (2015).
26. van Helden, M.J. *et al.* Terminal NK cell maturation is controlled by concerted actions of T-bet and Zeb2 and is essential for melanoma rejection. *J Exp Med* **212**, 2015-2025 (2015).
27. Delconte, R.B. *et al.* CIS is a potent checkpoint in NK cell-mediated tumor immunity. *Nat Immunol* **17**, 816-824 (2016).
28. Jeevan-Raj, B. *et al.* The Transcription Factor Tcf1 Contributes to Normal NK Cell Development and Function by Limiting the Expression of Granzymes. *Cell Rep* **20**, 613-626 (2017).

29. Sun, J.C. *et al.* Proinflammatory cytokine signaling required for the generation of natural killer cell memory. *J Exp Med* **209**, 947-954 (2012).

30. O'Sullivan, T.E. *et al.* Atg5 Is Essential for the Development and Survival of Innate Lymphocytes. *Cell Rep* **15**, 1910-1919 (2016).

31. Rapp, M. *et al.* Core-binding factor beta and Runx transcription factors promote adaptive natural killer cell responses. *Sci Immunol* **2** (2017).

32. Ramirez, K. *et al.* Gene deregulation and chronic activation in natural killer cells deficient in the transcription factor ETS1. *Immunity* **36**, 921-932 (2012).

33. Nausch, N. *et al.* Cutting edge: the AP-1 subunit JunB determines NK cell-mediated target cell killing by regulation of the NKG2D-ligand RAE-1epsilon. *J Immunol* **176**, 7-11 (2006).

34. Adams, N.M. *et al.* Transcription Factor IRF8 Orchestrates the Adaptive Natural Killer Cell Response. *Immunity* **48**, 1172-1182 e1176 (2018).

35. Geary, C.D. *et al.* Non-redundant ISGF3 Components Promote NK Cell Survival in an Auto-regulatory Manner during Viral Infection. *Cell Rep* **24**, 1949-1957 e1946 (2018).

36. Wiedemann, G.M. *et al.* Divergent Role for STAT5 in the Adaptive Responses of Natural Killer Cells. *Cell Rep* **33**, 108498 (2020).

37. Cook, K.D. *et al.* T Follicular Helper Cell-Dependent Clearance of a Persistent Virus Infection Requires T Cell Expression of the Histone Demethylase UTX. *Immunity* **43**, 703-714 (2015).

38. Beyaz, S. *et al.* The histone demethylase UTX regulates the lineage-specific epigenetic program of invariant natural killer T cells. *Nat Immunol* **18**, 184-195 (2017).

39. Mitchell, J.E. *et al.* UTX promotes CD8(+) T cell-mediated antiviral defenses but reduces T cell durability. *Cell Rep* **35**, 108966 (2021).

40. Maj, T. *et al.* Oxidative stress controls regulatory T cell apoptosis and suppressor activity and PD-L1-blockade resistance in tumor. *Nat Immunol* **18**, 1332-1341 (2017).

41. Pomeroy, C., Delong, D., Clabots, C., Riciputi, P. & Filice, G.A. Role of interferon-gamma in murine cytomegalovirus infection. *J Lab Clin Med* **132**, 124-133 (1998).

42. Biron, C.A., Byron, K.S. & Sullivan, J.L. Severe herpesvirus infections in an adolescent without natural killer cells. *N Engl J Med* **320**, 1731-1735 (1989).

43. van der Heiden, M. *et al.* Differential effects of Cytomegalovirus carriage on the immune phenotype of middle-aged males and females. *Sci Rep* **6**, 26892 (2016).

44. Banka, S. *et al.* Novel KDM6A (UTX) mutations and a clinical and molecular review of the X-linked Kabuki syndrome (KS2). *Clin Genet* **87**, 252-258 (2015).

45. Thrasher, B.J., Hong, L.K., Whitmire, J.K. & Su, M.A. Epigenetic Dysfunction in Turner Syndrome Immune Cells. *Curr Allergy Asthma Rep* **16**, 36 (2016).

46. Cribbs, A. *et al.* Inhibition of histone H3K27 demethylases selectively modulates inflammatory phenotypes of natural killer cells. *J Biol Chem* **293**, 2422-2437 (2018).

47. Kruidenier, L. *et al.* A selective jumonji H3K27 demethylase inhibitor modulates the proinflammatory macrophage response. *Nature* **488**, 404-408 (2012).

48. Anders, S., Pyl, P.T. & Huber, W. HTSeq--a Python framework to work with high-throughput sequencing data. *Bioinformatics* **31**, 166-169 (2015).

49. Love, M.I., Huber, W. & Anders, S. Moderated estimation of fold change and dispersion for RNA-seq data with DESeq2. *Genome Biol* **15**, 550 (2014).

50. Kechin, A., Boyarskikh, U., Kel, A. & Filipenko, M. cutPrimers: A New Tool for Accurate Cutting of Primers from Reads of Targeted Next Generation Sequencing. *J Comput Biol* **24**, 1138-1143 (2017).

51. Langmead, B. & Salzberg, S.L. Fast gapped-read alignment with Bowtie 2. *Nat Methods* **9**, 357-359 (2012).

52. Zhang, Y. *et al.* Model-based analysis of ChIP-Seq (MACS). *Genome Biol* **9**, R137 (2008).

53. Heinz, S. *et al.* Simple combinations of lineage-determining transcription factors prime cis-regulatory elements required for macrophage and B cell identities. *Mol Cell* **38**, 576-589 (2010).

Concluding Remarks

In recent years, NK cells are being recognized as important players in cell therapy for treatment against cancer and even infections such as COVID-19[146, 147]. However, the basic biology of many NK cell processes still remain incompletely understood. Our studies on NK cells during MCMV infection, offer a robust model to study the transcriptional and epigenetic regulation of effector NK cell expansion, cytotoxicity and memory formation. In summary, our work has identified a subset of $Ly6C^{-}$ MP NK cells, which due to enhanced persistence, make up a majority of the memory $Ly6C^{+}$ NK cell pool. In addition, we identified Fli1, a transcription factor with no known previous role in NK cells, as an important negative regulator of the accumulation of these MP NK cells. CRISPR mediated deletion of Fli1 ($Fli1^{KO}$) in NK cells resulted in enhanced fitness demonstrated by decreased Bim levels and $Fli1^{KO}$ NK cells made up a majority of the memory NK cell pool at Day 28 post infection.

Although NK cells offer many advantages for immunotherapy, current NK immunotherapy approaches suggest persistence could be an issue since NK cells do not form lifelong memory[147]. Genetic deletion of Fli1 in NK cell immunotherapies may improve NK cell persistence and the outcome of these therapies, although future work is needed to support this hypothesis. In addition to the advances in basic NK cell biology, our work has outlined a robust and efficient method for using CRISPR to study gene function in a wide array of innate immune cells. This method will allow for rapid study of gene function to advance basic biology and for translational advancement to quickly screen gene targets to identify additional negative regulators for NK cell responses.

However, future work is needed to fully adapt our CRISPR method to an *in vivo* tumor model.

In summary, our work here has described the process by which MP NK cells are formed, a novel transcriptional regulator Fli1 which controls MP NK cell fitness, the upstream signals which induce Fli1 and an improved method to study gene function in NK cells and other innate immune cells. In addition, our findings demonstrate an important role for UTX in promoting NK cell effector responses during viral infection. Deletion of UTX in mature NK cells resulted in decreased IFN-γ production during MCMV infection, suggesting that continuous UTX expression is required for optimal NK cell effector function. These advances will not only add to the understanding of basic NK cell biology but could potentially offer new targets for NK immunotherapies in the future.